



Study of hybrid baryons in a constituent model of the quantum chromodynamics and prospects for a large- N extension

Université de Mons

Thèse présentée par

Lorenzo CIMINO

en vue de l'obtention du grade académique de *Doctorat en Sciences*

Promoteurs

Claude SEMAY (UMONS)

Cintia T. WILLEMYNS (UMONS - VUB)

Jury

Pascal QUINET (UMONS)

Evelyne DAUBIE (UMONS)

Barbara CLERBAUX (Université Libre de Bruxelles)

Vicente VENTO (Universidad de Valencia)

Année académique 2024-2025

- Faculté des sciences • Université de Mons •
- Place du Parc 20, 7000 Mons Belgique •

Contents

Acknowledgements/Remerciements	i
Units and abbreviations	v
1 SI units and fundamental constants	v
1.1 Natural units	vi
2 Table of abbreviations	vii
Introduction and state of the art	ix
1 State of the art	x
2 Structure of the thesis	xiii
1 Brief history of the strong interaction	1
1.1 Isospin, flavour and colour	2
1.1.1 Heavy quarks	5
1.1.2 Hypothesis of the colour	6
1.2 Quantum chromodynamics	8
1.2.1 Quantum electrodynamics	9
1.2.2 Non-abelian gauge symmetry	10
1.2.3 Hadronic states	12
1.3 QCD approaches	13
1.3.1 One-gluon exchange	15
1.3.2 Confinement	17
2 Many-body systems and the envelope theory	23
2.1 Generalities	24
2.2 <i>N</i> -body harmonic oscillator	24
2.2.1 Jacobi coordinates	25
2.2.2 Diagonalisation procedure	27
2.2.3 Identical particles	29
2.2.4 Sets of identical particles	31
2.3 Envelope theory	34
2.3.1 Auxiliary Hamiltonian	34
2.3.2 Compact equations for identical particles	39
2.3.3 Compact equations for two sets of identical particles	41
2.4 Improved envelope theory	44
2.4.1 Dominantly orbital state method	45
2.4.2 Coupling of the ET and the DOS method	47
2.4.3 Generalisation to different particles	47

2.5	Example of results with the envelope theory	51
2.5.1	Results for identical particles	51
2.5.2	Results for different particles	53
3	Helicity formalism	59
3.1	One-body states	59
3.1.1	Massive particles and canonical states	60
3.1.2	Massless particles and helicity states	62
3.1.3	Massive particles and helicity states	63
3.1.4	Parity and opposite momentum states	66
3.2	Two-body states	67
3.2.1	Two-body helicity states	67
3.2.2	Helicity angular momentum states	68
3.2.3	Two-body canonical states	71
3.3	Application of the helicity formalism to hybrid baryons	72
3.3.1	Quark core with $J_C = 1/2$	73
3.3.2	Quark core with $J_C = 3/2$	74
3.3.3	Physical states	76
4	Hybrid baryons in a constituent approach	83
4.1	Flux tubes for hybrid baryons	84
4.2	Quark core Hamiltonian	85
4.2.1	Wavefunction of the quark core	87
4.2.2	Spectrum of the quark core	89
4.3	Core-gluon interaction	91
4.4	Spectrum of heavy hybrid baryons	93
	Conclusions and prospects	99
1	Contributions of this work	99
2	Future works	102
3	Farewell	104
A	Wavefunction of the N-body harmonic oscillator	107
A.1	One-body oscillator wavefunction	107
A.1.1	Degeneracy of the harmonic oscillator	108
A.2	N -body oscillator wavefunction	109
A.2.1	Properties	109
A.2.2	Bosonic ground state	111
A.2.3	Fermionic ground state	111
A.3	Symmetrised three-body oscillator states	112
A.4	Wavefunction in the envelope theory	114
A.4.1	Modified global quantum number	115
B	Notions of the Poincaré group and $SO(3)$	119
B.1	Poincaré algebra and generators	119
B.1.1	Casimir operators	120
B.1.2	Classification of particles	121
B.2	Little group and $SO(3)$	122
B.2.1	Wigner- D matrices	122
C	Lagrange mesh method	127

Acknowledgements

Remerciements

As is customary, these acknowledgements are written in my mother tongue, French. However, parts that are addressed to non-French speakers are written in English and italicised. The rest of the manuscript is, of course, entirely written in English.

Comme il est de coutume, les remerciements sont rédigés dans ma langue maternelle, le français. Cependant, les parties adressées aux personnes ne parlant pas français sont écrites en anglais et en italique. Le reste du manuscrit est évidemment écrit en anglais.

It is very difficult to write an exhaustive list of all the people to thank, especially since a PhD is a long endeavour (four years of hard work for me) and above all a team effort where I had the opportunity to meet many people.

Il est très difficile de faire une liste exhaustive de toutes les personnes à remercier, tant un doctorat est un travail long (quatre années de dur labeur pour moi) et surtout un travail d'équipe, durant lequel j'ai pu côtoyer de nombreuses personnes.

Toutefois, il me semble naturel de commencer par mon promoteur, Claude Semay, sans qui cette aventure n'aurait jamais commencé. Je le remercie particulièrement pour sa pédagogie qui m'a inspirée quand ce fut mon tour de donner cours, ses nombreux conseils, sa bonne humeur, sa disponibilité, et les nombreuses discussions que nous avons eues au cours de ces quatre dernières années. Je me rappelle notamment de la conférence à Kanazawa que nous étions censés suivre sur place, mais que nous avons finalement suivie depuis la Belgique, avec l'horaire japonais évidemment, à cause d'une petite pandémie qu'on préfère oublier. Je retiendrai également un conseil important pour l'avenir : "Le Diable est dans les détails".

Dans la même lignée, je remercie ma co-promotrice, Cintia T. Willemyns, pour ses conseils et son aide sur la QCD à large- N_c , qui m'ont été utiles pour mieux comprendre cette approche.

J'aimerais également remercier Vincent Mathieu pour ses divers conseils et propositions de projets, ainsi que pour nos discussions lors de la conférence NSTAR 2024 à York.

I also wish to thank the members of the Jury, Pascal Quinet, Evelyne Daublie,

Barbara Clerboux, and Vicente Vento, for their careful review of this manuscript, as well as for their numerous questions and discussions.

Je remercie également les membres du Jury, Pascal Quinet, Evelyne Daublie, Barbara Clerboux et Vicente Vento, pour leur relecture attentive de ce manuscrit ainsi que pour leurs nombreuses questions et discussions.

Je n'oublie évidemment pas le F.R.S.-FNRS qui m'a donné l'opportunité de poursuivre un doctorat en m'accordant la bourse d'Aspirant FNRS.

Cependant, un doctorat, ce n'est pas seulement rencontrer des collaborateurs, mais également d'autres doctorants avec qui partager nos expériences. En particulier, je tiens à remercier Cyrille Chevalier qui, en plus d'être un collègue, a été un véritable compagnon de route lors de ce doctorat. Je le remercie pour nos nombreuses discussions sur la théorie des enveloppes, le formalisme d'hélicité, la théorie quantique des champs, etc. Mais également sur des sujets non-scientifiques, dont la ducasse d'Ath que j'ai découverte pendant mon doctorat. Les différentes conférences et écoles d'été auxquelles nous avons assisté ont également été l'occasion de vivre des expériences à deux (c'est bien plus amusant de voyager en groupe que seul). Je me rappelle notamment du voyage à Salamanque où, suite à quelques petits retards à gauche et à droite, nous avons raté notre correspondance à Madrid alors que nous étions à l'arrêt, dans le métro, à moins de 100 mètres de la gare.

Je tiens également à remercier tous les joueurs de cartes invétérés des temps de midi comme Alice, Antoine, Florent, Guillaume, Ismaël, Pierre, Steve, Thomas, et bien d'autres, pour nos nombreuses parties de Belote, Tarot ou Whist. Je pense notamment aux parties de Tarot en Garde Sans avec le roi appelé se trouvant dans le chien (seuls les connaisseurs comprendront).

Je tiens aussi à remercier Ludovic Ducobu qui, en plus d'avoir été un excellent assistant lors de mes études, m'a fourni de nombreux conseils pédagogiques lorsque j'ai repris le cours de Mécanique Newtonienne et Relativiste, et qui m'a aussi énormément aidé avec le template de ce manuscrit.

Enfin, je tiens à remercier tous les autres doctorants de Mons que j'ai pu rencontrer comme Arnaud, David, Helena, Lea, Noémie, Sébastien, Simon, et bien d'autres.

During my numerous conferences and summer schools, I had the opportunity to meet many PhD students with whom I had great moments. I notably think of André, Di, Enrico and Guilherme at Trento, Giorgia at Seville, Elena and Jana at Salamanca, and finally Sebastian at York.

En plus de mes travaux de recherche, j'ai également eu l'opportunité de donner des séances de cours. Dans cette optique, je tiens à remercier tous les étudiants à qui j'ai eu l'occasion d'enseigner et de discuter, que ce soit de sujets scientifiques ou non. J'ai pris ma tâche d'enseignement à cœur et ce fut un véritable plaisir de pouvoir donner cours et répondre aux diverses questions.

En dehors du cadre académique, je remercie évidemment ma famille, dont mes parents, grands-parents, beaux-parents, et belle-sœur, pour leur soutien inconditionnel lors de mon doctorat. Je n'oublie évidemment pas ma compagne, Mathilde, qui partage ma vie depuis plus de six ans et m'a aidé durant toute la durée de mon doctorat, et qui a su être patiente à chacun de mes départs à l'étranger pour une conférence.

Finalement, je tiens à remercier tous mes professeurs, de la maternelle à l'université, en passant par le primaire et le secondaire, qui m'ont aidé à devenir ce que je suis maintenant et ont su transmettre leur savoir. On sait ô combien le métier d'enseignant est difficile, donc il me semble naturel de les remercier. En particulier, je tiens à remercier Mme Angelaki, ma professeure de Physique en secondaire, qui a su me donner goût à la Physique, à l'époque où je me tournais plutôt vers des études de chimie, et de nous avoir initiés à la physique nucléaire et des particules en rhéto.

Pour terminer, j'aimerais remercier toutes les personnes qui ont participé directement ou indirectement à cette thèse et que j'ai oublié de citer, à ma plus grande honte.

To finish, I would like to thank all the persons that contributed directly or not at this thesis and that I have forgotten to cite, at my greatest shame.

Units and abbreviations

The purpose of this section is to provide an overview of the fundamental constants employed throughout this text, alongside their values in the International System of Units (SI units). Additionally, the concept of natural units, which is utilised extensively in this thesis, is explained. A table of abbreviations used in the text is also provided.

1 SI units and fundamental constants

The SI base units are: the second (s) for time, the metre (m) for length, the kilogram (kg) for mass, the ampere (A) for electric current, the kelvin (K) for temperature, the mole (mol) for the amount of substance, and the candela (cd) for luminous intensity. These seven base units serve as the foundation for deriving other units by combining powers of the base units. For instance, the SI unit of electric potential, the volt (V), is expressed as $\text{kg m}^2 \text{s}^{-3} \text{A}^{-1}$.

The values of the fundamental constants, expressed in SI units, were verified using the NIST (National Institute of Standards and Technology) database¹, accessed on 16th September 2024. Digits in parentheses indicate the uncertainty in the value, expressed in concise form². Throughout this text

- The speed of light in vacuum is denoted c . Its value in SI units is

$$c = 299\,792\,458 \text{ m s}^{-1}.$$

- Planck's constant is denoted h . Its value in SI units is

$$h = 6.626\,070\,15 \times 10^{-34} \text{ m}^2 \text{ kg s}^{-1}.$$

The reduced Planck's constant $\hbar = h/(2\pi)$ is often used in calculations.

- The vacuum electric permittivity is denoted ϵ_0 . Its value in SI units is

$$\epsilon_0 = 8.854\,187\,8188(14) \times 10^{-12} \text{ m}^{-3} \text{ kg}^{-1} \text{ s}^4 \text{ A}^2.$$

The vacuum magnetic permeability, denoted μ_0 , is related to the vacuum electric permittivity by the relation $\epsilon_0\mu_0 = 1/c^2$.

¹<https://pm1.nist.gov/cuu/Constants/>

²For example, 2.1969811(22) represents 2.1969811 ± 0.0000022

- The elementary charge is denoted e . Its value in SI units is

$$e = 1.602\,176\,634 \times 10^{-19} \text{ A s.}$$

The fine-structure constant, denoted α , is defined as

$$\alpha = \frac{e^2}{4\pi\epsilon_0\hbar c} = 7.297\,352\,5643(11) \times 10^{-3},$$

which is dimensionless.

With the exception of ϵ_0 , the other fundamental constants are defined as exact. This is due to the modern redefinition of SI units, which fixes the values of certain fundamental constants to exact numbers in order to define the units themselves. For instance, the metre (m) is defined as the distance light travels in $1/(299\,792\,458)$ seconds³. Similarly, the kilogram (kg) is defined in terms of Planck's constant, while the ampere (A) is defined based on the elementary charge.

The SI unit for energy is the joule (J), defined as $1 \text{ J} = 1 \text{ kg m}^2 \text{ s}^{-2}$. However, in particle physics, the electron-volt (eV) is more commonly used as a unit of energy. The eV is defined as the amount of kinetic energy gained by a single electron when accelerated through an electric potential difference of one volt (V) in a vacuum. It is related to SI units by

$$1 \text{ eV} = (1 e) \times (1 \text{ V}) = 1.602\,176\,634 \times 10^{-36} \text{ J.}$$

In this thesis, the electron-volt (eV) will be used as the unit of energy instead of the joule.

1.1 Natural units

In theoretical physics, it is often convenient to use a system of units where certain fundamental constants are normalised to unity, known as natural units. In this thesis, natural units are adopted such that

$$c = \hbar = 1.$$

This approach simplifies the expression of equations and facilitates the numerical evaluation of physical quantities. For instance, a particle with a velocity of $74\,948\,114.5 \text{ m s}^{-1}$ is equal to $1/4$ in natural units. The conversion is achieved by multiplying the velocity in natural units by the value of c in SI units. Similarly, the intrinsic spin of an electron is simply given by $1/2$ in natural units, instead of $5\,272\,858.5 \times 10^{-34} \text{ m}^2 \text{ kg s}^{-1}$ in SI units.

Thanks to natural units, various physical quantities can be expressed in the same unit. Notably, through Einstein's relation $E = mc^2$, mass can be expressed as energy divided by c^2 . In natural units, where $c = 1$, mass is directly expressed in units of energy, such as electron-volts (eV). For example, the masses of the electron, proton, and neutron are given in natural units as

³The second is defined based on the hyperfine transition frequency of caesium-133, $\Delta\nu_{\text{Cs}} = 9\,192\,631\,770 \text{ s}^{-1}$, which is an exact value.

$$\begin{aligned}
m_e &= 0.510\,998\,950\,69(16) \text{ MeV}, \\
m_p &= 938.272\,089\,43(29) \text{ MeV}, \\
m_n &= 939.565\,421\,94(48) \text{ MeV}.
\end{aligned}$$

To convert mass from natural units to kilograms, the relationship is

$$1 \text{ eV [natural units]} = \frac{1 \text{ eV[SI]}}{c^2[\text{SI}]} = 1.782\,661\,92 \times 10^{-36} \text{ kg}.$$

Similarly, momentum is expressed in units of eV, while length and time are expressed in units of eV^{-1} .

Additionally, by setting $\epsilon_0 = 1$ in natural units, the electric charge can be expressed in units of $\sqrt{\epsilon_0 \hbar c}$, leading to the elementary charge being represented as

$$e = \sqrt{4\pi\alpha} = 0.303.$$

It is important to note that the definition of natural units may vary depending on the field of study. For example, in atomic physics, natural units are often defined by setting $m_e = e = \hbar = 4\pi\epsilon_0 = 1$. In this system, the speed of light is no longer equal to one, but rather $c = 1/\alpha$. As a result, energy is expressed in electron volts (eV) by multiplying by $m_e\alpha^2c^2 = 27.21 \text{ eV}$.

2 Table of abbreviations

Hereunder, we offer a table of the abbreviations used in the different chapters of this manuscript.

Abbreviation	Full name
BGS	Bosonic Ground State
BM	Brody-Moshinsky (coefficients)
CEBAF	Continuous Electron Beam Accelerator Facility
CLAS	CEBAF Large Acceptance Spectrometer
CM	Centre of Mass
DOS	Dominantly Orbital State (method)
ET	Envelope Theory
EOB	Expansion in Oscillator Bases
FGS	Fermionic Ground State
FT	Fourier Transform
HB	Hybrid Baryon
HO	Harmonic Oscillator
IET	Improved Envelope Theory
LM	Lagrange-Mesh (method)
LQCD	Lattice Quantum ChromoDynamics
MA	Mixed Antisymmetric
MS	Mixed Symmetric
NR	Non-Relativist
OGE	One-Gluon Exchange (process)
OPE	One-Photon Exchange (process)
PL	Pauli-Lubanski (operator/vector)
QCD	Quantum ChromoDynamics
QED	Quantum ElectroDynamics
SI	Système International d'unités (International System of Units)
SM	Standard Model

Introduction and state of the art

The study of elementary particles which constitute the universe has often been a central theme in the history of science. In Antiquity, the Greek philosopher Democritus proposed that all matter was composed of small, indivisible particles he termed “atoms”. However, it was not until the 18th and 19th centuries that modern atomic theory began to emerge, notably through the work of scientists such as Lavoisier and Dalton.

Fast-forwarding to the first half of the 20th century, it was discovered that the atom is not an elementary particle. Instead, it consists of a nucleus at its centre, which is positively charged and contains most of the atom’s mass, and electrons, which are negatively charged particles that “orbit” around the nucleus and are bound to it by the electromagnetic force. Electrons were discovered by Thomson in 1897 through his work on cathode rays, and the nucleus was identified by Rutherford, Geiger, and Marsden in 1911 by studying the scattering of α particles¹ on gold foil. The nucleus itself is composed of protons, positively charged particles whose number, called the atomic number, determines the type of atom (e.g., hydrogen has a single proton, iron has 26, and gold has 79), and neutrons, neutral particles discovered by Chadwick in 1932, which determine the isotopes of the nucleus. If only the electromagnetic force were present, the nucleus would not be stable since the protons would repel each other. The cohesion of the nucleus is explained by the attraction between the protons and neutrons due to a new force, the strong (nuclear) interaction, which is stronger than the electromagnetic one.

Advancing to the present time, the early 21st century, numerous subatomic and subnuclear particles have been discovered, leading to the emergence of a new field of physics: particle physics. A comprehensive list of all known elementary particles and their properties can be found in the Particle Data Group [1]. Our current understanding indicates that protons and neutrons are not elementary particles; rather, they are composite particles made of quarks, which are bound together by the strong interaction. Other composite particles made of quarks exist and are collectively termed hadrons [1]. Their study lies in the

¹ α particles are positively charged particles of matter that are spontaneously emitted from certain radioactive elements. From our current knowledge, we understand that these particles are, in fact, helium-4 nuclei.

field of hadronic physics. Hadrons made of three quarks, such as the proton and neutron, are called baryons, and those composed of a quark-antiquark pair are called mesons.

The current theoretical framework of particle physics is the Standard Model (SM), which unifies three of the four fundamental forces: electromagnetism, strong interaction, and weak interaction, with gravitation notably excluded from this theory. The strong interaction is specifically explained by the theory of Quantum Chromodynamics (QCD). QCD describes the strong interaction between quarks through the exchange of particles known as gluons, which are themselves elementary particles.

In theory, knowledge of the fundamental principles of QCD should enable us to explain all phenomena associated with the strong interaction, including the properties of all possible hadrons. However, in practice, the high complexity of the QCD equations presents significant challenges to this quest. Despite these difficulties, QCD is known to be a rich theory, predicting various configurations of quarks beyond ordinary baryons and mesons. One such configuration is the hybrid baryon, which can be described as a system consisting of three quarks (like a baryon) plus a valence gluon, the particle responsible for mediating the strong interaction. Hybrid baryons have not yet been experimentally observed, and their discovery would provide further confirmation of the theory of the strong interaction. The aim of this thesis is to develop a theoretical model of hybrid baryons to aid experimentalists in their search.

1 State of the art

QCD is an established part of the SM of particle physics, responsible for the confinement of quarks and gluons inside hadrons. Despite the comprehensive framework provided by QCD, significant mysteries remain regarding how hadrons are constructed from quarks and gluons.

A successful method to study the properties of hadrons is the constituent approach, in which quarks interact via potentials that encapsulate the effects of the gluonic field. This method involves solving a many-body quantum problem with interactions deduced or inspired by QCD. Although this approach is theoretically justified primarily for heavy quarks, it has also yielded very good results in the light quark sector, provided constituent quarks are treated as effective degrees of freedom with semi-relativistic dynamics [2, 3]. Another analytical scheme to study the phenomenology of hadrons involves starting from the large number of colours (N_c) limit of QCD [4, 5]. This method has been successfully applied to the study of the properties of ground state baryons, as well as the masses and decays of excited baryons. This approach requires experimental inputs or predictions from other models when no data is available. These two very different approaches can be combined to gain new insights into the structure of hadrons [6, 7, 8, 9].

Besides ordinary hadrons, QCD allows for the existence of states in which the excitation of the gluonic field plays the role of valence particles, either alone in a glueball or coupled to quarks in a hybrid. Consequently, hybrid baryons, composed of three quarks and a gluon, can theoretically exist. These exotic

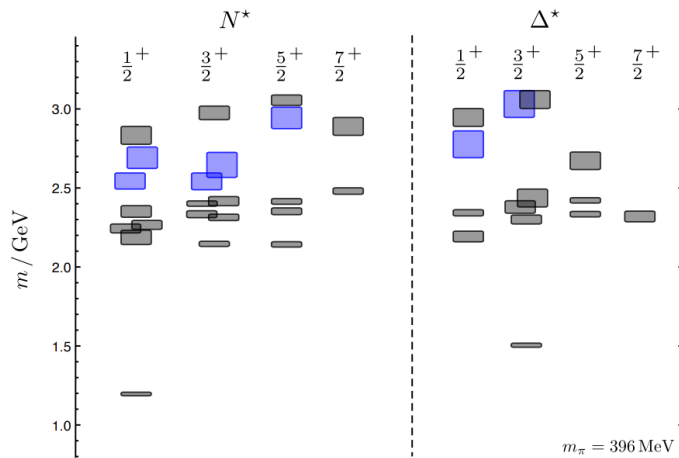


Figure 1: The light-quark baryon spectrum predicted in LQCD at a pion mass of 396 MeV [14]. Grey boxes represent conventional qqq states, and blue boxes represent states identified as hybrid baryons. Note that both the mass of the nucleon ground state and the $\Delta(1232)$ are shifted by nearly 300 MeV to higher masses.

hadrons have been studied using various models: the bag model [10], the flux-tube model [11], QCD sum rules [12], the large- N_c approach [13], and lattice QCD (LQCD) [14]. Unfortunately, although these models predict the existence of hybrid baryons, their predictions for the masses and structures differ considerably. For example, recent LQCD calculations for light hybrid baryons predict the existence of a common energy scale of about 1.3 GeV for the lowest gluonic excitations and a low mixing between hybrid and ordinary baryons with the same spin and parity J^P (see Fig. 1). On the other hand, the possible hybrid baryon nature of the $\Lambda(1405)$ state is suggested by a recent QCD sum rules study [12], and the possibility of significant mixing between the ground states of hybrid and ordinary light baryons is predicted in a detailed large- N_c calculation [13].

A priori, the LQCD technique, in which the gauge theory is formulated on a lattice of points in space and time, can be a powerful method to study these hadrons [14]. Accurate results can be obtained without free parameters, but they require extremely intensive numerical calculations. There is still a long way to go in the study of hybrid baryons with this approach. To gain a better understanding of these exotic baryons using LQCD will require calculations at light quark masses, close to their physical values, coupled with large lattice volumes, which can dramatically increase computational costs. Another issue with this method is the difficulty of investigating the various physical processes occurring inside hadrons. Moreover, efforts currently being made using LQCD and other available approaches (numerical or analytical) focus mainly on hybrid mesons, as these methods are usually simpler due to the fewer constituent particles involved. It is, therefore, worthwhile to explore a method that seems promising for the study of hybrid baryons.

From the experimental side, there is no clear signal yet regarding the existence

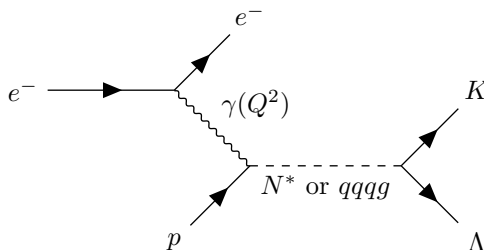


Figure 2: Electroproduction process for a $K\Lambda$ pair on a proton. The four-momentum squared transferred by the photon is Q^2 . The dashed line represents an intermediate state, which could be either an excited nucleon N^* or a hybrid baryon $qq\bar{q}\bar{g}$.

of these hybrid baryons. However, current experimental efforts are focused on searching for hybrid baryons at the CEBAF Large Acceptance Spectrometer (CLAS12) in the experimental Hall B at Jefferson Laboratory (USA) [15, 16]. Hybrid baryons are anticipated to be produced via electroproduction processes, where a polarised electron beam is directed at a liquid hydrogen target (denoted LH_2 , which serves as a proton target). The beam, generated by the CEBAF accelerator, reaches energies up to 10 GeV and operates at a maximum luminosity² of $10^{35} \text{ s}^{-1} \text{ cm}^{-2}$. In the experiment, the electron beam interacts with the proton target through the exchange of virtual photons, characterised by a four-momentum squared Q^2 . The resulting final state includes a scattered electron and a meson-baryon pair, for example $K\Lambda$, produced from the interaction of the proton and photon. During this process, intermediate states appear as resonances, which could either be excited nucleons or exotic particles like hybrid baryons. A schematic of this process is depicted in Fig. 2.

Data will likely become available in the coming years [17]. Identifying hybrid baryons will be more challenging than identifying hybrid mesons, as the latter can have exotic quantum numbers forbidden for states containing only constituent quarks. This is not the case for hybrid baryons, which have quantum numbers also populated by ordinary baryons. Consequently, mixings are possible between hybrid baryons and excited three-quark states. Hybrid baryons should then appear as overpopulated states compared to some models of qqq excitation. Fortunately, the nature of the states produced at CLAS12 can be explored by investigating the Q^2 dependence of the resonance coupling in electroproduction processes [15, 16]. Differences with ordinary baryons are expected due to the additional gluonic component in the wave function of hybrids. For the same reason, the decay products of hybrid baryons must differ from those of ordinary baryons.

The differences between the various models of hybrid baryons and their potential detection in the near future make a better understanding of these objects crucial

²The luminosity L is defined as the ratio of the number of events detected dN in a certain period of time dt to the cross-section σ

$$L = \frac{1}{\sigma} \frac{dN}{dt}.$$

It is expressed in $\text{s}^{-1} \text{ b}^{-1}$ in SI units, where $1 \text{ b} = 10^{-28} \text{ m}^2$.

for their correct identification. The purpose of this thesis is to develop a reliable model of hybrid baryons to guide experimenters, by combining, as has already been done for ordinary baryons, two different approaches: the large- N_c theory and a constituent model.

2 Structure of the thesis

This present work is structured in four chapters. We propose here a brief explanation of each of them. At the end of each chapter, a concise conclusion summarises the key contributions of the research presented.

First, a brief history of the strong interaction and QCD is presented in Chapter 1. This chapter starts from the state of 20th century physics and explores the emergence of particle physics. In particular, the classification of hadrons and the hypothesis of quarks as elementary particles are discussed. The introduction of the concept of colour charges is also explained, along with the evidence supporting it. Following this historical discussion, the main steps in the construction of QCD, the fundamental theory of the strong interaction, are outlined, starting from the colour invariance of the interaction. Finally, some approaches for obtaining information from QCD are proposed, with an emphasis on the constituent approach, which is the primary approach used in this work. In particular, models of the strong interaction potential are explored.

Next, the problem of solving the many-body Schrödinger equation, which is a key component of the constituent approach, is presented in Chapter 2. The chapter begins with an illustration of a particular many-body system, the harmonic oscillator. It is shown that this system can be exactly solved for an arbitrary number of particles and dimensions. Following this, an approximation method called the envelope theory (ET) is introduced. This method proves useful in the context of large- N_c QCD as in this approach baryons are systems of N_c quarks. An improvement procedure for the ET is also subsequently discussed. Finally, some results obtained with the ET and its improvement procedure are presented. This chapter is accompanied by Appendix A, which discusses the wavefunction of the many-body harmonic oscillator and its connection to the ET.

The implications of the masslessness of the gluon are treated in Chapter 3. Indeed, the masslessness of the gluon implies it has only two projections of spin, ± 1 . To correctly couple the spin of the massive quarks with the helicity of the gluon, the helicity formalism of Jacob and Wick is used. The chapter begins with an explanation of this formalism and a derivation of the helicity states for one- and two-body systems. Some properties of the helicity states are also discussed. Subsequently, the helicity states of a hybrid baryon in a quark core model, allowing the hybrid baryon to be reduced to a two-body system, are computed. The chapter is accompanied by Appendix B, which explores the Poincaré and rotation groups, aiding in the understanding of the definitions and derivations presented earlier.

Eventually, results for the spectrum of heavy hybrid baryons are presented in Chapter 4. The interactions between the quarks and the gluon are discussed, and the quark core model is justified. Following this model, the mass and size of

the quark core are computed using a suitable method, the expansion in oscillator bases (EOB). The spectrum of hybrid baryons as quark core-gluon systems is then computed using another method, the Lagrange-mesh (LM) method. The inclusion of the helicity states in the model is also discussed. Appendix C provides additional information about the LM method.

In this first study, only *cccg* and *bbbg* systems are studied, for reasons elaborated upon in the text. Prospects for future research are proposed at the conclusion of this study. Improvements to the model concerning heavy quarks are presented, alongside potential extensions to the light quark sector, which holds greater experimental interest. Additionally, the integration of the large- N_c approach into the constituent model is examined, with an emphasis on the challenges and potential solutions. The justification for employing the ET is also provided.

With the context and plan of this thesis established, it is now time to delve into the vast field of hadronic physics and explore the uncharted territory of hybrid baryons within a constituent model.

Bibliography

- [1] Navas, S. *et al.* Review of particle physics. *Phys. Rev. D* **110**, 030001 (2024).
- [2] Godfrey, S. & Isgur, N. Mesons in a relativized quark model with chromodynamics. *Phys. Rev. D* **32**, 189 (1985).
- [3] Capstick, S. & Isgur, N. Baryons in a relativized quark model with chromodynamics. *Phys. Rev. D* **34**, 2809 (1986).
- [4] 't Hooft, G. A planar diagram theory for strong interactions. *Nucl. Phys. B* **72**, 461 (1974).
- [5] Witten, E. Baryons in the $1/N$ expansion. *Nucl. Phys. B* **160**, 57 (1979).
- [6] Buisseret, F. & Semay, C. Light baryon masses in different large- N_c limits. *Phys. Rev. D* **82**, 056008 (2010).
- [7] Buisseret, F., Matagne, N. & Semay, C. Spin contribution to light baryons in different large- N limits. *Phys. Rev. D* **85**, 036010 (2012).
- [8] Buisseret, F., Willemyns, C. T. & Semay, C. Many-quark interactions: large- N scaling and contribution to baryon masses. *Universe* **8**, 311 (2022).
- [9] Willemyns, C. & Schat, C. Operator analysis of effective spin-flavor interactions for $L = 1$ excited baryons. *Phys. Rev. D* **93**, 034007 (2016).
- [10] Barnes, T. & Close, F. E. Where are hermaphrodite baryons? *Phys. Lett. B* **123**, 89 (1983).
- [11] Page, P. R. Hybrid and conventional baryons in the flux-tube and quark models. *Int. J. Mod. Phys. A* **20**, 1791 (2005).
- [12] Azizi, K., Barsbay, B. & Sundu, H. Mass and residue of $\lambda(1405)$ as hybrid and excited ordinary baryon. *Eur. Phys. J. Plus* **133**, 121 (2018).
- [13] Chow, C.-K., Pirjol, D. & Yan, T.-M. Hybrid baryons in large- N_c QCD. *Phys. Rev. D* **59**, 056002 (1999).
- [14] Dudek, J. J. & Edwards, R. G. Hybrid baryons in QCD. *Phys. Rev. D* **85**, 054016 (2012).
- [15] Burkert, V. *et al.* A search for hybrid baryons in Hall B with CLAS12. https://www.jlab.org/exp_prog/proposals/16/PR12-16-010.pdf (2016). Report of the 44th Program Advisory Committee (PAC44) Meeting.
- [16] Burkert, V. D. Jefferson Lab at 12 GeV: The science program. *Annu. Rev. Nucl. and Part. Sci.* **68**, 405 (2018).
- [17] Lanza, L. Search for hybrid baryons and KY electroproduction at CLAS12. <https://indico.jlab.org/event/729/contributions/14461/> (2024). Oral presentation during the NSTAR 2024 conference at York (UK).

Brief history of the strong interaction

1

Who ordered that ?

Reaction of physicist I.I. Rabi
after the discovery of the muon.

At the beginning of the 20th century, physicists believed the Universe was composed of four elementary particles: the proton p , neutron n , electron e^- and photon γ . In subsequent years, new particles were discovered in cloud chambers through the study of cosmic radiation, such as the positron e^+ (the anti-electron) by Anderson in 1932 [1], and the muon μ^- (the heavy cousin of the electron) by Anderson and Neddermeyer in 1936 [2]. Advancing to the 1950s, newly developed particle accelerators enabled the production of new particles like the pions (π^+ , π^0 , π^-), the deltas (Δ^{++} , Δ^+ , Δ^0 , Δ^-), and many others, leading to what became known as the particle zoo. It soon became clear that all these particles, termed hadrons, could not be elementary particles. The primary objectives for physicists at the time were to (1) classify these particles and (2) determine their elementary constituents. Hadrons can be initially classified according to their spin J and parity P . Integer spin hadrons are called mesons, whereas half-integer spin hadrons are called baryons.

The study of the hadron spectrum reveals the existence of particle families sharing the same J^P quantum numbers and similar masses. Members of the same family, called a multiplet, are distinguished by their electric charges. For instance, the proton and neutron are $J^P = 1/2^+$ particles, each with a mass of around 939 MeV. The pions and deltas are further examples of multiplets, comprising three and four particles, respectively.

These mass degeneracies are significant because they suggest an underlying symmetry of the Hamiltonian describing hadronic states. The symmetry transformations form the symmetry group¹. For example, the eigenfunctions of a Hamiltonian invariant under spatial rotations, such as the Hamiltonian of the

¹Consider a Hamiltonian H with an eigenvector $|\psi_\alpha\rangle$ and eigenvalue E . Now consider a transformation of the eigenstate under a group G , $|\psi_\alpha\rangle \rightarrow g_i |\psi_\alpha\rangle$ with $g_i \in G$, such that the set of functions $\{g_i |\psi_\alpha\rangle\}$ is degenerate. Then

$$H g_i |\psi_\alpha\rangle = E g_i |\psi_\alpha\rangle = g_i E |\psi_\alpha\rangle = g_i H |\psi_\alpha\rangle.$$

hydrogen atom, form a multiplet of $2l + 1$ degenerate eigenfunctions, where l is the orbital angular momentum. In this case, the symmetry group is $SO(3)$. This degeneracy can be lifted by applying a magnetic field, resulting in the Zeeman effect. The magnetic field favours a particular direction, often chosen as the z -axis, thereby breaking the rotational symmetry. The reasoning is similar for hadrons: the underlying Hamiltonian of strong interaction is invariant under a certain group G , which we will identify as the group $SU(N)$, leading to mass degeneracy that is broken by electromagnetic forces.

In this introductory chapter, we propose to review the main concepts surrounding the strong interaction. First, in Sec. 1.1, the notions of isospin, flavour, and colour are introduced. Next, the theory of quantum chromodynamics (QCD) is presented along with some of its properties in Sec. 1.2. Finally, in Sec. 1.3, various approaches to QCD are discussed, with particular emphasis on the constituent quark model. Throughout this chapter, natural units are employed, where $\hbar = c = 1$.

1.1 Isospin, flavour and colour

In the early 20th century, before the discovery of hadrons, Heisenberg introduced a new quantum number for describing the proton p and neutron n , known as isotopic spin or *isospin* I . Due to the mass degeneracy of these two particles, he proposed that they are projections of a single particle, the nucleon, with $I = 1/2$. The two projections along the third axis, $I_3 = 1/2$ and $I_3 = -1/2$, correspond to the proton and neutron, respectively, and are degenerate under the strong interaction. This situation is analogous to the two projections $S_z = 1/2$ and $S_z = -1/2$ of a spin-1/2 particle. This concept can be extended to other multiplets. For example, pions form an isospin triplet with $I = 1$, and deltas form an isospin quadruplet with $I = 3/2$. Isospin singlets with $I = 0$ also exist, such as the lambda Λ .

Mathematically, spin and isospin are described by the group $SU(2)$, the group of complex 2×2 unitary matrices with unit determinant. More generally, the group $SU(N)$ is defined as

$$SU(N) = \{U \in \mathcal{M}_{N \times N}(\mathbb{C}) | U^\dagger U = \mathbf{1} \text{ and } \det U = 1\}. \quad (1.1)$$

The isospin multiplets are associated with the irreducible representations of the group $SU(2)$. Interested readers can refer to [3] for an introduction to the $SU(N)$ group and its representations. We recall that a group representation is a mapping of each element of the group g_i to an operator or matrix $R(g_i)$ acting on a vector space V . The dimension of the representation is the dimension of V . The nucleon doublet (p, n) is associated with the fundamental two-dimensional representation of the group $SU(2)$. This means that if we take a state $|\psi\rangle$ in a

two-dimensional vector space with the basis vectors $|p\rangle = \begin{pmatrix} 1 \\ 0 \end{pmatrix}$ and $|n\rangle = \begin{pmatrix} 0 \\ 1 \end{pmatrix}$,

then a transformation under the group $SU(2)$ on the state is given by

Thus, the degeneracy implies $[H, g_i] = 0$, indicating that H is invariant under the action of the group G .

$$|\psi\rangle \rightarrow \exp\left(\frac{i}{2}\theta^a\sigma_a\right)|\psi\rangle, \quad (1.2)$$

where θ^a are the real parameters of the transformation, and σ_a are the three 2×2 Pauli matrices

$$\sigma_1 = \begin{pmatrix} 0 & 1 \\ 1 & 0 \end{pmatrix}, \quad \sigma_2 = \begin{pmatrix} 0 & -i \\ i & 0 \end{pmatrix}, \quad \sigma_3 = \begin{pmatrix} 1 & 0 \\ 0 & -1 \end{pmatrix}, \quad (1.3)$$

which are the generators of $SU(2)$ and satisfy the commutation relations

$$\left[\frac{\sigma_a}{2}, \frac{\sigma_b}{2}\right] = i\epsilon_{abc}\frac{\sigma_c}{2}, \quad (1.4)$$

with ϵ_{abc} being the completely antisymmetric Levi-Civita tensor. In the above equations and the following ones, repeated indices are summed.

Other multiplets correspond to higher-dimensional representations of $SU(2)$. For example, the triplet of pions (π^+, π^0, π^-) is associated with the three-dimensional representation of $SU(2)$, called the adjoint representation, and the quadruplet of deltas ($\Delta^{++}, \Delta^+, \Delta^0, \Delta^-$) corresponds to the four-dimensional representation of $SU(2)$. In general, states in the n -dimensional representation of $SU(2)$ transform similarly to (1.2), but with the Pauli matrices σ_a replaced by $n \times n$ matrices S_a that respect the $SU(2)$ algebra (1.4). For example, the generators of the adjoint representation are often chosen as [3]

$$S_1 = \frac{1}{\sqrt{2}} \begin{pmatrix} 0 & -1 & 0 \\ -1 & 0 & 1 \\ 0 & 1 & 0 \end{pmatrix}, \quad S_2 = \frac{i}{\sqrt{2}} \begin{pmatrix} 0 & 1 & 0 \\ -1 & 0 & -1 \\ 0 & 1 & 0 \end{pmatrix}, \quad S_3 = \begin{pmatrix} 1 & 0 & 0 \\ 0 & 0 & 0 \\ 0 & 0 & -1 \end{pmatrix}. \quad (1.5)$$

The study of strange hadrons² reveals they can also form isospin multiplets with the same spin, parity, and strangeness quantum number \mathcal{S} , such as the kaons (K^+, K^-) and sigmas ($\Sigma^+, \Sigma^0, \Sigma^-$), characterised by isospin $I = 1/2$ and $I = 1$, respectively. Some of these strange multiplets have similar masses to the non-strange ones, making it tempting to merge them into super-multiplets. The hadrons of a super-multiplet can be arranged in a graph where the x -axis represents the third projection of isospin I_3 , and the y -axis represents the strangeness quantum number \mathcal{S} . Such graphs are shown in Fig. 1.1 for the $1/2^+$ and $3/2^+$ baryons. Particles on the same diagonal have the same electric charge Q , yielding the Gell-Mann–Nishijima formula [5, 6]

$$Q = I_3 + \frac{1}{2}(B + \mathcal{S}) \quad (\text{in units of } e), \quad (1.6)$$

where B is the baryon number (equal to 1 for baryons and 0 for mesons). From these graphs, Gell-Mann [7] and Ne'eman [8] independently discovered in 1961

²Strange hadrons are named this way because of their slower decay rates compared to non-strange hadrons. For instance, the mean lifetime of kaons is about 10^{-10} seconds, whereas deltas have a mean lifetime of around 10^{-24} seconds [4]. To explain this behaviour, the concept of the strangeness quantum number was introduced. Strangeness is conserved in strong interactions but not in weak interactions, which accounts for the slower decay of strange hadrons via weak interactions, during which their strangeness can change.

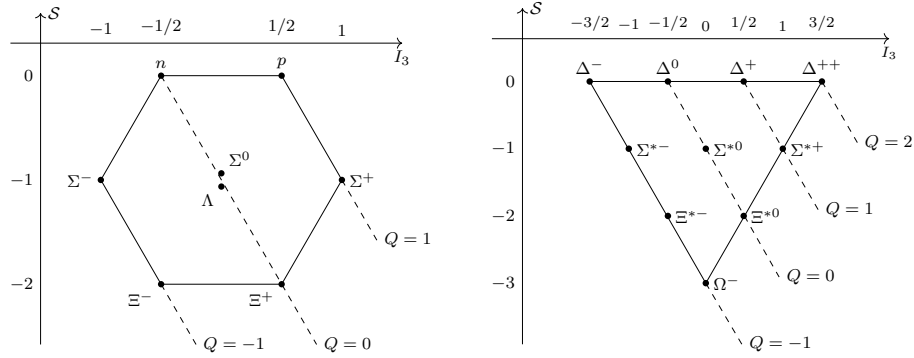


Figure 1.1: Baryon octet (on the left) and baryon decuplet (on the right). Particles are placed horizontally according to their third component of isospin I_3 , and vertically according to their strangeness \mathcal{S} . Particles on the same diagonal have the same electric charge Q .

Flavour	I	I_3	\mathcal{S}	Q
Up u	1/2	1/2	0	2/3
Down d	1/2	-1/2	0	-1/3
Strange s	0	0	-1	-1/3

Table 1.1: Properties of the three quark flavours: isospin I , third component of isospin I_3 , strangeness \mathcal{S} , and electric charge Q in units of e . The charge is determined via (1.6) assuming $B = 1/3$ for quarks (see text).

that they can be put into a one-to-one correspondence with the irreducible representations of the group $SU(3)$. More precisely, the $1/2^+$ states are associated with the octet representation, denoted by its dimension $\mathbf{8}$, and the $3/2^+$ states correspond to the decuplet representation $\mathbf{10}$. A similar reasoning applies to mesons, but for simplicity, we will focus on baryons.

This observation led to a classification scheme for hadrons. However, some questions arise from this conclusion, notably: (1) Why does Nature not use the fundamental representation $\mathbf{3}$? (2) Why do spin-1/2 hadrons only form an octet, and spin-3/2 a decuplet? Gell-Mann [9] and Zweig [10] proposed an answer to the first question in 1964 by suggesting the fundamental representation $\mathbf{3}$ exists and corresponds to a triplet of elementary particles (u, d, s), called quarks. Each quark state is characterised by a flavour. The properties of each flavour can be deduced and are summarised in Table 1.1.

Hadrons can then be understood as composite particles made of quarks. For instance, consider a system composed of three quarks qqq , with $q = \{u, d, s\}$. Mathematically, this system is associated with the tensor products of the fundamental representation $\mathbf{3}$. The decomposition into irreducible representations of $SU(3)$ leads to [3]

$$\mathbf{3} \otimes \mathbf{3} \otimes \mathbf{3} = \mathbf{10}^S \oplus \mathbf{8}^{MS} \oplus \mathbf{8}^{MA} \oplus \mathbf{1}^A, \quad (1.7)$$

where S, MS, MA, A denote symmetric, mixed symmetric³, mixed antisymmetric, and antisymmetric wavefunctions under the exchange of quarks. The baryon octet and decuplet are then recovered. Thus, baryonic states can be visualised as systems of three quarks, implying quarks are spin-1/2 particles with a baryon number $B = 1/3$. The flavour wavefunctions of hadrons can be computed following the irreducible representations of $SU(3)$. For example, the proton is in the $\mathbf{8}$, mixed symmetric, representation. Since the proton has no strangeness and a positive charge, we conclude its quark content is uud . The complete expression of the wavefunction is given by [3]

$$|p\rangle^{MS} = \frac{1}{\sqrt{6}}[(ud + du)u - 2uud], \quad (1.8a)$$

$$|p\rangle^{MA} = \frac{1}{\sqrt{2}}(ud - du)u. \quad (1.8b)$$

These two wavefunctions can be combined to form a completely symmetric or antisymmetric wavefunction [3]. The Δ^+ baryon has the same quark content as the proton but is in the $\mathbf{10}$, symmetric, representation. Thus, its flavour wavefunction is given by

$$|\Delta^+\rangle = \frac{1}{\sqrt{3}}[uud + udu + duu]. \quad (1.9)$$

Thanks to Gell-Mann's quark model, the internal structure of hadrons has been discovered. Notably, the omega baryon Ω^- , which has a quark content sss , was predicted by Gell-Mann in 1961 and discovered in 1964 [11], confirming the quark model. However, questions remain, such as why spin-1/2 particles form only an octet and why quarks are not observed directly.

Before addressing these questions, note that if the flavour symmetry $SU(3)_F$ was exact, meaning the strong interaction treats the three flavours (u, d, s) the same way, the hadrons in a super-multiplet would be degenerate. This is not the case, as the inclusion of a strange quark adds around 150 MeV of mass. Thus, the flavour symmetry is only approximate but remains a powerful tool for classifying hadronic states. On the other hand, the isospin $SU(2)$ symmetry is better reproduced but still not exact.

1.1.1 Heavy quarks

Following the hypothesis of the quarks u, d and s by Gell-Mann and Zweig in 1964, which revealed the internal structure of light hadrons, new quark flavours were predicted and subsequently discovered through advancements in particle accelerators. These accelerators enabled the production of heavier hadrons. Currently, six quark flavours are known [4], grouped into three families: (u, d) , (c, s) and (t, b) , where c represents the charm quark, b the bottom (or beauty) quark, and t the top (or truth) quark. Since these quarks are more massive than the light quarks (u, d, s), the (c, b, t) quarks are referred to as heavy quarks.

Experimentally, the charm quark was discovered in 1974 at Brookhaven National Laboratory [12] and at SLAC (Stanford Linear Accelerator Center) [13]

³A mixed symmetric function is one that is symmetric only under the exchange of the first two particles, and similarly for a mixed antisymmetric wavefunction.

independently, through the detection of a new particle, the J/ψ meson, which is interpreted as a $c\bar{c}$ state. In a manner analogous to the strange quark, a charm quantum number \mathcal{C} is introduced, with $\mathcal{C} = 1$ for charm quarks. This quantum number is conserved in both electromagnetic and strong interactions, though it is violated by weak interactions.

The bottom quark was discovered in 1977 at Fermilab [14] through the detection of a new resonance, the Υ meson, which is interpreted as a $b\bar{b}$ state. A corresponding bottom quantum number \mathcal{B} is assigned, where $\mathcal{B} = -1$ for bottom quarks.

Finally, the top quark was discovered at Fermilab in 1995 [15, 16]. Due to its high mass, the top quark decays more rapidly than the other flavours, with a lifetime on the order of 10^{-25} s. This is shorter than the timescale for strong interactions, meaning that the top quark does not form hadrons. For this reason, the top quark is frequently excluded from studies of hadronic matter.

To incorporate the charm and bottom quarks, the flavour symmetry group must be extended to $SU(4)$ and $SU(5)$, respectively. However, since the charm and bottom quarks are significantly heavier than the light quarks (u, d, s), the flavour symmetry is even more violated than $SU(3)$. Additionally, with the introduction of the charm and bottom quantum numbers, the Gell-Mann–Nishijima formula (1.6) is extended to

$$Q = I_3 + \frac{Y}{2} \quad (\text{in units of } e), \quad (1.10)$$

where $Y = B + S + \mathcal{C} + \mathcal{B}$ is the hypercharge.

1.1.2 Hypothesis of the colour

The hypothesis of quarks allows the classification of hadronic states in terms of the irreducible representations of the flavour group $SU(3)_F$. It is interesting to consider the other degrees of freedom of hadrons, such as space and spin. Since we are focusing on the lowest energy states, we assume there is no excitation between the quarks, implying a symmetric spatial wavefunction.

For a system of three spin-1/2 particles, the total spin and symmetry are given by decomposition into the irreducible representation of $SU(2)$ [3]

$$\mathbf{1/2} \otimes \mathbf{1/2} \otimes \mathbf{1/2} = \mathbf{3/2}^S \oplus \mathbf{1/2}^{MS} \oplus \mathbf{1/2}^{MA}, \quad (1.11)$$

where the representations are denoted by the corresponding spin. Thus, spin-3/2 states have a symmetric spin wavefunction, and since their flavour wavefunction is also symmetric, their spatial-spin-flavour wavefunction is totally symmetric. A similar reasoning applies to the spin-1/2 octet [3].

The problem arises from the fact that quarks are fermions, meaning the total wavefunction should be antisymmetric under the exchange of quarks. To resolve this issue, Greenberg [17] introduced a new degree of freedom for the quarks, known as colour. Assuming quarks can choose from three colours, typically denoted as (R, B, G) , an antisymmetric colour wavefunction can be constructed using a Slater determinant (up to a normalisation factor)

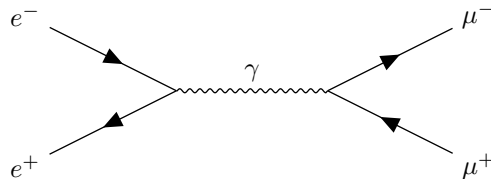


Figure 1.2: Feynman diagram, at the lowest order, for the $e^-e^+ \rightarrow \mu^-\mu^+$ scattering.

$$\begin{vmatrix} R(1) & R(2) & R(3) \\ B(1) & B(2) & B(3) \\ G(1) & G(2) & G(3) \end{vmatrix} = R(BG - GB) - B(RG - GR) + G(RB - BR). \quad (1.12)$$

This makes the total wavefunction of the baryons antisymmetric, as required for fermions.

By associating the colour degree of freedom with the colour group $SU(3)_C$, similar to how we treated flavour, it can be shown that the antisymmetric wavefunction corresponds to a singlet state, which is invariant under the action of the $SU(3)$ group [3]. Since the colour degree of freedom has never been observed directly, as evidenced by the absence of isolated quarks, we assume that all observable hadronic states must be colour singlets. This hypothesis is known as *confinement*. Hence, spin-1/2 hadrons can only form a flavour octet, and spin-3/2 hadrons can only form a flavour decuplet to respect colour confinement.

Proof of the colour

Even though there is no direct proof of colour, its inclusion in the models leads to good agreement with experiments. One such example is the cross-section ratio R . Other examples can be found in [18].

Consider the scattering process $e^-e^+ \rightarrow \mu^-\mu^+$. At the lowest order in energy, this process occurs via the annihilation of the initial electron-positron pair into a virtual photon, which then transforms into a $\mu^-\mu^+$ pair, as shown in Fig. 1.2. On the other hand, the scattering process $e^-e^+ \rightarrow$ hadrons involves an additional step, where a quark-antiquark pair $q\bar{q}$ is produced and subsequently hadronises into hadrons. This hadronisation process is highly complex, but if we measure the total cross-section for all possible final hadronic states, we can assume that the probability for a $q\bar{q}$ pair to transform into hadrons is unity. Thus, we can write

$$\sigma(e^-e^+ \rightarrow \text{hadrons}) = \sum_q \sigma(e^-e^+ \rightarrow q\bar{q}), \quad (1.13)$$

where the sum runs over all quark pairs $q\bar{q}$ whose threshold energy $2m_q$ is lower than the centre of mass energy \sqrt{s} of the reaction. At the lowest order, the cross-section for the production of a fermion-antifermion pair is given by

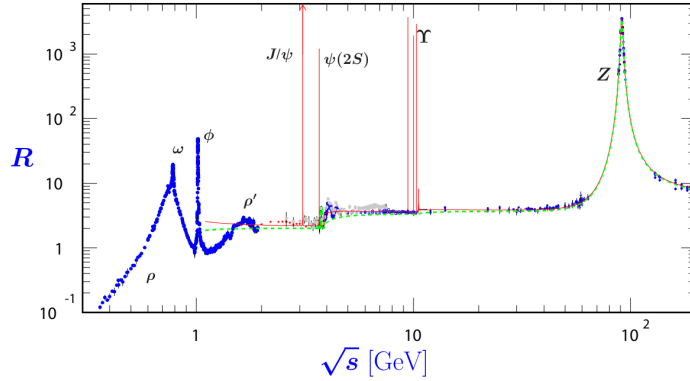


Figure 1.3: Cross-section ratio R defined by (1.15) as a function of the centre of mass energy \sqrt{s} [4]. The green dashed lines correspond to the predictions of the quark model.

$$\sigma(e^-e^+ \rightarrow f\bar{f}) = \frac{4\pi\alpha^2}{3s} Q_f^2, \quad (1.14)$$

where $\alpha = e^2/(4\pi)$ is the fine-structure constant, and Q_f is the electric charge of the fermion f in units of e . Hence,

$$R \equiv \frac{\sigma(e^-e^+ \rightarrow \text{hadrons})}{\sigma(e^-e^+ \rightarrow \mu^-\mu^+)} = \sum_q Q_q^2, \quad (1.15)$$

where Q_q is the electric charge of the quark q in units of e .

At the energies where only the u, d and s quarks can be produced, R becomes

$$R = \left(\frac{4}{9} + \frac{1}{9} + \frac{1}{9} \right) N_c = \frac{2N_c}{3}, \quad (1.16)$$

where N_c is the number of colours. If the colour assumption is correct, $R = 2$ instead of $R = 2/3$. Experimental data [4], shown in Fig. 1.3, are in better agreement with the value for coloured quarks. For energies above the charm quark threshold, corresponding to the production of the J/ψ meson, the ratio R takes the value $R = 10/3$. Considering the bottom quark, the ratio R becomes $R = 11/3$, which is observed for energies above the Υ meson production.

1.2 Quantum chromodynamics

The quark hypothesis and the classification of hadrons according to the (approximate) flavour symmetry are only the first steps in the study of hadrons. A complete theoretical study of their spectroscopy should allow computing their masses starting from the quark interactions. By analogy with electric charge, a theory of strong interaction is constructed as a theory of colour charges, known as Quantum Chromodynamics (QCD). This theory is built similarly to Quantum Electrodynamics (QED), that is, as a gauge theory based on the local

invariance of the colour group $SU(3)_C$, which is supposed to be an exact symmetry unlike the flavour group $SU(3)_F$. Before introducing QCD, let us recall the main ingredients of a gauge theory by reviewing QED.

1.2.1 Quantum electrodynamics

The Lagrangian density of a free spin-1/2 particle of mass m is given by the Dirac Lagrangian

$$\mathcal{L}_D = \bar{\psi}(i\gamma^\mu \partial_\mu - m)\psi, \quad (1.17)$$

where $\psi = \psi(x)$ is a four-component Dirac spinor, which is a function of space-time coordinates x , γ^μ are the four Dirac matrices

$$\gamma^0 = \begin{pmatrix} \mathbf{1} & 0 \\ 0 & -\mathbf{1} \end{pmatrix}, \quad \gamma^i = \begin{pmatrix} 0 & \sigma^i \\ -\sigma^i & 0 \end{pmatrix}, \quad (1.18)$$

and $\bar{\psi} = \psi^\dagger \gamma^0$ is the Dirac adjoint. Applying the Euler-Lagrange equation to \mathcal{L}_D yields the Dirac equation

$$(i\gamma^\mu \partial_\mu - m)\psi = 0. \quad (1.19)$$

Consider now the transformation $\psi \rightarrow e^{i\theta}\psi$, where θ is a real constant. Since the transformation is the same for every spacetime point, it is referred to as a global transformation. The set of these transformations for all values of θ forms the unitary group $U(1)$. It is easy to see that the action of $U(1)$ leaves the Dirac Lagrangian invariant. According to Noether's theorem, this invariance leads to a conserved current $\partial_\mu j^\mu = 0$, namely the electromagnetic current

$$j^\mu = \bar{\psi}\gamma^\mu\psi. \quad (1.20)$$

From Gauss's theorem, the current conservation law $\partial_\mu j^\mu = 0$ leads to a conserved charge

$$Q = \int d^3x j^0(x), \quad (1.21)$$

which is the electric charge. Consider now the local transformation

$$\psi \rightarrow e^{ie\theta(x)}\psi, \quad (1.22)$$

with e being the electric charge of the particle described by the spinor ψ , and where θ is now a real function of x . The Dirac Lagrangian is no longer invariant under these local transformations since

$$\partial_\mu \psi \rightarrow \partial_\mu (e^{ie\theta(x)}\psi) = e^{ie\theta(x)}[ie\partial_\mu\theta(x) + \partial_\mu]\psi \neq e^{ie\theta(x)}\partial_\mu\psi. \quad (1.23)$$

To restore the invariance, a vector field A_μ , called the *gauge field*, is introduced such that its transformation law cancels the $\partial_\mu\theta(x)$ term. To this end, the usual derivative is replaced by the covariant derivative

$$D_\mu \equiv \partial_\mu - ieA_\mu, \quad (1.24)$$

such that it transforms under the local $U(1)$ transformation as

$$D_\mu \psi \rightarrow e^{ie\theta(x)} D_\mu \psi. \quad (1.25)$$

Following this constraint, the transformation law of A_μ is deduced

$$A_\mu \rightarrow A_\mu + \partial_\mu \theta(x), \quad (1.26)$$

which is recognised as the gauge transformation of the four-vector potential in electromagnetism. Thus, the Dirac Lagrangian is invariant under the simultaneous local transformations $\psi \rightarrow e^{ie\theta(x)}\psi$ and $A_\mu \rightarrow A_\mu + \partial_\mu \theta(x)$.

The substitution of the usual derivative by the covariant derivative D_μ is equivalent to adding the coupling term $e A_\mu \psi$ in the Dirac Lagrangian, which represents the minimal coupling between a spin-1/2 particle of charge e and the electromagnetic field. Thus, an interaction term is obtained from the local gauge invariance principle.

Finally, a term describing the dynamics of the free gauge field must be added. This term must be Lorentz and gauge invariant, and quadratic in its derivative. From electromagnetism, the term

$$\mathcal{L}_g = -\frac{1}{4} F^{\mu\nu} F_{\mu\nu}, \quad (1.27)$$

with $F_{\mu\nu} = \partial_\mu A_\nu - \partial_\nu A_\mu$ being the Faraday tensor, respects these conditions. The factor $-1/4$ is added to recover Maxwell's equations. Hence, we obtain the Lagrangian of QED

$$\mathcal{L}_{\text{QED}} = -\frac{1}{4} F^{\mu\nu} F_{\mu\nu} + \bar{\psi}(i\gamma^\mu \partial_\mu - m)\psi + e \bar{\psi}\gamma^\mu \psi A_\mu. \quad (1.28)$$

Note the Lagrangian contains no term quadratic in A_μ because such terms are not gauge invariant. Thus, gauge fields are massless.

1.2.2 Non-abelian gauge symmetry

The QED case is particularly simple since the gauge group $U(1)$ is abelian, meaning its elements commute among themselves. Consider now a transformation under the colour group $SU(3)_C$

$$\psi \rightarrow \exp\left(\frac{i}{2}\theta^a \lambda_a\right) \psi, \quad (1.29)$$

where $\psi = \begin{pmatrix} \psi^R \\ \psi^B \\ \psi^G \end{pmatrix}$ is a vector in the three-dimensional colour space (R, B, G) , and λ_a , with $a = \{1, \dots, 8\}$, are the eight Gell-Mann matrices

$$\lambda_1 = \begin{pmatrix} 0 & 1 & 0 \\ 1 & 0 & 0 \\ 0 & 0 & 0 \end{pmatrix}, \quad \lambda_2 = \begin{pmatrix} 0 & -i & 0 \\ i & 0 & 0 \\ 0 & 0 & 0 \end{pmatrix}, \quad \lambda_3 = \begin{pmatrix} 1 & 0 & 0 \\ 0 & -1 & 0 \\ 0 & 0 & 0 \end{pmatrix},$$

$$\lambda_4 = \begin{pmatrix} 0 & 0 & 1 \\ 0 & 0 & 0 \\ 1 & 0 & 0 \end{pmatrix}, \quad \lambda_5 = \begin{pmatrix} 0 & 0 & -i \\ 0 & 0 & 0 \\ i & 0 & 0 \end{pmatrix}, \quad \lambda_6 = \begin{pmatrix} 0 & 0 & 0 \\ 0 & 0 & 1 \\ 0 & 1 & 0 \end{pmatrix}, \quad (1.30)$$

$$\lambda_7 = \begin{pmatrix} 0 & 0 & 0 \\ 0 & 0 & -i \\ 0 & i & 0 \end{pmatrix}, \quad \lambda_8 = \frac{1}{\sqrt{3}} \begin{pmatrix} 1 & 0 & 0 \\ 0 & 1 & 0 \\ 0 & 0 & -2 \end{pmatrix},$$

corresponding to the generators of $SU(3)$ and respecting the commutation relations

$$\left[\frac{\lambda_a}{2}, \frac{\lambda_b}{2} \right] = i f_{abc} \frac{\lambda_c}{2}, \quad (1.31)$$

where f_{abc} are the structure constants of the group [3]. Since the Gell-Mann matrices do not commute with each other, it is clear that $SU(3)$ is a non-abelian group. Suppose now the parameters θ^a are real constants. Then, the Lagrangian

$$\mathcal{L}_D = \sum_j \bar{\psi}_j (i\gamma^\mu \partial_\mu - m_j) \psi_j, \quad (1.32)$$

where the sum runs over the flavours j , is invariant under these global $SU(3)$ transformations. From Noether's theorem, there are eight conserved currents for each flavour j

$$j_{ji}^\mu = \bar{\psi}_j^a \gamma^\mu (\lambda_i)_{ab} \psi_j^b. \quad (1.33)$$

We move on now to local transformations by promoting the parameters to real functions of spacetime coordinates $\theta^a(x)$. The above Lagrangian is no longer invariant under the local transformations. To overcome this problem, and following the steps of QED, the usual derivative is replaced by the covariant one, which is now a 3×3 matrix in the colour space

$$(D_\mu)_{kl} \equiv \delta_{kl} \partial_\mu - \frac{i}{2} g (\lambda_a)_{kl} A_\mu^a, \quad (1.34)$$

where we introduced eight gauge vector fields A_μ^a , called the gluon field. By imposing that the gauge fields transform under $SU(3)$ as

$$A_\mu^a \rightarrow A_\mu^a - \partial_\mu \theta^a + g f_{cba} \theta^c A_\mu^b, \quad (1.35)$$

where f_{abc} are the structure constants of $SU(3)$, it is possible to show that the Lagrangian density

$$\mathcal{L} = \sum_j \bar{\psi}_j (i\gamma^\mu D_\mu - m_j) \psi_j, \quad (1.36)$$

becomes invariant under the local $SU(3)$ transformation (1.29) and (1.35). If the quarks transform under the fundamental representation of $SU(3)$, then it can be shown that the gluons transform under the adjoint, eight-dimensional, representation of the colour group [19].

As for QED, the substitution with the covariant derivative corresponds to the inclusion of an interaction term between the quarks and gluons, which is responsible for the strong interaction. We still need to add a term describing the free gluon fields. The situation is more complicated than for QED because the Faraday tensor $F_{\mu\nu}^a = \partial_\mu A_\nu^a - \partial_\nu A_\mu^a$ is not invariant under the local gauge transformations. We then need to generalise it to

$$F_{\mu\nu}^a = \partial_\mu A_\nu^a - \partial_\nu A_\mu^a + g f_{abc} A_\mu^b A_\nu^c, \quad (1.37)$$

such that

$$\mathcal{L}_g = \sum_{a=1}^8 F_{\mu\nu}^a F^{a\mu\nu}, \quad (1.38)$$

is indeed gauge invariant [19]. The complete expression of the QCD Lagrangian is then

$$\mathcal{L}_{\text{QCD}} = -\frac{1}{4} \sum_{a=1}^8 F_{\mu\nu}^a F^{a\mu\nu} + \sum_j \bar{\psi}_j^a (i\delta_{ab} \gamma^\mu \partial_\mu + \frac{g}{2} \gamma^\mu (\lambda_i)_{ab} A_\mu^i - m_j \delta_{ab}) \psi_j^b. \quad (1.39)$$

As for the photon, the gluons are also massless particles since a mass term would not be gauge invariant.

Even though the construction of QCD is analogous to that of QED, a major difference appears: gluons carry colour charge. Since colour plays the same role in QCD as electric charge does in QED, this implies that gluons can interact with each other, contrary to photons, which have no electric charge. In addition to the quark-gluon interaction term, the QCD Lagrangian contains three- and four-gluon interaction terms corresponding to third- and fourth-order terms in A_μ^a in $\sum_a F_{\mu\nu}^a F^{a\mu\nu}$.

1.2.3 Hadronic states

Having now a theory of strong interactions, we can deduce the allowed hadronic states following the confinement hypothesis. Quarks transform under the fundamental representation $\mathbf{3}$ of the colour group $SU(3)_C$, antiquarks transform under the conjugate representation $\bar{\mathbf{3}}$, and gluons transform under the adjoint representation $\mathbf{8}$, as discussed above. Since gluons are coloured particles, they can interact with quarks or with themselves. Let us look first at the (anti)quarks only.

We already know that three quarks can form a hadron, the baryon, since it is possible to form a colour singlet $\mathbf{1}$ from three quarks (see (1.7) for instance). Can two quarks form a hadron? The decomposition into irreducible representations yields

$$\mathbf{3} \otimes \mathbf{3} = \mathbf{6} \oplus \bar{\mathbf{3}}, \quad (1.40)$$

where there is no colour singlet. Thus, a diquark alone cannot form a hadron. However, a diquark in the $\bar{\mathbf{3}}$ representation coupled with a quark can form a baryon since

$$\bar{\mathbf{3}} \otimes \mathbf{3} = \mathbf{1} \oplus \mathbf{8}. \quad (1.41)$$

The $\bar{\mathbf{3}}$ representation corresponds also to the antiquark representation, so a quark-antiquark pair $q\bar{q}$ can also form a hadron, called a meson.

Following these principles, we can construct various hadrons. In general, a system with a quark content

$$(q\bar{q})^m (qqq)^n (\bar{q}\bar{q}\bar{q})^p, \quad (1.42)$$

with m, n and p integers, can form a colour singlet. In particular, we can find tetraquarks ($m = 2, n = 0$) or pentaquarks ($m = 1, n = 1$).

Consider now systems with a constituent gluon. An important relation, which can be generalised to $SU(N)$, is

$$\mathbf{8} \otimes \mathbf{8} = \mathbf{1} \oplus \dots \quad (1.43)$$

The $\mathbf{8}$ representation can correspond to a gluon and in this case, the hadron associated with this decomposition is a pure gluonic state, known as a glueball. However, the adjoint representation can also be reached from a $q\bar{q}$ pair (1.41) or a baryon (1.7). The corresponding state in this case is a *hybrid* state.

In the following discussion, baryons and mesons are referred to as ordinary hadrons, whereas the other hadrons are referred to as exotic hadrons.

1.3 QCD approaches

If QCD is indeed the theory describing strong interactions, it should be possible to derive all pertinent information about hadrons, such as their spectrum, widths, and decay channels, starting from the QCD Lagrangian. However, this task is complex because QCD fundamentally describes quarks and gluons rather than hadrons, although hadrons are implicitly embedded in the theory.

In quantum field theories, a common approach to studying scattering processes is the *perturbative* method. This involves expanding the scattering amplitude in powers of the coupling constant g and considering only the lowest order terms, with higher-order terms providing corrections. This method is often illustrated using Feynman diagrams. It works well for QED because the coupling constant $\alpha = e^2/(4\pi) \approx 1/127 \ll 1$. However, this is not the case for QCD, particularly in the context of hadrons.

The evolution of the strong coupling constant $\alpha_s = g^2/(4\pi)$ with the energy scale Q , represented by the β function

$$\beta(\alpha_s) \equiv \frac{\partial \alpha_s}{\partial \ln Q} = - \left(11 - \frac{2n_f}{3} \right) \frac{\alpha_s^2}{2\pi}, \quad (1.44)$$

with n_f denoting the number of flavours, shows that the strong coupling constant decreases with increasing energy scale for $n_f \leq 16$. This property is known as *asymptotic freedom*. Experimental data [4] confirms this behaviour, as illustrated in Fig. 1.4. Thus, the perturbative approach is valid for high-energy experiments. However, at the hadronic energy scale (approximately 1 GeV), the strong coupling constant is around unity, making a perturbative approach unfeasible for studying hadrons.

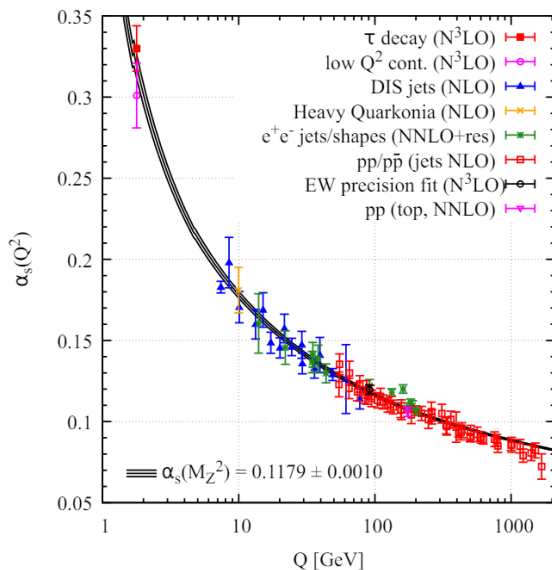


Figure 1.4: Evolution of the QCD running coupling constant α_s as a function of the energy scale Q [4].

To address this challenge, several alternative approaches have been developed to understand hadron phenomenology. Some notable methods include

- Large- N_c QCD [20, 21, 22], which involves considering a large number of colours ($N_c \rightarrow \infty$) and expanding observables in powers of $1/N_c$.
- Lattice QCD [23, 24, 25], which entails discretising spacetime and writing the QCD Lagrangian on this lattice.
- Effective field theories [26, 27, 28], which derive new Lagrangians from the QCD Lagrangian, with hadrons as the degrees of freedom.
- Functional methods [29, 30, 31], which start from the Dyson-Schwinger and Bethe-Salpeter equations, representing the equations of motion in a quantum field theory.

All these approaches have a common point, they start from the QCD Lagrangian. Another popular approach is the constituent one. The idea is to consider a hadron as only consisting of valence particles interacting by QCD-inspired potentials. Then, the hadron is represented as the bound state of a many-body Schrödinger-like equation. Even though this approach does not start from the QCD Lagrangian, it allows to obtain results in a simple way and is a good starting point for the study of ordinary and exotic hadrons. This approach presents two main problems (1) there is not a unique potential for describing the strong interaction [32], (2) the resolution of a many-body Schrödinger equation is not the simplest task.

The solution to the second problem is discussed in more detail in Chapter 2. For the potential, the Cornell (or funnel) potential is frequently employed. It has the form

$$V(r) = Ar - \frac{B}{r}, \quad (1.45)$$

in a meson, where A and B are constants determined from experimental or lattice QCD results. The derivation of this potential will be outlined briefly, and its extension to other hadrons.

1.3.1 One-gluon exchange

In a quantum field theory such as QCD, the scattering amplitude $\mathcal{A} = \langle f|i\rangle$ between an initial $|i\rangle$ and final $|f\rangle$ state can be computed. Consider, for example, the evolution operator

$$\hat{S} = \mathcal{T} \exp \left(i g \int dx \mathcal{L}_I \right), \quad (1.46)$$

where \mathcal{T} is the time-ordering operator⁴ and \mathcal{L}_I is the interaction Lagrangian in the interaction picture [19]. The evolution operator describes all possible outcomes from an initial state. The scattering amplitude is then given by the S -matrix elements

$$S_{fi} = \langle f|\hat{S}|i\rangle. \quad (1.47)$$

The cross-section, which can be measured experimentally, is proportional to the square of the scattering amplitude. Since the S -matrix elements contain all the information about the interaction, it should be possible to deduce an effective potential from them.

Consider, for example, the scattering of two electrons, $e^-e^- \rightarrow e^-e^-$. Since in QED the coupling constant is less than one, it is possible to expand the exponential in (1.46) in powers of g , which is the fundamental electric charge e . This is the perturbative approach explained above. The lowest non-vanishing term in the expansion is given by the Feynman diagram in Fig. 1.5, which corresponds to the exchange of one photon between the pair, known as the One-Photon Exchange (OPE) phenomenon. Following the Feynman rules for QED, the scattering amplitude associated with this diagram can be computed. Since the sought potential will appear in a Schrödinger equation, which is a non-relativistic equation, we take the non-relativistic (NR) limit of the scattering amplitude by expanding it in powers of v^2/c^2 . Finally, since the scattering amplitude is often written in momentum space and the potential in position space, a Fourier transform (FT) is applied to the result. This approach for finding a potential is summarised by the equation

$$V_{\text{OPE}}(r) = \text{FT} \left\{ \lim_{\text{NR}} S_{fi} \right\}. \quad (1.48)$$

For instance, at the lowest order in v^2/c^2 , the associated potential for the e^-e^- interaction is given by [33]

⁴The time-ordering operator is defined as

$$\mathcal{T}(\hat{A}(t_1)\hat{B}(t_2)) = \begin{cases} \hat{A}(t_1)\hat{B}(t_2) & \text{if } t_1 > t_2 \\ \hat{B}(t_2)\hat{A}(t_1) & \text{if } t_2 > t_1 \end{cases}.$$

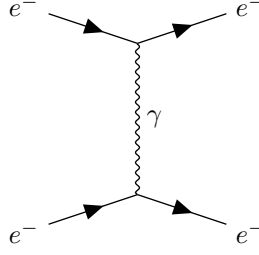


Figure 1.5: Feynman diagram, at the lowest order, for the $e^-e^- \rightarrow e^-e^-$ scattering.

$$V_{\text{OPE}}(r) = -\frac{\alpha}{r}, \quad (1.49)$$

which is the Coulomb potential, as expected. Relativistic corrections can be obtained by considering higher-order terms in v^2/c^2 during the non-relativistic limit. These terms give rise, for instance, to the Darwin, hyperfine, spin-orbit, and tensor interactions. The complete expression of the potential, sometimes called the Fermi-Breit potential, can be found in [3, 33].

Returning to the strong interaction, the quark-quark potential is determined in a similar fashion. The first Feynman diagram of the $qq \rightarrow qq$ scattering involves the exchange of one gluon, known as the One-Gluon Exchange (OGE) phenomenon. The scattering amplitude of QCD is similar to that of QED (as QCD was modelled after QED), except for the inclusion of a colour factor $F(1) \cdot F(2)$, defined by

$$F(i) \cdot F(j) \equiv \frac{1}{4} \sum_{a=1}^8 \lambda^a(i) \lambda^a(j), \quad (1.50)$$

where $\lambda^a(i)$ is the Gell-Mann matrix associated to the i th quark. Hence, the quark-quark potential is given, at the lowest order in v^2/c^2 , by

$$V_{\text{OGE}}(r) = F(1) \cdot F(2) \frac{\alpha_s}{r}. \quad (1.51)$$

We now compute the colour factor as given by (1.50), which can be re-expressed as

$$F(i) \cdot F(j) = \frac{1}{2} [(F(i) + F(j))^2 - F(i)^2 - F(j)^2], \quad (1.52)$$

with

$$F(i)^2 = \frac{1}{4} \sum_{a=1}^8 \lambda^a(i) \lambda^a(i). \quad (1.53)$$

From a group theory perspective, F^2 is the quadratic Casimir operator of $SU(3)$. A Casimir operator is a combination of the generators that commutes with all the other generators. The value of the Casimir operator F^2 is given in Tab. 1.2 for different irreducible representations of $SU(3)$. Since we are dealing with quarks, we obtain $F(i)^2 = 4/3$. The value of $(F(i) + F(j))^2$ is more subtle since

	3	$\bar{\mathbf{3}}$	6	8
F^2	4/3	4/3	10/3	3

Table 1.2: Values of the quadratic Casimir operator of $SU(3)$, F^2 , defined by (1.53), for some of the irreducible representations of $SU(3)$ denoted by their dimension [3].

it corresponds to the Casimir of the quark pair $q_i q_j$. For quarks inside a baryon, each pair must form a $\bar{\mathbf{3}}$ state so that the baryon can be in a singlet state. Thus, $(F(i) + F(j))^2 = 4/3$. Consequently, the colour factor for a quark pair (inside a baryon) is given by $F(1) \cdot F(2) = -2/3$. Thus, the quark-quark interaction is attractive.

A similar reasoning can be applied to find the quark-antiquark potential, which is the potential of a meson, for which the colour factor is given by $-4/3$. Therefore, the quark-antiquark interaction is twice as strong as the quark-quark interaction

$$V_{q\bar{q}} = 2V_{qq}. \quad (1.54)$$

1.3.2 Confinement

Following the above discussion, the strong interaction would behave identically to the electromagnetic one, that is with a Coulomb potential, except for the inclusion of some colour factors. Of course, this is not the case because quarks must be confined into hadrons. The fault in the previous discussion originates from the fact we considered only OGE processes, that is the first possible Feynman diagram. However, as explained in the beginning of this section, a perturbative approach cannot be used for hadronic states because the strong coupling constant is around one. In order to correct this fault, a potential reproducing confinement is added.

From lattice QCD, it is possible to prove that QCD is indeed a confining theory thanks to the so-called area law [19], and to show from this result that the associated potential is linear in the distance between the quarks.

$$V_c(r) = \sigma r, \quad (1.55)$$

where σ is some constant that will be explained later. Thus, the combination of a Coulomb and linear term can reproduce the effect of strong interaction inside a meson. This form is also compatible with the existence of Regge trajectories for mesons [34, 35, 36].

Another way to understand the linear confining potential is from the string model. Consider a system of two point-like particles connected by a relativistic string. Constructing the Lagrangian of the system and then its Hamiltonian, it is possible to show [34] that the associated potential is linear in the distance between the two particles, which is in agreement with the previous paragraph. The constant σ in the potential is then interpreted as the string tension. More realistically, we can see the system as two particles generating a colour flux tube and neutralising to form a colour singlet.

This picture can be extended to baryons: each quarks produce a flux tube that neutralise in a single point, forming a Y -junction as represented in Fig. 1.6. The position of the junction is determined by minimising the strings length, leading to the corresponding potential

$$V_Y = \sigma \min_{\mathbf{Y}} (|\mathbf{r}_1 - \mathbf{Y}| + |\mathbf{r}_2 - \mathbf{Y}| + |\mathbf{r}_3 - \mathbf{Y}|), \quad (1.56)$$

with \mathbf{r}_i the position of the i th quark. As for the mesons, the spectrum of baryons can be reproduced with this potential [37]. However, the complexity of the potential (1.56) can be difficult to handle in some models. One way to simplify the potential would be to replace the linear confinement by a quadratic one [38, 39, 40, 41]. The minimisation on \mathbf{Y} then implies that the connection occurs at the geometrical centre of the triangle formed by the quarks. The confinement potential then becomes

$$V_{\text{quad}} = \frac{\sigma}{3} [(\mathbf{r}_1 - \mathbf{r}_2)^2 + (\mathbf{r}_1 - \mathbf{r}_3)^2 + (\mathbf{r}_2 - \mathbf{r}_3)^2], \quad (1.57)$$

which is a sum of two-body potential. If one still wants a linear confining potential, one can tries

$$V \propto \sqrt{(\mathbf{r}_1 - \mathbf{r}_2)^2 + (\mathbf{r}_1 - \mathbf{r}_3)^2 + (\mathbf{r}_2 - \mathbf{r}_3)^2}, \quad (1.58)$$

which is a three-body potential [42]. Another possibility to replace the Y -junction potential (1.56) is to approximate the position of the Y -junction by the centre of mass of the system. It can be shown that this replacement leads to a small error when quarks have similar masses [43]. Finally, the potential (1.56) can also be replaced by half the perimeter of the triangle formed by the quarks [37]

$$V_{\Delta} = \frac{\sigma}{2} (|\mathbf{r}_1 - \mathbf{r}_2| + |\mathbf{r}_1 - \mathbf{r}_3| + |\mathbf{r}_2 - \mathbf{r}_3|), \quad (1.59)$$

which is a linear two-body confining potential. It is shown in [37, 43] that multiplying this potential by a geometrical factor $f \approx 1.086$ allows to improve the agreement between V_Y and V_{Δ} .

In conclusion, this chapter has presented the fundamental concepts related to the strong interaction, including quark flavours, colours, and the theory of quantum chromodynamics (QCD), as described by the QCD Lagrangian (1.39), within a historical context. It was emphasised that observable hadronic states must form colour singlets to satisfy the principle of confinement. In this framework, QCD permits the existence of hybrid baryons with a colour octet quark core, as allowed by relation (1.43). Lastly, the constituent approach to QCD was introduced, featuring the Cornell potential (1.45) and its extension to systems involving three quarks.

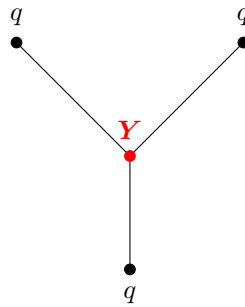


Figure 1.6: Flux-tube model of a baryon. Black dots represent quarks and the red dot marks the connection of flux tubes.

Bibliography

- [1] Anderson, C. D. The positive electron. *Phys. Rev.* **43**, 491 (1933).
- [2] Street, J. C. & Stevenson, E. C. New evidence for the existence of a particle of mass intermediate between the proton and electron. *Phys. Rev.* **52**, 1003 (1937).
- [3] Close, F. E. *An Introduction to Quarks and Partons* (Academic Press, London, 1979).
- [4] Navas, S. *et al.* Review of particle physics. *Phys. Rev. D* **110**, 030001 (2024).
- [5] Nakano, T. & Nishijima, K. Charge Independence for V -particles. *Prog. Theor. Phys.* **10**, 581 (1953).
- [6] Gell-Mann, M. The interpretation of the new particles as displaced charged multiplets. *Nuovo Cim* **4**, 848 (1956).
- [7] Gell-Mann, M. The eightfold way: A theory of strong interaction symmetry. <https://www.osti.gov/biblio/4008239> (1961). Technical Report.
- [8] Ne'eman, Y. Derivation of strong interactions from a gauge invariance. *Nucl. Phys.* **26**, 222 (1961).
- [9] Gell-Mann, M. A schematic model of baryons and mesons. *Phys. Lett.* **8**, 214 (1964).
- [10] Zweig, G. An SU_3 model for strong interaction symmetry and its breaking; Version 2. <https://cds.cern.ch/record/570209> (1964). CERN Report TH-412.
- [11] Barnes, V. E. *et al.* Observation of a hyperon with strangeness minus three. *Phys. Rev. Lett.* **12**, 204 (1964).
- [12] Aubert, J. J. *et al.* Experimental observation of a heavy particle J . *Phys. Rev. Lett.* **33**, 1404 (1974).

-
- [13] Augustin, J. E. *et al.* Discovery of a narrow resonance in e^+e^- annihilation. *Phys. Rev. Lett.* **33**, 1406 (1974).
- [14] Herb, S. W. *et al.* Observation of a dimuon resonance at 9.5 GeV in 400-GeV proton-nucleus collisions. *Phys. Rev. Lett.* **39**, 252 (1977).
- [15] Abe, F. *et al.* Observation of top quark production in $\bar{p}p$ collisions with the collider detector at Fermilab. *Phys. Rev. Lett.* **74**, 2626 (1995).
- [16] Abachi, S. *et al.* Observation of the top quark. *Phys. Rev. Lett.* **74**, 2632 (1995).
- [17] Greenberg, O. W. Spin and unitary-spin independence in a paraquark model of baryons and mesons. *Phys. Rev. Lett.* **13**, 598 (1964).
- [18] Amsler, C. *The Quark Structure of Hadrons. An Introduction to the Phenomenology and Spectroscopy* (Springer, Cham, 2018).
- [19] Srednicki, M. *Quantum Field Theory* (Cambridge University Press, Cambridge, 2007).
- [20] 't Hooft, G. A planar diagram theory for strong interactions. *Nucl. Phys. B* **72**, 461 (1974).
- [21] Witten, E. Baryons in the $1/N$ expansion. *Nucl. Phys. B* **160**, 57 (1979).
- [22] Matagne, N. & Stancu, F. Baryon resonances in large N_c QCD. *Rev. Mod. Phys.* **87**, 211 (2015).
- [23] Wilson, K. G. Confinement of quarks. *Phys. Rev. D* **10**, 2445 (1974).
- [24] Kogut, J. B. An introduction to lattice gauge theory and spin systems. *Rev. Mod. Phys.* **51**, 659 (1979).
- [25] ETM collaboration, Baron, R. *et al.* Light hadrons from lattice QCD with light (u, d), strange and charm dynamical quarks. *J. High Energ. Phys.* **2010**, 111 (2010).
- [26] Weinberg, S. Phenomenological lagrangians. *Physica A Stat. Mech. Appl.* **96**, 327 (1979).
- [27] Georgi, H. An effective field theory for heavy quarks at low energies. *Phys. Lett. B* **240**, 447 (1990).
- [28] Brambilla, N., Pineda, A., Soto, J. & Vairo, A. Effective-field theories for heavy quarkonium. *Rev. Mod. Phys.* **77**, 1423 (2005).
- [29] Maris, P. & Roberts, C. D. Dyson–Schwinger equations: A tool for hadron physics. *Int. J. Mod. Phys. E* **12**, 297 (2003).
- [30] Eichmann, G., Sanchis-Alepuz, H., Williams, R., Alkofer, R. & Fischer, C. S. Baryons as relativistic three-quark bound states. *Prog. Part. Nucl. Phys.* **91**, 1 (2016).
- [31] Eichmann, G., Fischer, C. S., Heupel, W., Santowsky, N. & Wallbott, P. C. Four-quark states from functional methods. *Few-Body Syst.* **61**, 38 (2020).

-
- [32] Sreelakshmi, M. & Akhilesh, R. Models and potentials in hadron spectroscopy. *J. Phys. G: Nucl. Part. Phys.* **50**, 073001 (2023).
- [33] Lucha, W., Schöberl, F. F. & Gromes, D. Bound states of quarks. *Phys. Rep.* **200**, 127 (1991).
- [34] LaCourse, D. & Olsson, M. G. String potential model: Spinless quarks. *Phys. Rev. D* **39**, 2751 (1989).
- [35] Olsson, M. G. Universal behavior in excited heavy-light and light-light mesons. *Phys. Rev. D* **55**, 5479 (1997).
- [36] Morgunov, V., Nefediev, A. V. & Simonov, Y. A. Rotating QCD string and the meson spectrum. *Phys. Lett. B* **459**, 653 (1999).
- [37] Takahashi, T. T., Matsufuru, H., Nemoto, Y. & Suganuma, H. Three-quark potential in $SU(3)$ lattice QCD. *Phys. Rev. Lett.* **86**, 18 (2001).
- [38] Dmitrašinović, V. Cubic casimir operator of $SU_C(3)$ and confinement in the nonrelativistic quark model. *Phys. Lett. B* **499**, 135 (2001).
- [39] Pepin, S. & Stancu, F. Three-body confinement force in hadron spectroscopy. *Phys. Rev. D* **65**, 054032 (2002).
- [40] Ping, J., Deng, C., Wang, F. & Goldman, T. Quantum chromodynamic quark benzene. *Phys. Lett. B* **659**, 607 (2008).
- [41] Deng, C., Ping, J., Wang, H., Zhou, P. & Wang, F. QCD quark cyclobutadiene and light tetraquark spectra. *Phys. Rev. D* **86**, 114035 (2012).
- [42] Cimino, L., Tourbez, C., Chevalier, C., Lacroix, G. & Semay, C. Tests of the envelope theory for three-body forces. *Few-Body Syst.* **65**, 20 (2024).
- [43] Silvestre-Brac, B., Semay, C., Narodetskii, I. M. & Veselov, A. I. The baryonic Y-shape confining potential energy and its approximants. *Eur. Phys. J. C* **32**, 385 (2004).

Many-body systems and the envelope theory

2

The Schrödinger equation $\left(-\frac{\hbar^2}{2m}\nabla^2 + V(\mathbf{r})\right)\psi = E\psi$ is the fundamental stationary equation of motion describing quantum systems involving one particle or relative motion. Solving this equation yields the eigenvalues E and eigenfunctions $\psi = \psi(\mathbf{r})$ of the system. Analytical solutions are feasible for certain potentials V , such as the harmonic oscillator and the Coulomb potential. Techniques like supersymmetric quantum mechanics [1] can be employed to identify these solvable cases. For other potentials, numerical methods are utilised.

In practice, physical systems often contain more than two particles, making the resolution of the Schrödinger equation significantly more complex. This complexity increases with the number of particles, rendering the equation analytically intractable even for systems with as few as three particles. Despite these challenges, solving the many-body Schrödinger equation is crucial in various fields of physics, including condensed matter, atomic and hadronic physics. This necessity has driven the development of numerous approximation and numerical techniques. These techniques include the expansion in oscillator bases (EOB) [2], Gaussian expansion [3], hyperspherical harmonics expansion [4], and Lagrange-mesh (LM) method [5], among others. Each technique offers varying degrees of accuracy, computational cost, and applicability. For instance, while the hyperspherical harmonics expansion is easier to extend to systems with more than three particles, it cannot handle easily semi-relativistic kinematics as the EOB. Consequently, each method is employed in scenarios where it performs optimally, balancing the trade-offs between computational efficiency and the specific requirements of the physical system under study.

The use of the Schrödinger equation in hadronic physics may seem unconventional, given that the theory describing the strong interaction, quantum chromodynamics (QCD), is fundamentally based on the Dirac equation, which is a covariant equation. However, in the context of heavy quarks, relativistic effects can often be neglected, making the Schrödinger equation a viable approximation. For light quarks, the Schrödinger equation still provides good results by substituting the non-relativistic kinematics by a semi-relativistic one [6, 7]. In this chapter, we introduce an approximation method known as the envelope theory, which proves to be particularly useful in hadronic physics, especially within the large- N approach where the number of baryon constituents becomes

very large. The main advantage of this method is that it treats the number of particles N as a simple parameter.

In Section 2.1, we present the general form of the many-body Schrödinger equation that we aim to solve. Subsequently, in Section 2.2, we examine the specific case of the harmonic oscillator, which is the only known solvable many-body system for arbitrary dimensions. Next, the knowledge of the exact spectrum of the harmonic oscillator is used to develop the envelope theory and its improved version in Sections 2.3 and 2.4, respectively. Finally, Sec. 2.5 presents some results derived from the envelope theory and its improved version.

2.1 Generalities

Consider a D -dimensional system of N particles with kinetic energy T_i and interacting via a two-body potential V_{ij} . The inclusion of one- and K -body potentials will be discussed later. The position of the i th particle is denoted by \mathbf{r}_i and its conjugate variable, the momentum, by \mathbf{p}_i , satisfying the commutation relation $[r_i^a, p_j^b] = i\delta_{ij}\delta^{ab}$, where a and b are vector components. While remaining general, we impose that $T_i = T_i(p_i)$, with $p_i = |\mathbf{p}_i|$ (and additional constraints such as differentiability and positivity [8]), and $V_{ij} = V_{ij}(r_{ij})$, with $r_{ij} = |\mathbf{r}_i - \mathbf{r}_j|$. The corresponding many-body Schrödinger equation is

$$\left(\sum_{i=1}^N T_i(p_i) + \sum_{i<j=2}^N V_{ij}(r_{ij}) \right) \psi = E\psi, \quad (2.1)$$

where $\psi = \psi(\mathbf{r}_1, \dots, \mathbf{r}_N)$ is the wavefunction and E is the energy of the system. The expression in parentheses represents the Hamiltonian H of the system. Although it is not explicitly stated here, computations will be performed in the centre of mass (CM) frame and natural units $\hbar = c = 1$ are used.

Few N -body Hamiltonians can be exactly solved, such as the Calogero model in $D = 1$ [9] or the harmonic oscillator [10]. In fact, the harmonic oscillator is the only system known as totally solvable for arbitrary N and D and thus warrants investigation.

2.2 N -body harmonic oscillator

We specify our Hamiltonian for the harmonic oscillator as follows

$$H_{\text{ho}} = \sum_{i=1}^N \frac{p_i^2}{2m_i} + \sum_{i<j=2}^N k_{ij} r_{ij}^2 - \frac{\mathbf{P}^2}{2M}, \quad (2.2)$$

where m_i is the mass of the i th particle. The last term, where $M = \sum_i^N m_i$ is the total mass and $\mathbf{P} = \sum_i^N \mathbf{p}_i$ is the total momentum, accounts for the removal of the CM motion. To proceed, we introduce dimensionless parameters α_i such that $m_i = \alpha_i m$, with m being a reference mass. For notation convenience, we define $\alpha_{1\dots j} = \sum_{i=1}^j \alpha_i$ and, in particular, $\alpha_{1\dots N} = \sum_{i=1}^N \alpha_i = M/m$. In order to solve the Schrödinger equation (2.1) with the Hamiltonian (2.2), we first perform a change of basis.

2.2.1 Jacobi coordinates

The Jacobi coordinates are defined by

$$\begin{aligned}
\mathbf{x}_1 &= \mathbf{r}_1 - \mathbf{r}_2, \\
\mathbf{x}_2 &= \frac{\alpha_1 \mathbf{r}_1 + \alpha_2 \mathbf{r}_2}{\alpha_{12}} - \mathbf{r}_3, \\
&\vdots \\
\mathbf{x}_j &= \frac{\sum_{i=1}^j \alpha_i \mathbf{r}_i}{\alpha_{1\dots j}} - \mathbf{r}_{j+1}, \\
&\vdots \\
\mathbf{x}_N &= \frac{\sum_{i=1}^N \alpha_i \mathbf{r}_i}{\alpha_{1\dots N}},
\end{aligned} \tag{2.3}$$

where the last coordinate represents the CM position $\mathbf{x}_N = \mathbf{R}$ in a non-relativistic frame, which is the conjugate variable of \mathbf{P} . Equations (2.3) can also be expressed as $\mathbf{x}_i = \sum_{j=1}^N A_{ij} \mathbf{r}_j$, with A being a transformation matrix given by

$$A_{ij} = \begin{cases} \frac{\alpha_j}{\alpha_{1\dots i}} & \text{if } j \leq i, \\ -1 & \text{if } j = i + 1, \\ 0 & \text{if } j > i + 1. \end{cases} \tag{2.4}$$

The Jacobian of the transformation is given by $\det(A) = 1$. The conjugate variable of \mathbf{x}_i is defined as

$$\mathbf{\Pi}_i = \sum_{j=1}^N B_{ji} \mathbf{p}_j, \tag{2.5}$$

with $B = A^{-1}$, ensuring that the commutation relations between \mathbf{r}_i and \mathbf{p}_j are preserved. Although tedious, the computation of B yields

$$B_{ij} = \begin{cases} \frac{\alpha_{j+1}}{\alpha_{1\dots j+1}} & \text{if } i \leq j < N, \\ -\frac{\alpha_{1\dots j}}{\alpha_{1\dots j+1}} & \text{if } i = j + 1 \text{ and } j < N, \\ 1 & \text{if } j = N \forall i, \\ 0 & \text{if } i > j + 1. \end{cases} \tag{2.6}$$

In particular, $\mathbf{\Pi}_N = \mathbf{P}$. We now turn to the computation of Hamiltonian (2.2) in terms of the Jacobi coordinates (2.3). The following identities will be useful

$$\sum_{j=1}^N A_{ij} = \delta_{iN}, \tag{2.7}$$

$$\sum_{j=1}^N \alpha_j B_{ji} = \frac{M}{m} \delta_{iN}. \tag{2.8}$$

Kinetic operator

The kinetic operator of the harmonic oscillator is written as

$$\begin{aligned} T_{\text{ho}} &= \sum_{i=1}^N \frac{p_i^2}{2m_i} = \frac{1}{2m} \sum_{i=1}^N \frac{p_i^2}{\alpha_i} = \frac{1}{2m} \sum_{k,l=1}^N \mathbf{\Pi}_k \mathbf{\Pi}_l \left(\sum_{i=1}^N \frac{A_{ki} A_{li}}{\alpha_i} \right) \\ &= \frac{1}{2m} \left[\sum_{k=1}^N \mathbf{\Pi}_k^2 \left(\sum_{i=1}^N \frac{A_{ki}^2}{\alpha_i} \right) + 2 \sum_{k < l=2}^N \mathbf{\Pi}_k \mathbf{\Pi}_l \left(\sum_{i=1}^N \frac{A_{ki} A_{li}}{\alpha_i} \right) \right], \end{aligned} \quad (2.9)$$

where, in the second line, the expression is separated in diagonal and non-diagonal terms. Let us focus on the non-diagonal terms for the moment. Two cases arise. First, if $l = N$

$$\sum_{i=1}^N \frac{A_{ki} A_{Ni}}{\alpha_i} = \frac{m}{M} \sum_{i=1}^N A_{ki} = \frac{m}{M} \delta_{kN}. \quad (2.10)$$

The first equality follows from the definition (2.4) and the second from identity (2.7). However, since $k < l = N$, this term vanishes. Secondly, if $l < N$

$$\sum_{i=1}^N \frac{A_{ki} A_{li}}{\alpha_i} = \sum_{i=1}^k \frac{A_{ki} A_{li}}{\alpha_i} + \frac{A_{k k+1} A_{l k+1}}{\alpha_{k+1}} + \sum_{i=k+2}^N \frac{A_{ki} A_{li}}{\alpha_i}. \quad (2.11)$$

By definition (2.4), the third sum is equal to zero because $i > k+1$. The second term is

$$-\frac{A_{l k+1}}{\alpha_{k+1}} = -\frac{1}{\alpha_{k+1}} \frac{\alpha_{k+1}}{\alpha_{1\dots l}} = -\frac{1}{\alpha_{1\dots l}}, \quad (2.12)$$

and the first term is

$$\sum_{i=1}^k \frac{\alpha_i}{\alpha_{1\dots k}} \frac{A_{li}}{\alpha_i} = \frac{1}{\alpha_{1\dots k}} \sum_{i=1}^k \frac{\alpha_i}{\alpha_{1\dots l}} = \frac{1}{\alpha_{1\dots l}}. \quad (2.13)$$

Hence, all non-diagonal terms vanish.

We can now turn our attention to the diagonal terms. Again, two cases arise. First, if $k = N$

$$\sum_{i=1}^N \frac{A_{Ni}^2}{\alpha_i} = \frac{m}{M}. \quad (2.14)$$

Secondly, if $k < N$

$$\sum_{i=1}^N \frac{A_{ki}^2}{\alpha_i} = \sum_{i=1}^k \frac{A_{ki}^2}{\alpha_i} + \frac{A_{k k+1}^2}{\alpha_{k+1}} + \sum_{i=k+2}^N \frac{A_{ki}^2}{\alpha_i} = \frac{1}{\alpha_{1\dots k}} + \frac{1}{\alpha_{k+1}}. \quad (2.15)$$

The kinetic energy (2.9) thus becomes

$$T_{\text{ho}} = \sum_{i=1}^{N-1} \frac{1}{2m} \left(\frac{1}{\alpha_{1\dots k}} + \frac{1}{\alpha_{k+1}} \right) \mathbf{\Pi}_i^2 + \frac{1}{2M} \mathbf{P}^2, \quad (2.16)$$

remembering that $\mathbf{\Pi}_N = \mathbf{P}$.

We notice two important features in the above equation. First, the CM energy has been isolated and will be cancelled in (2.2). Secondly, the first term is diagonal, meaning there is no term proportional to $\mathbf{\Pi}_i \mathbf{\Pi}_j$ with $i \neq j$. The approach aims to diagonalise our Hamiltonian (2.2) to express it as the sum of individual solvable Hamiltonians.

Potential operator

Following the above demonstration, we now focus on the transformation of the two-body potential $V_{\text{ho}} = \sum_{i < j}^N k_{ij} r_{ij}^2$ into Jacobi coordinates. Unlike the kinetic operator, the non-diagonal elements of the potential do not vanish in the most general case [10, 11]. Therefore, Jacobi coordinates alone are insufficient to diagonalise the Hamiltonian H_{ho} . Consequently, a new set of coordinates must be found to achieve our goal.

2.2.2 Diagonalisation procedure

Let $\lambda_i = \left(\frac{\alpha_{1 \dots i+1}}{\alpha_{1 \dots i} \alpha_{i+1}} \right)^{1/2}$ and consider a new set of rescaled Jacobi coordinates $\mathbf{y}_i = \mathbf{x}_i / \lambda_i$ with their conjugates $\boldsymbol{\rho}_i = \lambda_i \mathbf{\Pi}_i$. Using these new coordinates, it can be shown that

$$\mathbf{r}_i - \mathbf{r}_j = \sum_{k=1}^{N-1} (B_{ik} - B_{jk}) \lambda_k \mathbf{y}_k, \quad (2.17)$$

by using $B_{iN} = 1 \forall i$, and

$$V_{\text{ho}} = \sum_{k,l=1}^{N-1} G_{kl} \mathbf{y}_k \mathbf{y}_l \quad \text{with} \quad G_{kl} = \lambda_k \lambda_l \sum_{i < j=2}^N k_{ij} (B_{ik} - B_{jk})(B_{il} - B_{jl}). \quad (2.18)$$

The square matrix G , of size $N - 1$, is non-diagonal but symmetric, meaning it can always be diagonalised with a unitary matrix U so that $G = U^{-1} D U$, where D is a diagonal matrix whose elements are the eigenvalues of G , denoted d_i . Thanks to this diagonalisation, a new set of variables is defined by $\mathbf{z}_i = \sum_j^{N-1} U_{ij} \mathbf{y}_j$ so that the potential now reads

$$V_{\text{ho}} = \sum_{i=1}^{N-1} d_i \mathbf{z}_i^2. \quad (2.19)$$

The conjugate of \mathbf{z}_i is $\boldsymbol{\sigma}_i = \sum_j^{N-1} (U^{-1})_{ji} \boldsymbol{\rho}_j$ and the kinetic term (2.16), with the CM energy removed, reads

$$T_{\text{ho}} = \frac{1}{2m} \sum_{i=1}^{N-1} \boldsymbol{\sigma}_i^2. \quad (2.20)$$

Eventually, our harmonic oscillator Hamiltonian (2.2) takes the form

$$H_{\text{ho}} = \sum_{i=1}^{N-1} \left(\frac{\boldsymbol{\sigma}_i^2}{2m} + d_i \mathbf{z}_i^2 \right), \quad (2.21)$$

which is a sum of $N-1$ decoupled one-body harmonic oscillators $h_i = \frac{\sigma_i^2}{2m} + d_i z_i^2$. The eigenvalue of h_i is the well-known result [12]

$$e_i = \begin{cases} \bar{\omega}_i (2n_i + l_i + \frac{D}{2}) & \text{if } D \geq 2 \\ \bar{\omega}_i (n_i + \frac{1}{2}) & \text{if } D = 1 \end{cases} \quad \text{with } \bar{\omega}_i^2 = \frac{2d_i}{m}, \quad (2.22)$$

where (n_i, l_i) are the principal and angular quantum numbers associated with the Jacobi coordinate z_i . The eigenfunction of h_i is denoted $\varphi_{n_i l_i}(z_i)$ (the magnetic quantum numbers are omitted). If the total wavefunction of (2.21) is written as $\psi(z_1, \dots, z_{N-1}) = \prod_i^{N-1} \varphi_{n_i l_i}(z_i)$, then the total intrinsic energy of the system is $E = \sum_i^{N-1} e_i$.

We have just demonstrated that it is always possible to solve the N -body harmonic oscillator at arbitrary D by diagonalising the matrix G given by (2.18). The diagonalisation procedure can be easily done numerically, but some cases remain analytical, as we shall see in the next sections.

Before moving on, let us note there is a hidden condition in (2.22). Indeed, $\bar{\omega}_i^2 > 0 \forall i$, thus $d_i > 0$, is necessary to take the square root. This is the case if the potential between all particles is attractive, that is $k_{ij} > 0 \forall i, j$, but a mix of repulsive and attractive potentials could lead to negative $\bar{\omega}_i^2$. Physically, this means that the repulsive potentials prevent the creation of a bound state.

One-body forces

In addition to two-body forces V_{ij} , one-body forces U_i can also be included in (2.1). Although they may seem non-physical, one-body forces can be used to model confinement inside baryons in a string model, where each quark produces a ‘‘colour’’ string that connects to a single point, forming a Y -junction [13], as explained in Sec. 1.3. The position of the Y -junction must minimise the string’s length, and thus the corresponding potential

$$U_Y = \min_{\mathbf{Y}} (|\mathbf{r}_1 - \mathbf{Y}| + |\mathbf{r}_2 - \mathbf{Y}| + |\mathbf{r}_3 - \mathbf{Y}|), \quad (2.23)$$

is difficult to implement. However, the Y -junction can be approximated by the CM position \mathbf{R} , at the cost of a small error when quarks have similar masses [14]. We will thus consider one-body potentials of the form $U_i = U_i(s_i)$, with $s_i = |\mathbf{r}_i - \mathbf{R}|$. For the case of the harmonic oscillator, the term $U_{\text{ho}} = \sum_i^N \tilde{k}_i s_i^2$ is added in (2.2).

In a similar fashion to the previous section, the one-body potential can be written in terms of the Jacobi coordinates \mathbf{y}_i as

$$U_{\text{ho}} = \sum_{k,l=1}^{N-1} F_{kl} \mathbf{y}_k \mathbf{y}_l \quad \text{with } F_{kl} = \lambda_k \lambda_l \sum_{i < j=2}^N \tilde{k}_i B_{ik} B_{il}, \quad (2.24)$$

where F is a symmetric square matrix. The total potential is then $V_{\text{tot}} = V_{\text{ho}} + U_{\text{ho}} = \sum_{k,l=1}^{N-1} J_{kl} \mathbf{y}_k \mathbf{y}_l$, with the symmetric matrix J given by the sum of (2.18) and (2.24). It is then possible to diagonalise J , leading to a set of Jacobi variables z_i that diagonalise the Hamiltonian.

2.2.3 Identical particles

If all particles are identical, then $\alpha_i = \alpha$, $\tilde{k}_i = \tilde{k} \forall i$ and $k_{ij} = k \forall i, j$. Computation of J shows that non-diagonal matrix elements vanish and all diagonal elements take the value $(Nk + \tilde{k})$ [10]. This result implies that in the original Jacobi coordinates $(\mathbf{x}_i, \mathbf{\Pi}_i)$, defined by (2.3), the crossed terms in the potential operator were equal to zero, greatly simplifying our work. Hamiltonian (2.21) then reduces to

$$H_{\text{ho}}^{\text{id}} = \sum_{i=1}^{N-1} \left(\frac{i+1}{2i\alpha m} \mathbf{\Pi}_i^2 + \frac{i\alpha}{i+1} (Nk + \tilde{k}) \mathbf{x}_i^2 \right). \quad (2.25)$$

We can set, without any loss of generality, $\alpha = 1$ so that the reference mass m represents the mass of the identical particles. The intrinsic energy of the system is then

$$E_{\text{ho}}^{\text{id}} = Q(N) \sqrt{\frac{2}{m} (Nk + \tilde{k})}, \quad (2.26)$$

where we define the global quantum number

$$Q(M) = \begin{cases} \sum_{i=1}^{M-1} (2n_i + l_i + \frac{D}{2}) & \text{if } D \geq 2 \\ \sum_{i=1}^{M-1} (n_i + \frac{1}{2}) & \text{if } D = 1 \end{cases}, \quad (2.27)$$

with the quantum numbers n_i and l_i associated with the Jacobi coordinate \mathbf{x}_i .

Symmetries

The wavefunction of (2.25) is given by $\psi = \prod_i^{N-1} \varphi_{n_i l_i}(\mathbf{x}_i)$, where $\varphi_{n_i l_i}$ is a one-body harmonic oscillator wavefunction (the magnetic quantum numbers are omitted). For systems with identical particles, the wavefunction must be either completely symmetric or completely antisymmetric under particle exchange to satisfy Bose-Einstein or Fermi-Dirac statistics, respectively. This symmetrisation can be achieved by applying the symmetriser operator \hat{S} on ψ . Explicitly, this operator is defined as

$$\hat{S}_{\pm} = \frac{1}{\sqrt{N!}} \sum_P (\pm 1)^\sigma \hat{P}, \quad (2.28)$$

where the sum runs over all permutations \hat{P} of signature σ , and \pm corresponds to symmetrisation or antisymmetrisation, respectively. Thus, the appropriate wavefunction is $\hat{S}\psi$ up to a normalisation factor.

Since the wavefunction ψ is expressed in terms of Jacobi coordinates \mathbf{x}_i rather than the individual coordinates \mathbf{r}_i , applying the symmetriser operator directly is not straightforward, even for $N = 3$. Fortunately, it is not necessary at this stage to explicitly construct the symmetrised wavefunctions; it suffices to acknowledge their existence. Similarly, calculating the global quantum number $Q(N)$ is challenging because the quantum numbers are not directly associated with the individual coordinates \mathbf{r}_i . Additional details on specific values of $Q(N)$ and the symmetrisation procedure can be found in Appendix A. Notably, it is shown that the ground state $n_i = l_i = 0 \forall i$ corresponds to a completely

symmetric wavefunction. This state is thus the bosonic ground state (BGS) and the associated global quantum number is

$$Q_{\text{BGS}}(N) = (N-1) \frac{D}{2}. \quad (2.29)$$

***K*-body forces**

Many-body forces, and especially three-body forces, are sometimes a crucial ingredient in atomic physics [15], nuclear physics [16], or hadronic physics [17, 18, 19, 20, 21]. The structures of many-body forces depend strongly on the system considered, and they are generally difficult to uncover and difficult to implement in numerical codes. The *Y*-junction presented above is an example of a three-body potential. That is the reason why effective forms can be used instead to simulate these complicated many-body contributions, avoiding some technical difficulties. A common structure used to this end for a *K*-body force is the square-root of the sum of two-body variables, given by

$$\sum_{\{i_1, \dots, i_K\}}^N W(r_{\{i_1, \dots, i_K\}}) \quad \text{with} \quad r_{\{i_1, \dots, i_K\}}^2 = \sum_{i < j=2}^{\{i_1, \dots, i_K\}} r_{ij}^2, \quad (2.30)$$

where $r_{ij} = |\mathbf{r}_i - \mathbf{r}_j|$ and $\{i_1, \dots, i_K\}$ is a set of *K* particles among the *N* possible ones, with $i_1 < \dots < i_K$. The sum $\sum_{\{i_1, \dots, i_K\}}^N$ runs over the C_N^K different sets $\{i_1, \dots, i_K\}$, while the sum $\sum_{i < j}^{\{i_1, \dots, i_K\}}$ runs over the C_K^2 different pairs in a particular set $\{i_1, \dots, i_K\}$, where C_A^B is a usual binomial coefficient

$$C_A^B = \binom{B}{A} = \frac{A!}{B!(A-B)!}. \quad (2.31)$$

If *K* = 2, the usual two-body case is recovered. For the harmonic oscillator, the corresponding *K*-body potential is

$$\begin{aligned} W_{\text{ho}} &= k \sum_{\{i_1, \dots, i_K\}}^N r_{\{i_1, \dots, i_K\}}^2 = k \sum_{\{i_1, \dots, i_K\}}^N \sum_{i < j=2}^{\{i_1, \dots, i_K\}} r_{ij}^2 \\ &= k C_{N-2}^{K-2} \sum_{i < j=2}^N r_{ij}^2. \end{aligned} \quad (2.32)$$

The binomial factor in the last line accounts for the fact there are C_N^2 elements in the last equality opposed to $C_N^K \times C_K^2$ elements in the second equality. In this particular case, a *K*-body potential reduces to a 2-body potential by changing $k \rightarrow k C_{N-2}^{K-2}$. The intrinsic energy of the system then becomes

$$E_{\text{ho}}^{\text{id}} = Q(N) \sqrt{\frac{2}{m} N C_{N-2}^{K-2} k}. \quad (2.33)$$

If an additional *K'*-body potential is included in the system, a new term is added in the energy expression by following similar calculations.

2.2.4 Sets of identical particles

Consider now a particular system composed of S different sets of N_α identical particles (where the index α refers to a particular set). The harmonic oscillator Hamiltonian, with the CM energy removed, can be expressed as

$$\begin{aligned}
H_{\text{ho}} = & \sum_{\alpha=1}^S \sum_{i_\alpha=1}^{N_\alpha} \frac{p_{i_\alpha}^2}{2m_\alpha} - \frac{\mathbf{P}^2}{2M} + \sum_{\alpha=1}^S \sum_{i_\alpha=1}^{N_\alpha} \tilde{k}_\alpha (\mathbf{r}_{i_\alpha} - \mathbf{R})^2 \\
& + \sum_{\alpha=1}^S \sum_{i_\alpha < j_\alpha=2}^{N_\alpha} k_{\alpha\alpha} r_{i_\alpha j_\alpha}^2 + \sum_{\alpha < \beta=2}^S \sum_{i_\alpha=1}^{N_\alpha} \sum_{j_\beta=1}^{N_\beta} k_{\alpha\beta} r_{i_\alpha j_\beta}^2.
\end{aligned} \tag{2.34}$$

In this context, many-body forces within a given set α of identical particles can be included by substituting $k_{\alpha\alpha} \rightarrow k_{\alpha\alpha} C_{N_\alpha-2}^{K-2}$. The total number of particles is $N = \sum_{\alpha}^S N_\alpha$. By defining $M_\alpha = N_\alpha m_\alpha$, so that $M = \sum_{\alpha}^S M_\alpha$, and introducing the total momenta $\mathbf{P}_\alpha = \sum_{i_\alpha}^{N_\alpha} \mathbf{p}_{i_\alpha}$ and the CM positions $\mathbf{R}_\alpha = \frac{1}{N_\alpha} \sum_{i_\alpha}^{N_\alpha} \mathbf{r}_{i_\alpha}$ for a set α , the Hamiltonian (2.34) can be decomposed as [22, 23]

$$H_{\text{ho}} = \sum_{\alpha=1}^S H_\alpha + H_{\text{CM}} \text{ with} \tag{2.35a}$$

$$\begin{aligned}
H_\alpha = & \sum_{i_\alpha=1}^{N_\alpha} \frac{p_{i_\alpha}^2}{2m_\alpha} - \frac{\mathbf{P}_\alpha^2}{2M_\alpha} + \sum_{i_\alpha=1}^{N_\alpha} \tilde{k}_\alpha (\mathbf{r}_{i_\alpha} - \mathbf{R}_\alpha)^2 \\
& + \sum_{i_\alpha < j_\alpha=2}^{N_\alpha} \frac{1}{N_\alpha} \left[\sum_{\beta=1}^S N_\beta k_{\alpha\beta} \right] r_{i_\alpha j_\alpha}^2,
\end{aligned} \tag{2.35b}$$

$$\begin{aligned}
H_{\text{CM}} = & \sum_{\alpha=1}^S \frac{\mathbf{P}_\alpha^2}{2M_\alpha} - \frac{\mathbf{P}^2}{2M} + \sum_{\alpha=1}^S N_\alpha \tilde{k}_\alpha (\mathbf{R}_\alpha - \mathbf{R})^2 \\
& + \sum_{\alpha < \beta=2}^S N_\alpha N_\beta k_{\alpha\beta} (\mathbf{R}_\alpha - \mathbf{R}_\beta)^2.
\end{aligned} \tag{2.35c}$$

The Hamiltonians H_α and H_{CM} are entirely decoupled since (2.35b) depends solely on the internal coordinates of their respective set α , and (2.35c) depends on the relative coordinates between the CM positions of the sets. Therefore, the energy of the system is the sum of the energies of each sub-Hamiltonian, $E = \sum_{\alpha}^S E_\alpha + E_{\text{CM}}$. Since H_α is a Hamiltonian composed of identical particles, its energy can be derived from the previous section results

$$E_\alpha = \sqrt{\frac{2}{m_\alpha} \left(\tilde{k}_\alpha + \sum_{\beta=1}^S N_\beta k_{\alpha\beta} \right)} Q(N_\alpha), \tag{2.36}$$

where $Q(N_\alpha)$ is the global quantum number of the set α .

The S -body Hamiltonian H_{CM} can be solved using the diagonalisation procedure described previously.

S = 2

When considering the simplest case of a system with only two sets of particles, denoted a and b , the CM Hamiltonian H_{CM} becomes a two-body Hamiltonian. This Hamiltonian can be solved by introducing the relative momentum $\mathbf{p} = (M_b \mathbf{P}_a - M_a \mathbf{P}_b)/M$ and the relative position $\mathbf{r} = \mathbf{R}_a - \mathbf{R}_b$ between the two sets. Consequently, (2.35c) simplifies to

$$H_{\text{CM}}^{S=2} = \frac{M}{M_a M_b} \frac{\mathbf{p}^2}{2} + \left[N_a \left(\frac{M_b}{M} \right)^2 \tilde{k}_a + N_b \left(\frac{M_a}{M} \right)^2 \tilde{k}_b + N_a N_b k_{ab} \right] \mathbf{r}^2, \quad (2.37)$$

where its corresponding eigenvalue is

$$\sqrt{\frac{2}{M_a M_b M} (N_a M_b^2 \tilde{k}_a + N_b M_a^2 \tilde{k}_b + N_a N_b M^2 k_{ab})} Q(2). \quad (2.38)$$

Thus, the total energy for a system composed of two sets of N_a and N_b particles is

$$\begin{aligned} E_{\text{ho}}^{N_a+N_b} &= \sqrt{\frac{2}{m_a} (\tilde{k}_a + N_a k_{aa} + N_b k_{ab})} Q(N_a) \\ &+ \sqrt{\frac{2}{m_b} (\tilde{k}_b + N_b k_{bb} + N_a k_{ab})} Q(N_b) \\ &+ \sqrt{\frac{2}{M_a M_b M} (N_a M_b^2 \tilde{k}_a + N_b M_a^2 \tilde{k}_b + N_a N_b M^2 k_{ab})} Q(2). \end{aligned} \quad (2.39)$$

Special consideration is required when N_a and/or $N_b = 1$. In these cases, the respective Hamiltonians H_a and/or H_b in (2.35) vanish, and their contributions to the total energy in (2.39) also vanish. Additionally, the global quantum number $Q(N)$ is not defined for $N = 1$ due to its definition (2.27), which involves a sum from 1 to $N - 1$.

It is also important to note that when all particles are identical, the result correctly reduces to the expression given in (2.26). This ensures that the derived formulae are consistent across different scenarios, whether dealing with identical particles or distinct sets of particles.

S = 3

To investigate the eigenvalue of the Hamiltonian H_{CM} for a system with $S = 3$ sets of particles, denoted as a, b and c , we utilise the diagonalisation procedure. The computation of the symmetric matrix J yields

$$J = m \begin{pmatrix} J_{11} & J_{12} \\ J_{12} & J_{22} \end{pmatrix} \text{ with} \quad (2.40a)$$

$$\left\{ \begin{array}{l} J_{11} = \frac{1}{M_a M_b (M_a + M_b)} [N_b M_a^2 (\tilde{k}_b + N_c k_{bc}) \\ \quad + N_a M_b^2 (\tilde{k}_a + N_c k_{ac}) + N_a N_b (M_a + M_b)^2 k_{ab}] \\ J_{12} = \frac{1}{M_a + M_b} [N_a \tilde{k}_a + N_b \tilde{k}_b + N_a N_c k_{ac} + N_b N_c k_{bc}] \\ \quad + \frac{1}{M_c} [N_c \tilde{k}_c + N_a N_c k_{ac} + N_b N_c k_{bc}] \\ \quad - \frac{1}{M} [N_a \tilde{k}_a + N_b \tilde{k}_b + N_c \tilde{k}_c] \\ J_{22} = -\frac{1}{(M_a + M_b) \sqrt{M M_a M_b M_c}} [M_c (N_b M_a \tilde{k}_b - N_a M_b \tilde{k}_a) \\ \quad + M M_a N_b N_c k_{bc} - M M_b N_a N_c k_{ac}] \end{array} \right. , \quad (2.40b)$$

where we recall m is a reference mass. The diagonalization of this matrix leads to the following expression for the energy [10]

$$E_{\text{CM}}^{S=3} = \left(\frac{1}{M M_a M_b M_c} \right)^{1/2} \left(\sqrt{s + \delta} Q(2) + \sqrt{s - \delta} Q'(2) \right), \quad (2.41)$$

where δ and s are defined as

$$\delta = \sqrt{s^2 - 4 M M_a M_b M_c r}, \quad (2.42a)$$

$$\begin{aligned} r = & N_a N_b \tilde{k}_a \tilde{k}_b M_c^2 + N_a N_c \tilde{k}_a \tilde{k}_b M_b^2 + N_b N_c \tilde{k}_b \tilde{k}_c M_a^2 \\ & + N_a N_b N_c M^2 (N_a k_{ab} k_{ac} + N_c k_{ac} k_{bc} + N_b k_{ab} k_{bc}) \\ & + N_a N_b k_{ab} [(N_a \tilde{k}_a + N_b \tilde{k}_b) M_c^2 + N_c \tilde{k}_c (M_a + M_b)^2] \\ & + N_a N_c k_{ac} [(N_a \tilde{k}_a + N_c \tilde{k}_c) M_b^2 + N_b \tilde{k}_b (M_a + M_c)^2] \\ & + N_b N_c k_{bc} [(N_b \tilde{k}_b + N_c \tilde{k}_c) M_a^2 + N_a \tilde{k}_a (M_b + M_c)^2], \end{aligned} \quad (2.42b)$$

$$\begin{aligned} s = & N_a \tilde{k}_a M_b M_c (M_b + M_c) + N_b \tilde{k}_b M_a M_c (M_a + M_c) \\ & + N_c \tilde{k}_c M_a M_b (M_a + M_b) \\ & + M (N_a N_b k_{ab} M_c (M_a + M_b) + N_a N_c k_{ac} M_b (M_a + M_c) \\ & + N_b N_c k_{bc} M_a (M_b + M_c)). \end{aligned} \quad (2.42c)$$

This eigenvalue $E_{\text{CM}}^{S=3}$ does not depend on the reference mass and is symmetric under the exchange of the sets' labels, ensuring no set is favoured over the others. Furthermore, it can be verified that the solution correctly reduces to the expected form in the limit of identical particles.

$S > 3$

The eigenvalues of H_{CM} can be analytically determined for up to $S = 5$ sets of particles. This is because the diagonalisation process involves solving a quartic equation at most, which is always possible to solve analytically. However, the solutions to these equations can be extremely complex and cumbersome to express.

2.3 Envelope theory

We have demonstrated that it is always possible to solve the N -body harmonic oscillator through a diagonalisation procedure, with some analytical solutions being attainable for specific configurations. These configurations include N identical particles (2.26), two and three distinct sets of identical particles (2.39) and (2.41), respectively. This interesting property will be utilised to develop an approximation method for determining approximate eigensolutions of the Schrödinger equation (2.1), known as the envelope theory.

2.3.1 Auxiliary Hamiltonian

Before continuing, let us make a brief mathematical detour. Consider the Lagrangian of a relativistic point particle [24], $\mathcal{L}_r(x) = -m\sqrt{\dot{x}^2}$, where $x^\mu(\tau)$ denotes the world line of the particle and $\dot{x}^\mu = \frac{dx^\mu}{d\tau}$ its derivative with respect to the proper time τ . The equation of motion of the particle is derived from the Euler-Lagrange equation, and the associated Hamiltonian is obtained via a Legendre transformation. In both cases, the square root in the Lagrangian complicates computation compared to the non-relativistic Lagrangian $\mathcal{L}_{nr}(x) = \dot{x}^2/(2m)$. Now, consider the Lagrangian $\mathcal{L}_{aux}(x, \mu) = \dot{x}^2/(2\mu) + m^2\mu/2$, where μ is an *auxiliary field*. At first glance, Lagrangians \mathcal{L}_r and \mathcal{L}_{aux} may not seem related. However, considering the Euler-Lagrange equation for the field μ , we obtain

$$\left. \frac{\partial \mathcal{L}_{aux}}{\partial \mu} \right|_{\mu_0} = 0 \Leftrightarrow \mu_0 = -\frac{\sqrt{\dot{x}^2}}{m}. \quad (2.43)$$

Substituting μ_0 into \mathcal{L}_{aux} , we find $\mathcal{L}_{aux}(x, \mu_0) = \mathcal{L}_r(x)$. These two Lagrangians are actually equivalent, but \mathcal{L}_{aux} is simpler to work with due to its similarity to \mathcal{L}_{nr} . The idea is to perform the computations with the auxiliary Lagrangian and, ultimately, eliminate the auxiliary fields. This technique can also be applied to the Nambu-Goto Lagrangian describing a relativistic string [25]. Auxiliary fields differ from ordinary fields in that their equations of motion are not dynamical (there is no kinematic term) but lead to algebraic relations that allow them to be expressed in terms of the other degrees of freedom in the problem.

Returning to our Hamiltonian H in (2.1), and based on the above discussions, it is replaced with the auxiliary Hamiltonian [26]

$$\begin{aligned} \tilde{H} = & \sum_{i=1}^N \left[\frac{p_i^2}{2\mu_i} + T_i(G_i(\mu_i)) - \frac{G_i^2(\mu_i)}{2\mu_i} \right] \\ & + \sum_{i<j=2}^N [\rho_{ij}r_{ij}^2 + V_{ij}(J_{ij}(\rho_{ij})) - \rho_{ij}J_{ij}^2(\rho_{ij})], \end{aligned} \quad (2.44)$$

with the functions G_i and J_{ij} defined such that

$$T'_i(G_i(x)) - \frac{G_i(x)}{x} = 0, \quad (2.45a)$$

$$V'_{ij}(J_{ij}(x)) - 2xJ_{ij}(x) = 0, \quad (2.45b)$$

where $A'(y) = dA(y)/dy$. The auxiliary Hamiltonian depends on a set of auxiliary fields $\{\alpha\} = \{\{\mu_i\}, \{\rho_{ij}\}\}$ with $i, j = \{1, \dots, N\}$. The definition of the

functions $G_i(x)$ and $J_{ij}(x)$ arises from the requirement that \tilde{H} must reduce to the original Hamiltonian H after the auxiliary fields are removed by a similar procedure as in (2.43). The auxiliary Hamiltonian can also be written as

$$\tilde{H} = \sum_{i=1}^N \tilde{T}_i(p_i) + \sum_{i<j=2}^N \tilde{V}_{ij}(r_{ij}), \quad (2.46)$$

where the auxiliary parts \tilde{T}_i and \tilde{V}_{ij} are easily derived from (2.44). So far, our calculations are exact. We then make an approximation by replacing our auxiliary fields $\{\alpha\}$ with *auxiliary parameters*. The key difference is that fields depend on the positions and momenta, whereas parameters are merely numbers. By doing so, the auxiliary Hamiltonian \tilde{H} becomes a harmonic oscillator Hamiltonian (2.2)

$$\tilde{H} = H_{\text{ho}}(\{\alpha\}) + B(\{\alpha\}), \quad (2.47)$$

with

$$\begin{aligned} B(\{\alpha\}) = & \sum_{i=1}^N \left[T_i(G_i(\mu_i)) - \frac{G_i^2(\mu_i)}{2\mu_i} \right] \\ & + \sum_{i<j=2}^N \left[V_{ij}(J_{ij}(\rho_{ij})) - \rho_{ij} J_{ij}^2(\rho_{ij}) \right], \end{aligned} \quad (2.48)$$

a function that solely depends on the auxiliary parameters and is entirely determined by the original Hamiltonian via the functions G_i and J_{ij} . The eigenvalue of \tilde{H} is then

$$\tilde{E} = E_{\text{ho}}(\{\alpha\}) + B(\{\alpha\}), \quad (2.49)$$

which depends on the parameters $\{\alpha\}$. The auxiliary parameters are eliminated by finding the set $\{\alpha_0\} = \{\{\mu_{i0}\}, \{\rho_{ij0}\}\}$ that extremise the eigenvalue of (2.44)

$$\left. \frac{\partial \tilde{E}}{\partial \mu_i} \right|_{\alpha_0} = \left. \frac{\partial \tilde{E}}{\partial \rho_{ij}} \right|_{\alpha_0} = 0 \quad \forall i, j. \quad (2.50)$$

The set $\{\alpha_0\}$ depends on the specific state considered. Once eliminated, the eigenvalue $\tilde{E}_0 \equiv \tilde{E}(\{\alpha_0\})$ is interpreted as an approximation of the eigenvalue of the original Hamiltonian H . If one knows an analytic solution of $E_{\text{ho}}(\{\alpha\})$, such as those presented in the previous section, then equations (2.50) are merely minimisation equations that can be easily solved numerically, and sometimes analytically. This procedure forms the basis of the approximation method called *envelope theory* (ET), or sometimes the *auxiliary field method* (the origin of the name will be explained later).

A difficulty in the method may arise during the computation of the function $B(\{\alpha\})$, and thus the functions G_i and J_{ij} , which may not exist. We will assume this is always the case, except when dealing with quadratic kinematic or potential terms. Indeed, consider non-relativistic kinematics $T_i = p_i^2/(2m_i)$. In this scenario, the function $G_i(x)$ in (2.45) is undefined. We can resolve this by noting that equation (2.45) is always valid if one sets $\mu_i = m_i \forall i$. By doing so, the first sum in (2.48) vanishes, which is equivalent to not introducing auxiliary

fields in the first place. A similar situation occurs if $V_{ij}(r_{ij}) \propto r_{ij}^2$. When both T_i and V_{ij} are quadratic in their argument, H is actually a harmonic oscillator Hamiltonian for which exact solutions are known.

Hellmann-Feynman theorem

The Hellmann-Feynman theorem states that the derivative of an eigenvalue E of a Hamiltonian H , with respect to a parameter λ , is equal to the mean value of the derivative of the Hamiltonian, with respect to the same parameter, evaluated between the corresponding eigenstate $|\psi\rangle$

$$\frac{\partial E}{\partial \lambda} = \left\langle \frac{\partial H}{\partial \lambda} \right\rangle_{\psi}, \quad (2.51)$$

where $\langle \cdot \rangle_{\psi}$ is a shorthand notation for $\langle \psi | \cdot | \psi \rangle$. Denoting an eigenstate of $\tilde{H}_0 \equiv \tilde{H}(\alpha_0)$ as $|\alpha_0\rangle$, the application of the Hellmann-Feynman theorem for the parameter μ_i yields

$$\begin{aligned} 0 &= \left. \frac{\partial \tilde{E}}{\partial \mu_i} \right|_{\alpha_0} = \left\langle \frac{\partial \tilde{H}_0}{\partial \mu_i} \right\rangle_{\alpha_0} \\ &= \left\langle \frac{G_i^2(\mu_{i0}) - p_i^2}{2\mu_{i0}^2} + G_i'(\mu_{i0}) \left[T_i'(G_i(\mu_{i0})) - \frac{G_i(\mu_{i0})}{\mu_{i0}} \right] \right\rangle_{\alpha_0} \\ &= \frac{1}{2\mu_{i0}^2} \left(G_i^2(\mu_{i0}) - \langle p_i^2 \rangle_{\alpha_0} \right), \end{aligned} \quad (2.52)$$

where the last line is obtained thanks to the definition (2.45). Similar computations for the derivatives with respect to ρ_{ij} ultimately lead to

$$G_i^2(\mu_{i0}) = \langle p_i^2 \rangle_{\alpha_0} \equiv p_{i0}^2, \quad (2.53a)$$

$$J_{ij}^2(\rho_{ij0}) = \langle r_{ij}^2 \rangle_{\alpha_0} \equiv r_{ij0}^2. \quad (2.53b)$$

These relations show that the new quantities p_{i0} and r_{ij0} are defined such that p_{i0} is the mean modulus of the momentum for the i th particle, and r_{ij0} the mean distance between the i th particle and the j th one. All these observables are directly obtained by determining the set $\{\alpha_0\}$, and therefore depend on the quantum numbers of the state considered.

We now turn our attention to the computation of $\langle \tilde{T}_i(p_i) \rangle_{\alpha_0}$ using (2.53)

$$\langle \tilde{T}_i(p_i) \rangle_{\alpha_0} = \frac{\langle p_i^2 \rangle_{\alpha_0}}{2\mu_{i0}} + T_i(G_i(\mu_{i0})) - \frac{G_i^2(\mu_{i0})}{2\mu_{i0}} = T_i(p_{i0}). \quad (2.54)$$

With similar calculations, it is straightforward to show that

$$\tilde{E}_0 = \langle \tilde{H}_0 \rangle_{\alpha_0} = \sum_{i=1}^N T_i(p_{i0}) + \sum_{i < j=2}^N V_{ij}(r_{ij0}). \quad (2.55)$$

Given the definitions of p_{i0} and r_{ij0} , and the structure of the Hamiltonian H under study, the interpretation of (2.55) is quite evident: each part of the Hamiltonian H is evaluated at a mean value of its argument. This provides a direct estimation of the kinetic and potential contributions.

Virial theorem

The quantum virial theorem for an N -body Hamiltonian states [27]

$$\sum_{i=1}^N \left\langle \mathbf{p}_i \cdot \frac{\partial T_i(\mathbf{p}_i)}{\partial \mathbf{p}_i} \right\rangle_{\psi} = \sum_{i<j=2}^N \left\langle \mathbf{r}_{ij} \cdot \frac{\partial V_{ij}(\mathbf{r}_{ij})}{\partial \mathbf{r}_{ij}} \right\rangle_{\psi}. \quad (2.56)$$

Since the terms in (2.48) are constant, the application of the virial theorem on \tilde{H}_0 yields

$$\sum_{i=1}^N \frac{\langle p_i^2 \rangle_{\alpha_0}}{\mu_{i0}} = 2 \sum_{i<j=2}^N \rho_{ij0} \langle r_{ij}^2 \rangle_{\alpha_0}. \quad (2.57)$$

The auxiliary fields $\{\alpha_0\}$ can be eliminated using the relations (2.53) and definitions (2.45)

$$T'_i(p_{i0}) = \frac{p_{i0}}{\mu_{i0}}, \quad (2.58a)$$

$$V'_{ij}(r_{ij0}) = 2\rho_{ij0} r_{ij0}. \quad (2.58b)$$

Equation (2.57) then implies

$$\sum_{i=1}^N p_{i0} T'_i(p_{i0}) = \sum_{i<j=2}^N r_{ij0} V'_{ij}(r_{ij0}). \quad (2.59)$$

Identical particles

In the most general case, one must determine N parameters μ_{i0} and C_N^2 parameters ρ_{ij0} through the minimisation equations (2.50). However, if two particles numbered i and j are identical, then

$$p_{i0}^2 = \langle \alpha_0 | p_i^2 | \alpha_0 \rangle = \langle \alpha_0 | \hat{P}_{ij}^\dagger \left(\hat{P}_{ij}^{-1} p_i^2 \hat{P}_{ij} \right) \hat{P}_{ij} | \alpha_0 \rangle = \langle \alpha_0 | p_j^2 | \alpha_0 \rangle = p_{j0}^2, \quad (2.60)$$

where the properties of the permutation operator \hat{P}_{ij}^{-1} and the (anti-)symmetry of the state $|\alpha_0\rangle$ under the exchange of the particles i and j have been used. Relations (2.58) then imply

$$\mu_{i0} = \frac{p_{i0}}{T'_i(p_{i0})} = \frac{p_{j0}}{T'_j(p_{j0})} = \mu_{j0}, \quad (2.61)$$

since $T_i = T_j$ for identical particles. It is then clear that parameters $\{\mu_{i0}\}$ are all equal for a set of identical particles. If $\{i, j, k, l\}$ number any set of identical particles in the system and h numbers a different one, similar calculations show that $\rho_{ih0} = \rho_{jh0}$ and $\rho_{ij0} = \rho_{kl0}$. Many parameters are equal when the system contains identical particles, which can drastically reduce the number of equations (2.50) to solve.

If all particles are identical ($T_i = T, V_{ij} = V$), then one is left with only two parameters $\{\mu_0, \rho_0\}$ to find. The symmetry of the wavefunction also implies $p_{i0} = p_0$ and $r_{ij0} = r_0 \forall i, j$.

¹In particular, \hat{P}_{ij}^\dagger is hermitian $\hat{P}_{ij}^\dagger = \hat{P}_{ij}$ and unitary $\hat{P}_{ij}^\dagger = \hat{P}_{ij}^{-1}$, implying $\hat{P}_{ij}^{-1} = \hat{P}_{ij}$.

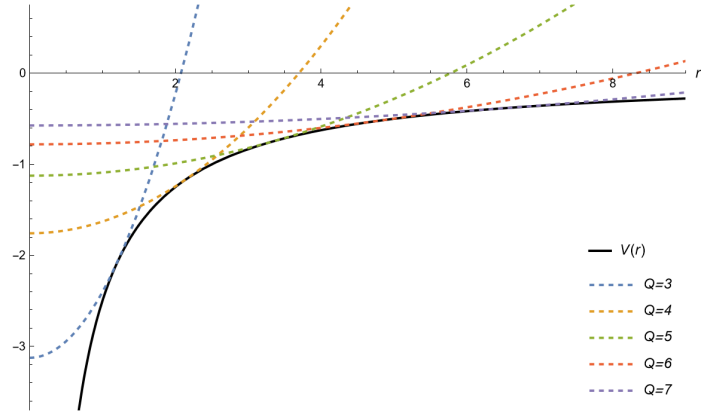


Figure 2.1: Example of envelopes for a three-dimensional and three-body system with kinematics $T(p) = p^2/2$ and potential $V(r) = -2.5/r$. In black straight line, the potential is plotted and in coloured dashed lines, the auxiliary potential for various values of Q , as defined by (2.27), from 3 to 7.

Equations (2.55) and (2.59) then reduce to

$$\tilde{E}_0 = NT(p_0) + C_N^2 V(r_0), \quad (2.62)$$

$$Np_0 T'(p_0) = C_N^2 r_0 V'(r_0). \quad (2.63)$$

Possible bounds

According to equations (2.53) and (2.58), the auxiliary kinetic part can be written as

$$\tilde{T}_i(p_i) = T_i(p_{i0}) + \frac{T'_i(p_{i0})}{2p_{i0}}(p_i^2 - p_{i0}^2). \quad (2.64)$$

This indicates that

$$\tilde{T}_i(p_{i0}) = T_i(p_{i0}) \text{ and } \tilde{T}'_i(p_{i0}) = T'_i(p_{i0}), \quad (2.65)$$

implying that the auxiliary kinetic parts \tilde{T}_i are tangent to the original kinetic parts T_i at $p_i = p_{i0}$, at least. Since the quantity p_{i0} is determined by the set $\{\alpha_0\}$, it depends on the quantum numbers of the system. All the tangent functions \tilde{T}_i for all possible quantum numbers form an *envelope* of the kinetic parts T_i . Similar envelopes can be obtained for the potential V_{ij} through analogous reasoning. An example of such envelopes is illustrated in Fig. 2.1. This is actually the procedure first developed to create the envelope theory and the origin of its name [28, 29].

The primary interest of these envelopes lies in examining the potential variational character of the method. Define a function b_i^T such that $b_i^T(x^2) = T_i(x)$. Then, equation (2.64) can be rewritten as

$$\tilde{b}_i^T(p_i^2) = b_i^T(p_{i0}^2) + b_i^{T'}(p_{i0}^2)(p_i^2 - p_{i0}^2), \quad (2.66)$$

which represents the equation of the tangent to the function b_i^T . If b_i^T is a concave (convex) function over the entire domain of interest, then $b_i^T(p^2) = T_i(p)$ is less (greater) than its tangent $\tilde{b}_i^T(p^2) = \tilde{T}_i(p)$ in each point. Similarly, we can define $b_{ij}^V(x^2) = V_{ij}(x)$. If $b_{ij}^V(x)$ is a concave (convex) function, then $V_{ij}(r_{ij})$ is less (greater) than $\tilde{V}_{ij}(r_{ij})$ everywhere, respectively.

Assume now that all b functions are all concave simultaneously. In this case, $T_i \leq \tilde{T}_i$ and $V_{ij} \leq \tilde{V}_{ij}$ everywhere. The comparison theorem [30] then states $\tilde{E} \leq E$, meaning the ET provides a lower bound for the energy. Conversely, if all b functions are convex, then the result of the ET is an upper bound. This is a recipe to determine the variational character of the method. If one of the functions is neither concave nor convex over its entire domain, or the functions do not share the same concavity simultaneously, it becomes impossible to determine the bound of the ET.

A special case arises when identifying the bound. If a term in the Hamiltonian is quadratic in its argument, the associated b function is a constant, neither concave nor convex. Since this term is identical to that in a harmonic oscillator, the associated auxiliary field vanishes, and thus this term does not contribute to the above discussion.

2.3.2 Compact equations for identical particles

The determination of the auxiliary parameters through equations (2.50) can be cumbersome due to the complexity of computing the functions G_i and J_{ij} in (2.48). However, for the case of identical particles, we have demonstrated that the approximated eigenvalue \tilde{E}_0 can be determined by two variables, p_0 and r_0 , as shown in equation (2.62). While equation (2.63) provides one relation for these variables, an additional equation is needed. Given the known exact eigenvalue of the harmonic oscillator Hamiltonian, we compute

$$\langle H_{\text{ho}}(\alpha_0) \rangle_{\alpha_0} = N \frac{p_0^2}{2\mu_0} + C_N^2 \rho_0 r_0^2 = \sqrt{\frac{2}{\mu_0}} N \rho_0 Q(N). \quad (2.67)$$

Applying the virial theorem on $H_{\text{ho}}(\alpha_0)$ yields

$$N \frac{p_0^2}{\mu_0} = 2\rho_0 C_N^2 r_0^2 \Leftrightarrow \rho_0 = \frac{N p_0^2}{2\mu_0 C_N^2 r_0^2}. \quad (2.68)$$

Inserting this result into the previous equation gives

$$\frac{N p_0^2}{2\mu_0} + C_N^2 \frac{N p_0^2}{2\mu_0 C_N^2 r_0^2} r_0^2 = \sqrt{\frac{2}{\mu_0}} N \frac{N p_0^2}{2\mu_0 C_N^2 r_0^2} Q(N), \quad (2.69)$$

which simplifies to the relation between p_0 and r_0

$$Q(N) = \sqrt{C_N^2} p_0 r_0. \quad (2.70)$$

The resulting set of three equations

$$\tilde{E}_0 = NT(p_0) + C_N^2 V(r_0), \quad (2.71a)$$

$$Np_0 T'(p_0) = C_N^2 r_0 V'(r_0), \quad (2.71b)$$

$$Q(N) = \sqrt{C_N^2} p_0 r_0, \quad (2.71c)$$

is equivalent to solving the minimisation equations (2.50) but without the need to compute the functions (2.45). The variables p_0 and r_0 also leads to interesting mean values. Hence, equations (2.71) will be referred to as the *compact equations* of the envelope theory. Additionally, these equations exhibit a semi-classical interpretation, as will be seen in the next section. A simple verification of these equations can be performed by applying them to the harmonic oscillator Hamiltonian and confirming that the exact solution (2.26) is recovered.

One-body forces

Consider a one-body potential $U_i(s_i)$, with $s_i = |\mathbf{r}_i - \mathbf{R}|$, in the original Hamiltonian H . Since the harmonic oscillator can be solved with such type of potential, the envelope theory can be adapted. First, a new set of auxiliary parameters $\{\nu_i\}$ is introduced and a term [26]

$$\sum_{i=1}^N \tilde{U}_i(s_i) = \sum_{i=1}^N [\nu_i s_i^2 + U_i(I_i(\nu_i)) - \nu_i I_i^2(\nu_i)], \quad (2.72)$$

is added to the auxiliary Hamiltonian (2.44). Here, I_i is defined similarly to the functions in (2.45). The auxiliary parameters are determined by minimising the energy \tilde{E} .

Using the Hellmann-Feynman theorem, we define new variables

$$I_i^2(\nu_{i0}) = \langle s_i^2 \rangle_{\alpha_0} \equiv s_{i0}^2. \quad (2.73)$$

When all particles are identical ($U_i = U$), the symmetry of the state $|\alpha_0\rangle$ implies $\nu_{i0} = \nu_0$ and $s_{i0} = s_0 \forall i$. It seems now that a new compact equation has to be determined in order to compute s_0 . However, it is not necessary as s_0 and r_0 are related, as we shall see. First, one can show

$$\sum_{i=1}^N \mathbf{s}_i^2 = \frac{1}{N} \sum_{i<j=2}^N (\mathbf{s}_i - \mathbf{s}_j)^2 = \frac{1}{N} \sum_{i<j=2}^N (\mathbf{r}_i - \mathbf{r}_j)^2, \quad (2.74)$$

where the first equality is obtained from $\sum_i^N \mathbf{s}_i = \mathbf{0}$. Hence,

$$\left\langle \sum_{i=1}^N s_i^2 \right\rangle_{\alpha_0} = N \langle s_i^2 \rangle_{\alpha_0} = \frac{1}{N} \left\langle \sum_{i<j=2}^N r_{ij}^2 \right\rangle_{\alpha_0} = \frac{C_N^2}{N} \langle r_{ij}^2 \rangle_{\alpha_0}, \quad (2.75)$$

leading to

$$2N \langle s_i^2 \rangle_{\alpha_0} = (N-1) \langle r_{ij}^2 \rangle_{\alpha_0}. \quad (2.76)$$

This shows the variables s_0 and r_0 are related for identical particles. The compact equations (2.71), with the inclusion of one-body forces, now read

$$\tilde{E}_0 = NT(p_0) + NU \left(\sqrt{\frac{N-1}{2N}} r_0 \right) + C_N^2 V(r_0), \quad (2.77a)$$

$$Np_0 T'(p_0) = \sqrt{C_N^2} r_0 U' \left(\sqrt{\frac{N-1}{2N}} r_0 \right) + C_N^2 r_0 V'(r_0), \quad (2.77b)$$

$$Q(N) = \sqrt{C_N^2} p_0 r_0. \quad (2.77c)$$

Note that the last equation remains unchanged when including one-body forces. In some references [26, 31], the variable $d_0 = N s_0$ was used so that $\langle s_i^2 \rangle_{\alpha_0} = d_0^2 / N^2$.

***K*-body forces**

Instead of two-body forces V , one can consider K -body forces W . In the case of identical particles, the harmonic oscillator Hamiltonian can be solved with K -body forces of the form (2.30), so the ET can be adapted. For notation convenience, we denote the set of K particles among N as $\{i_1, \dots, i_K\} = \{K\}$ and the variable $r_{\{i_1, \dots, i_K\}} = r_K$. The auxiliary Hamiltonian \tilde{H} is then modified by introducing a new auxiliary parameter κ in the auxiliary potential [26]

$$\sum_{\{K\}} \tilde{W}_K(r_K) = \sum_{\{K\}} [\kappa r_K^2 + W(Y(\kappa)) - \kappa Y^2(\kappa)], \quad (2.78)$$

where Y is a function defined similarly to (2.45). The determination of κ_0 is usually done by solving a minimisation equation of the energy. However, this new auxiliary parameter is related to ρ_0 . By applying the Hellmann-Feynman theorem for this new parameter, we find $Y^2(\kappa_0) = \langle r_K^2 \rangle_{\alpha_0}$. From the definition (2.30), it is straightforward to show $\langle r_K^2 \rangle_{\alpha_0} = C_K^2 \langle r_{ij}^2 \rangle_{\alpha_0} = C_K^2 r_0^2$.

To adapt the compact equations for handling K -body forces, we proceed as follows

1. Add the term $C_N^K W(\sqrt{C_K^2} r_0)$ to the energy expression (2.71a).
2. Add the term $C_N^K \sqrt{C_K^2} r_0 W'(\sqrt{C_K^2} r_0)$ to equation (2.71b).
3. The last compact equation (2.71c) remains unchanged.

Following this procedure allows us to incorporate any number of additional K' -body forces.

2.3.3 Compact equations for two sets of identical particles

In the previous section, the spectrum of the many-body harmonic oscillator was computed for a configuration of two sets, denoted a and b , of identical particles. This configuration is of particular interest, so the compact equations of the ET will be developed for such systems. Due to the symmetry of the system, only five auxiliary parameters need to be determined through (2.50), namely $\{\mu_a, \mu_b, \rho_{aa}, \rho_{bb}, \rho_{ab} = \rho_{ba}\}$. Equations (2.55) and (2.59) remain valid, but new equations must be determined to compute all auxiliary parameters.

To determine the compact equations, we rearrange the auxiliary Hamiltonian by following the decomposition of the harmonic oscillator in (2.35)

$$\begin{aligned}
H_{\text{ho}}(\{\alpha\}) &= \sum_{i=1}^{N_a} \frac{p_i^2}{2\mu_a} - \frac{\mathbf{P}_a^2}{2N_a\mu_a} + \sum_{i<i'=2}^{N_a} \left(\rho_{aa} + \frac{N_b}{N_a} \rho_{ab} \right) r_{ii'}^2 \\
&\quad + \sum_{j=1}^{N_b} \frac{p_j^2}{2\mu_b} - \frac{\mathbf{P}_b^2}{2N_b\mu_b} + \sum_{j<j'=2}^{N_b} \left(\rho_{bb} + \frac{N_a}{N_b} \rho_{ab} \right) r_{jj'}^2, \\
&\quad + \frac{p^2}{2} \frac{N_a\mu_a + N_b\mu_b}{N_a N_b \mu_a \mu_b} + N_a N_b \rho_{ab} r^2,
\end{aligned} \tag{2.79}$$

where indices i refer to the set a and indices j to the set b . We also recall that \mathbf{p} and \mathbf{r} are the relative momentum and distance between the CM of each sets, respectively. To be complete, the function $B(\{\alpha\})$ is given by

$$\begin{aligned}
B(\{\alpha\}) &= N_a \left[T_a(G_a(\mu_a)) - \frac{G_a^2(\mu_a)}{2\mu_a} \right] + N_b \left[T_b(G_b(\mu_b)) - \frac{G_b^2(\mu_b)}{2\mu_b} \right] \\
&\quad + C_{N_a}^2 [V_{aa}(J_{aa}(\rho_{aa})) - \rho_{aa} J_{aa}^2(\rho_{aa})] \\
&\quad + C_{N_b}^2 [V_{bb}(J_{bb}(\rho_{bb})) - \rho_{bb} J_{bb}^2(\rho_{bb})] \\
&\quad + N_a N_b [V_{ab}(J_{ab}(\rho_{ab})) - \rho_{ab} J_{ab}^2(\rho_{ab})].
\end{aligned} \tag{2.80}$$

Applying the Hellmann-Feynman theorem for each auxiliary parameter yields the following relations [32]

$$G_a^2(\mu_{a0}) = p_{a0}'^2 + \frac{P_0^2}{N_a^2} \text{ and } G_b^2(\mu_{b0}) = p_{b0}'^2 + \frac{P_0^2}{N_b^2}, \tag{2.81a}$$

$$J_{aa}^2(\rho_{aa0}) = r_{aa0}^2 \text{ and } J_{bb}^2(\rho_{bb0}) = r_{bb0}^2, \tag{2.81b}$$

$$J_{ab}^2(\rho_{ab0}) = \frac{N_a - 1}{2N_a} r_{aa0}^2 + \frac{N_b - 1}{2N_b} r_{bb0}^2 + R_0^2, \tag{2.81c}$$

where the six physical quantities are defined by

$$p_{a0}'^2 \equiv \left\langle p_i^2 - \frac{P_a^2}{N_a^2} \right\rangle \text{ and } p_{b0}'^2 \equiv \left\langle p_j^2 - \frac{P_b^2}{N_b^2} \right\rangle, \tag{2.82a}$$

$$P_0^2 \equiv \langle p^2 \rangle, \tag{2.82b}$$

$$r_{aa0}^2 \equiv \langle r_{ii'}^2 \rangle \text{ and } r_{bb0}^2 \equiv \langle r_{jj'}^2 \rangle, \tag{2.82c}$$

$$R_0^2 \equiv \langle r^2 \rangle, \tag{2.82d}$$

where the mean values are taken between a symmetrised eigenstate $|\alpha_0\rangle$ of the auxiliary Hamiltonian. Comparison between results (2.81) and (2.53) shows the following relations

$$\langle p_i^2 \rangle = p_{a0}^2 = p_{a0}'^2 + \frac{P_0^2}{N_a^2} \text{ and } \langle p_j^2 \rangle = p_{b0}^2 = p_{b0}'^2 + \frac{P_0^2}{N_b^2}, \tag{2.83a}$$

$$\langle r_{ij}^2 \rangle = r_{ab0}^2 = \frac{N_a - 1}{2N_a} r_{aa0}^2 + \frac{N_b - 1}{2N_b} r_{bb0}^2 + R_0^2, \tag{2.83b}$$

which can also be obtained starting from the mean values definitions. In the following, to lighten the notation, the index 0 will be omitted. Substituting relations (2.81) into $\langle \tilde{H}_0 \rangle$ leads to

$$\tilde{E}_0 = N_a T_a(p_a) + N_b T_b(p_b) + C_{N_a}^2 V_{aa}(r_{aa}) + C_{N_b}^2 V_{ab}(r_{bb}) + N_a N_b V_{ab}(r_{ab}). \quad (2.84)$$

Equation (2.55) is retrieved, as expected, but it is important to keep in mind that the variables p_a, p_b and r_{ab} are given by (2.83). The importance of the decomposition (2.35) is to write the harmonic oscillator Hamiltonian as a sum of decoupled Hamiltonians H_a, H_b and H_{CM} . Thanks to this property, the virial theorem can be applied separately to each line of (2.79), leading to

$$N_a T'_a(p_a) \frac{p_a'^2}{p_a} = C_{N_a}^2 V'_{aa}(r_{aa}) r_{aa} + \frac{N_b}{N_a} C_{N_a}^2 V'_{ab}(r_{ab}) \frac{r_{aa}^2}{r_{ab}}, \quad (2.85a)$$

$$N_b T'_b(p_b) \frac{p_b'^2}{p_b} = C_{N_b}^2 V'_{bb}(r_{bb}) r_{bb} + \frac{N_a}{N_b} C_{N_b}^2 V'_{ab}(r_{ab}) \frac{r_{bb}^2}{r_{ab}}, \quad (2.85b)$$

$$\frac{1}{N_a} T'_a(p_a) \frac{P_0^2}{p_a} + \frac{1}{N_b} T'_b(p_b) \frac{P_0^2}{p_b} = N_a N_b V'_{ab}(r_{ab}) \frac{R_0^2}{r_{ab}}. \quad (2.85c)$$

Finally, three equations are obtained by comparing the exact spectrum of the harmonic oscillator for this system (2.39) to $\langle H_{ho}(\{\alpha_0\}) \rangle$. Using the decomposition (2.35), a similar procedure as (2.67) is applied, leading to

$$Q(N_a) = \sqrt{C_{N_a}^2 p'_a r_{aa}}, \quad (2.86a)$$

$$Q(N_b) = \sqrt{C_{N_b}^2 p'_b r_{bb}}, \quad (2.86b)$$

$$Q(2) = P_0 R_0. \quad (2.86c)$$

The seven equations (2.84), (2.85), and (2.86), along with relations (2.83), form the compact equations of the ET for two sets of identical particles [32]. As in the case of identical particles, these compact equations can be checked to lead to the correct spectrum of the harmonic oscillator. The compact equations for identical particles (2.71) are also retrieved when assuming all particles are identical, with $p_a = p_b$ and $r_{aa} = r_{bb} = r_{ab}$.

N_a and/or $N_b = 1$

The seven compact equations (2.84), (2.85), and (2.86) were derived for a system comprising $N_a + N_b$ particles. It is insightful to examine the scenario where only a single particle is present in one set, for instance, $N_b = 1$. In this case, all the terms in $C_{N_b}^2$ and $Q(N_b)$ vanish. Consequently, the second equation in (2.86) becomes trivial, and the second equation of (2.85) results in $p'_b = 0$. This outcome further implies $p_b = P_0$. Ultimately, only five equations remain

$$\tilde{E}_0 = N_a T_a(p_a) + T_b(P_0) + C_{N_a}^2 V_{aa}(r_{aa}) + N_a V_{ab}(r_{ab}), \quad (2.87a)$$

$$N_a T'_a(p_a) \frac{p_a^2}{p_a} = C_{N_a}^2 V'_{aa}(r_{aa}) r_{aa} + \frac{N_a - 1}{2} V'_{ab}(r_{ab}) \frac{r_{aa}^2}{r_{ab}}, \quad (2.87b)$$

$$\frac{1}{N_a} T'_a(p_a) \frac{P_0^2}{p_a} + T'_b(P_0) P_0 = N_a V'_{ab}(r_{ab}) \frac{R_0^2}{r_{ab}}, \quad (2.87c)$$

$$Q(N_a) = \sqrt{C_{N_a}^2 p_a' r_{aa}}, \quad (2.87d)$$

$$Q(2) = P_0 R_0. \quad (2.87e)$$

The five equations (2.87) can also be derived from scratch using the aforementioned procedure.

Another notable case occurs when $N_a = N_b = 1$, resulting in a two-body system. Similar simplifications arise as in the previous case, leading to the compact equations of the ET for $N = 2$, which generalise the results obtained in [33, 34]

$$\tilde{E}_0 = T_a(P_0) + T_b(P_0) + V_{ab}(R_0), \quad (2.88a)$$

$$T'_a(P_0) P_0 + T'_b(P_0) P_0 = V'_{ab}(R_0) R_0, \quad (2.88b)$$

$$Q(2) = P_0 R_0. \quad (2.88c)$$

2.4 Improved envelope theory

As presented in the previous section, the envelope theory (ET) is an approximation method based on the exact solution of the many-body harmonic oscillator. The approximate spectrum depends on a characteristic global quantum number Q , whose common structure given by (2.27) implies a strong degeneracy of the levels, inherited from the harmonic oscillator. For arbitrary potentials, this degeneracy is, of course, absent, resulting in less accurate results for the ET. One potential improvement to the method involves modifying the structure of Q to (partially) break this degeneracy. Consider the modified global quantum number

$$Q_\phi = \phi \nu + \lambda \text{ with} \quad (2.89)$$

$$\nu = \sum_{i=1}^{N-1} \left(n_i + \frac{1}{2} \right) \text{ and } \lambda = \sum_{i=1}^{N-1} \left(l_i + \frac{D-2}{2} \right),$$

where ϕ is a parameter that depends on the considered system but not on the quantum numbers $\{n_i, l_i\}$. The choice for this modified quantum number originates from [35] where an effective quantum number for centrally symmetric two-body systems was found

$$q = \phi(n + 1/2) + l + (D - 2)/2. \quad (2.90)$$

Owing to this structure, λ can be interpreted as a purely orbital global quantum number and is not affected by the parameter ϕ . The goal now is to determine a procedure for computing ϕ . One approach is to fit the ET result to experimental data or more accurate results [36]. However, an approach independent of the

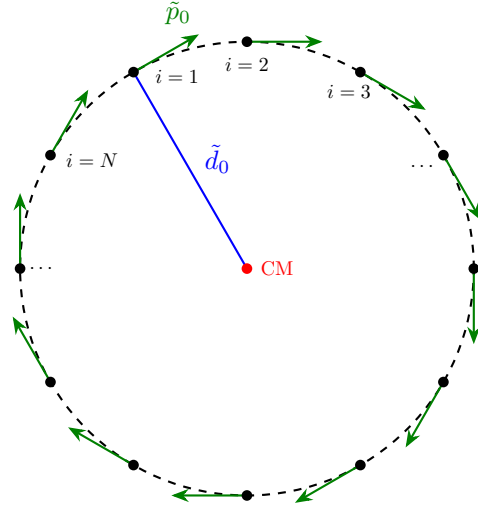


Figure 2.2: Example of a purely orbital motion of N particles, where \tilde{p}_0 denotes the mean momentum of the particles and \tilde{d}_0 the mean distance from the centre of mass (CM).

existence of accurate solutions is more desirable. Before presenting such an approach in Sec. 2.4.1, it is important to note that setting $\phi = 2$ recovers the original global quantum number Q and, consequently, the original ET.

2.4.1 Dominantly orbital state method

The dominantly orbital state (DOS) method is an approximation technique for solving the many-body Schrödinger equation. As its name implies, this method is based on states with high angular momentum. Initially, the DOS method was developed for two-body systems [37] and later generalised to N -body systems in [38]. Below, we briefly outline the main steps involved in constructing the DOS method.

1. Consider a classical system of N particles in purely symmetrical orbital motion, as represented in Fig. 2.2. Let \tilde{p}_0 denotes the mean momentum of the particles, \tilde{r}_0 the mean distance between each particle, and \tilde{d}_0 the mean distance from the centre of mass (the centre of the circle). The energy of the system is given by $E = NT(\tilde{p}_0) + C_N^2 V(\tilde{r}_0)$. The total angular momentum of the system is $L = N\tilde{p}_0 \tilde{d}_0$, which, after geometrical considerations [34], can be approximated as $L \approx \sqrt{C_N^2} \tilde{p}_0 \tilde{r}_0$ (for $N = 3$, this approximation is exact).

Careful readers will notice that these equations are similar to the compact equations of the ET for identical particles (2.71), but with the global quantum number Q replaced by the total angular momentum. The second compact equation (2.71b) can also be derived classically from considerations on the balance of forces [34]. From this discussion, we conclude that the compact equations of the ET have a semi-classical interpretation and correspond to the equations of the DOS method for N -body systems

$$\tilde{E} = NT(\tilde{p}_0) + C_N^2 V(\tilde{r}_0), \quad (2.91a)$$

$$N\tilde{p}_0 T'(\tilde{p}_0) = C_N^2 \tilde{r}_0 V'(\tilde{r}_0), \quad (2.91b)$$

$$\lambda = \sqrt{C_N^2 \tilde{p}_0 \tilde{r}_0}. \quad (2.91c)$$

Here, the total angular momentum has been assimilated to λ , the purely orbital part of the global quantum number. In the following, the notation $(\tilde{E}, \tilde{p}_0, \tilde{r}_0)$ will be used to denote the solutions of the compact equations with Q replaced by λ .

2. A small radial perturbation is introduced by replacing

$$\tilde{r}_0 \rightarrow \tilde{r}_0 + \Delta r \text{ and } \tilde{p}_0 \rightarrow \sqrt{p_r^2 + \frac{\lambda^2}{C_N^2 (\tilde{r}_0 + \Delta r)^2}}, \quad (2.92)$$

where p_r is the radial momentum, and we assume $\Delta r \ll \tilde{r}_0$ and $p_r \ll \tilde{p}_0$ to ensure the motion remains in a dominantly orbital state. Next, a Taylor expansion in Δr and p_r up to the first non-vanishing order is applied to (2.91a), leading to the radial contribution of the energy

$$\begin{aligned} \Delta E &\approx \frac{1}{2\mu} p_r^2 + \frac{k}{2} \Delta r^2 \text{ with} \\ \mu &= \frac{\tilde{p}_0}{NT'(\tilde{p}_0)}, \\ k &= \frac{2N\tilde{p}_0}{\tilde{r}_0^2} T'(\tilde{p}_0) + \frac{N\tilde{p}_0^2}{\tilde{r}_0^2} T''(\tilde{p}_0) + C_N^2 V''(\tilde{r}_0). \end{aligned} \quad (2.93)$$

Note that the terms linear in Δr are cancelled due to equation (2.91b).

3. The system is quantised by interpreting ΔE as a Hamiltonian and assuming p_r is the conjugate variable of Δr . This choice of conjugate variables is not straightforward since p_r and Δr are effective collective variables, and one could multiply p_r by some constants. This issue will be addressed later. By quantising the system, ΔE becomes a one-dimensional harmonic oscillator Hamiltonian whose eigenvalue is

$$\Delta E \approx \sqrt{\frac{k}{\mu}} (n + 1/2), \quad (2.94)$$

where n is an effective radial quantum number for the collective motion. Equation (2.94) can be tested on the N -body harmonic oscillator, where $T(p) = p^2/(2\mu)$ and $V(r) = kr/2$. The exact solution is retrieved by imposing

$$\sqrt{C_N^2} (n + 1/2) = \nu, \quad (2.95)$$

which allows an identification between the effective quantum number n and the individual quantum numbers $\{n_i\}$ in ν . This identification better

justifies the choice of the conjugate variable of Δr . If one considers another conjugate variable as in [38], the above identification would be different but the same result is obtained for ΔE . The complete solution for the DOS method is then $\tilde{E} + \Delta E$.

2.4.2 Coupling of the ET and the DOS method

The parameter ϕ in the modified global quantum number Q_ϕ , given by (2.89), is determined by comparing the modified ET, which has Q replaced by Q_ϕ , with the DOS method. For this comparison, the ET equations must be written under the same conditions as the DOS ones, i.e. for a dominantly orbital state. Rewriting the modified global quantum number as

$$Q_\phi = \lambda(1 + \epsilon) \text{ with } \epsilon = \phi \nu / \lambda, \quad (2.96)$$

the case $\epsilon = 0$ corresponds to a purely orbital state, and the associated solutions of the ET are $(\tilde{p}_0, \tilde{r}_0)$. A radial perturbation is achieved if $\epsilon \ll 1$, and so a Taylor expansion of the ET equations up to the first non-vanishing order in ϵ leads to the radial contribution

$$\Delta E \approx N \tilde{p}_0 T'(\tilde{p}_0) \epsilon. \quad (2.97)$$

Since the contribution (2.97) has been computed under the same conditions as (2.94), both results can be equated, leading to a formula for computing ϕ

$$\phi = \frac{\lambda}{N \tilde{p}_0 T'(\tilde{p}_0)} \sqrt{\frac{k}{C_N^2 \mu}}. \quad (2.98)$$

This value has been determined under specific conditions where the radial motion has a small contribution to the energy relative to the orbital motion, because it is computable with the DOS method. However, since the structure of ϕ is assumed to be valid for any quantum numbers, (2.98) can, in principle, be used for any state considered.

To summarise, the procedure for using the improved envelope theory (IET) is as follows

1. Specify the quantum numbers $\{n_i, l_i\}$ of the system, leading to the value of λ .
2. Solve the ET equations for a purely orbital motion, that is to say with $Q \rightarrow \lambda$, leading to the solutions $(\tilde{p}_0, \tilde{r}_0)$.
3. Compute the parameter ϕ via (2.98).
4. Solve the ET equations a second time with the modified global quantum number $Q \rightarrow Q_\phi$.

2.4.3 Generalisation to different particles

Since the ET has been generalised to systems with different particles, it seems natural to do the same for the IET. For simplicity, let us focus on systems consisting of N_a identical particles of type a and a single different particle of

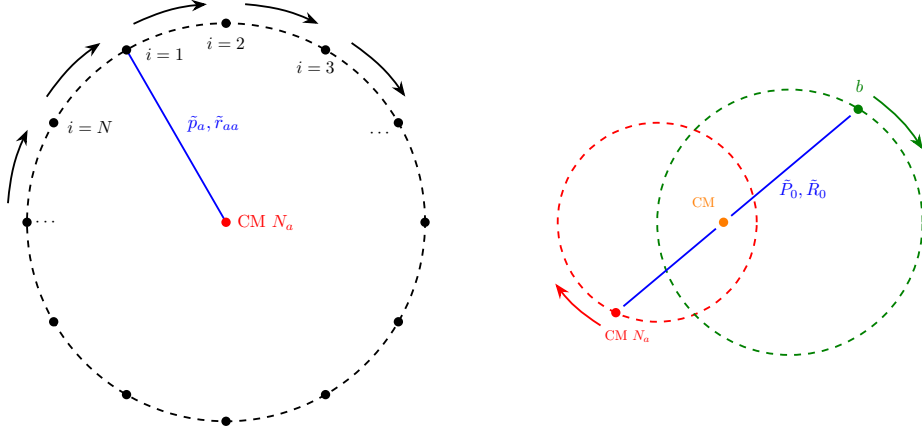


Figure 2.3: Semi-classical interpretation of the compact equations of the ET for a system of $N_a + 1$ particles. On the left, an orbital motion of the N_a identical particles, with a mean momentum \tilde{p}_a and distance \tilde{r}_{aa} . On the right, a decoupled orbital motion between the single particle b and the CM of the N_a particles, with a relative momentum \tilde{P}_0 and distance \tilde{R}_0 .

type b . The associated compact equations of the ET are given by the five equations (2.87). First, the two global quantum numbers $Q(N_a)$ and $Q(2)$ are modified by introducing two parameters ϕ_a and ϕ_b as follows

$$Q_\phi(N_a) = \phi_a \nu_a + \lambda_a \text{ with} \\ \nu_a = \sum_{i=1}^{N_a-1} \left(n_i + \frac{1}{2} \right) \text{ and } \lambda_a = \sum_{i=1}^{N_a-1} \left(l_i + \frac{D-2}{2} \right), \quad (2.99)$$

$$Q_\phi(2) = \phi_b \nu_b + \lambda_b \text{ with} \\ \nu_b = n_b + \frac{1}{2} \text{ and } \lambda_b = l_b + \frac{D-2}{2}. \quad (2.100)$$

Next, the DOS equations for $N_a + 1$ particles have to be established in a similar fashion as for the identical particles case

1. Starting from the compact equations (2.87), one can demonstrate [39] that they exhibit a semi-classical interpretation when $Q(N_a)$ is replaced by λ_a and $Q(N_b)$ is replaced by λ_b . This corresponds to an orbital motion of the N_a identical particles and a decoupled orbital motion between the single particle b and the CM of the N_a particles. This configuration is depicted in Fig. 2.3. An energy \tilde{E} is then computed with the associated parameters $(\tilde{p}'_a, \tilde{r}_{aa}, \tilde{P}_0, \tilde{R}_0)$.
2. Radial motions are introduced as small perturbations by computing the energy from (2.87a) with the following replacements

$$\tilde{r}_{aa} \rightarrow \tilde{r}_{aa} + \Delta r \text{ and } \tilde{p}'_a \rightarrow \sqrt{p_r^2 + \frac{\lambda_a^2}{C_{N_a}^2 (\tilde{r}_{aa} + \Delta r)^2}}, \quad (2.101a)$$

$$\tilde{R}_0 \rightarrow \tilde{R}_0 + \Delta R \text{ and } \tilde{P}_0 \rightarrow \sqrt{P_r^2 + \frac{\lambda_b^2}{(\tilde{R}_0 + \Delta R)^2}}. \quad (2.101b)$$

Assuming $\Delta r \ll \tilde{r}_{aa}$, $p_r \ll \tilde{p}'_a$, $\Delta R \ll R_0$ and $P_r \ll P_0$, a power expansion in these variables is applied to \tilde{E} , up to the first non-vanishing order, leading to the radial contribution of the energy [39]

$$\Delta E \approx \frac{1}{2} \left(\frac{1}{\mu_a} p_r^2 + \frac{1}{\mu_b} P_r^2 + k_a \Delta r^2 + k_b \Delta R^2 + k_c \Delta r \Delta R \right), \quad (2.102)$$

with

$$\mu_a = \frac{\tilde{p}_a}{N_a T'_a(\tilde{p}_a)}, \quad (2.103a)$$

$$\mu_b = \left(\frac{T'_a(\tilde{p}_a)}{N_a \tilde{p}_a} + \frac{T'_b(\tilde{P}_0)}{\tilde{P}_0} \right)^{-1}, \quad (2.103b)$$

$$\begin{aligned} k_a = & \frac{N_a T''_a(\tilde{p}_a) \tilde{p}_a^4}{\tilde{r}_{aa}^2 \tilde{p}_a^2} + \frac{N_a T'_a(\tilde{p}_a) \tilde{p}_a^2}{\tilde{r}_{aa}^2} \left(\frac{3}{\tilde{p}_a} - \frac{\tilde{p}_a^2}{\tilde{p}_a^3} \right) \\ & + C_{N_a}^2 V''_{aa}(\tilde{r}_{aa}) + \frac{(N_a - 1)^2 \tilde{r}_{aa}^2}{4 N_a \tilde{r}_{ab}^2} V''_{ab}(\tilde{r}_{ab}) \\ & + \frac{(N_a - 1)}{2} \left(\frac{1}{\tilde{r}_{ab}} - \frac{(N_a - 1) \tilde{r}_{aa}^2}{2 N_a \tilde{r}_{ab}^3} \right) V'_{ab}(\tilde{r}_{ab}), \end{aligned} \quad (2.103c)$$

$$\begin{aligned} k_b = & \frac{T''_a(\tilde{p}_a) \tilde{P}_0^4}{N_a^3 \tilde{R}_0^2 \tilde{p}_a^2} + \frac{T''_b(\tilde{P}_0) \tilde{P}_0^2}{\tilde{R}_0^2} + \frac{T'_a(\tilde{p}_a) \tilde{P}_0^2}{N_a \tilde{R}_0^2} \left(\frac{3}{\tilde{p}_a} - \frac{\tilde{P}_0^2}{N_a \tilde{p}_a^3} \right) \\ & + \frac{2 T'_b(\tilde{P}_0) \tilde{P}_0}{\tilde{R}_0^2} + \frac{N_a \tilde{R}_0^2}{\tilde{r}_{ab}^2} V''_{ab}(\tilde{r}_{ab}) \\ & + N_a \left(\frac{1}{\tilde{r}_{ab}} - \frac{\tilde{R}_0^2}{\tilde{r}_{ab}^3} \right) V'_{ab}(\tilde{r}_{ab}), \end{aligned} \quad (2.103d)$$

$$\begin{aligned} k_c = & \frac{2 \tilde{p}_a^2 \tilde{P}_0^2}{N_a \tilde{p}_a^2 \tilde{r}_{aa} \tilde{R}_0} \left(T''_a(\tilde{p}_a) - \frac{T'_a(\tilde{p}_a)}{\tilde{p}_a} \right) \\ & + \frac{(N_a - 1) \tilde{r}_{aa} \tilde{R}_0}{\tilde{r}_{ab}^2} \left(V''_{ab}(\tilde{r}_{ab}) - \frac{V'_{ab}(\tilde{r}_{ab})}{\tilde{r}_{ab}} \right). \end{aligned} \quad (2.103e)$$

Note there is no terms in Δr nor in ΔR , but a term $\Delta r \Delta R$ couples the two radial motions.

3. The energy ΔE is quantised by taking P_r and p_r as the conjugate variables of ΔR and Δr , respectively. Similar to the previous case, the choice of conjugate variables is not unique but will be justified later. The energy ΔE becomes that of two one-dimensional coupled oscillators, whose eigenvalue is [40]

$$\begin{aligned}
\Delta E &\approx \sqrt{\frac{A}{\mu}} \left(n + \frac{1}{2} \right) + \sqrt{\frac{B}{\mu}} \left(n' + \frac{1}{2} \right) \text{ with} \\
\mu &= \sqrt{\mu_a \mu_b}, \\
A &= \sqrt{\frac{\mu_b}{\mu_a}} k_a - \frac{k_c}{2} \left(\text{sgn}(\epsilon) \sqrt{1 + \epsilon^2} - \epsilon \right), \\
B &= \sqrt{\frac{\mu_a}{\mu_b}} k_b + \frac{k_c}{2} \left(\text{sgn}(\epsilon) \sqrt{1 + \epsilon^2} - \epsilon \right) \text{ and} \\
\epsilon &= \frac{1}{k_c} \left(\sqrt{\frac{\mu_a}{\mu_b}} k_b - \sqrt{\frac{\mu_b}{\mu_a}} k_a \right),
\end{aligned} \tag{2.104}$$

where $\text{sgn}(x)$ is the sign function.

4. Equations (2.104) are tested on the equivalent many-body harmonic oscillator, whose eigenvalues are known, leading to the following identification of the quantum numbers

$$\sqrt{C_{N_a}^2} \left(n + \frac{1}{2} \right) = \nu_a \text{ and } \left(n' + \frac{1}{2} \right) = \nu_b. \tag{2.105}$$

Once the DOS equations are known, the ET equations with $Q \rightarrow Q_\phi$ are computed in the same regime. The modified global quantum numbers are written as

$$Q_\phi(N_a) = \lambda_a(1 + \epsilon_a) \text{ with } \epsilon_a = \phi_a \nu_a / \lambda_a, \tag{2.106a}$$

$$Q_\phi(2) = \lambda_b(1 + \epsilon_b) \text{ with } \epsilon_b = \phi_b \nu_b / \lambda_b, \tag{2.106b}$$

so that the case $\epsilon_a = \epsilon_b = 0$ corresponds to a purely orbital state and $\epsilon_a, \epsilon_b \ll 1$ to a dominantly orbital state. The energy equation (2.87a) is then expanded to first order in ϵ_a and ϵ_b , yielding

$$\begin{aligned}
\Delta E &\approx D_a \frac{\phi_a}{\lambda_a} \sum_{i=1}^{N_a-1} \left(n_i + \frac{1}{2} \right) + D_b \frac{\phi_b}{\lambda_b} \left(n_b + \frac{1}{2} \right) \text{ with} \\
D_a &= T'_a(\tilde{p}_a) \frac{N_a \tilde{p}_a'^2}{\tilde{p}_a} \text{ and } D_b = T'_a(\tilde{p}_a) \frac{\tilde{P}_0^2}{N_a \tilde{p}_a} + T'_b(\tilde{P}_0) \tilde{P}_0.
\end{aligned} \tag{2.107}$$

The comparison between (2.104) and (2.107) leads to the expressions

$$\phi_a = \frac{\lambda_a}{D_a} \sqrt{\frac{A}{C_{N_a}^2 \mu}} \text{ and } \phi_b = \frac{\lambda_b}{D_b} \sqrt{\frac{B}{\mu}}, \tag{2.108}$$

where the quantities μ, A, B, D_a and D_b can be computed from the values of the solution $(\tilde{p}'_a, \tilde{r}_{aa}, \tilde{P}_0, \tilde{R}_0)$ fixed by the choice of the collective orbital quantum numbers λ_a and λ_b .

2.5 Example of results with the envelope theory

To conclude this chapter, we present some results computed using the ET and IET for systems with both identical and different particles. This will illustrate the main advantages and limitations of the method. A more exhaustive list of results derived with the ET and IET can be found in [31, 36, 38, 39, 41, 42].

2.5.1 Results for identical particles

Consider an N -body system of identical particles with a power-law kinematic and potential

$$T(p) = A p^\alpha \text{ and } V(r) = \text{sgn}(\beta) B r^\beta, \quad (2.109)$$

where A and B are positive constants, α is also positive to ensure the kinetic energy remains positive, and β can be either negative or positive. The sign function $\text{sgn}(x)$ ensures the potential is always attractive. This general form of the kinetic term allows for the treatment of non-relativistic kinematics with $A = 1/(2m)$ and $\alpha = 2$, as well as ultra-relativistic kinematics with $A = 1$ and $\alpha = 1$. Similarly, the potential form allows for various interactions such as linear ($\beta = 1$), quadratic ($\beta = 2$), or Coulomb ($\beta = -1$).

First, the compact equations for identical particles (2.71) are solved. By substituting (2.71c) into (2.71b), the following equation for r_0 is obtained

$$N \frac{Q(N)}{\sqrt{C_N^2 r_0}} A \alpha \left(\frac{Q(N)}{\sqrt{C_N^2 r_0}} \right)^{\alpha-1} = C_N^2 r_0 \text{sgn}(\beta) B \beta r_0^{\beta-1}, \quad (2.110)$$

with the solution given by

$$r_0 = \left(\frac{N \alpha A Q(N)^\alpha}{|\beta| B (\sqrt{C_N^2})^{\alpha+2}} \right)^{1/(\alpha+\beta)}. \quad (2.111)$$

This result is not merely an intermediate step in solving the compact equations but also provides an approximation for the mean value $\langle r^2 \rangle$ via (2.53). Substituting (2.111) back into (2.71a) yields the final approximate spectrum [39]

$$E = \text{sgn}(\beta)(\beta + \alpha) \left(\left(\frac{N A}{|\beta|} \right)^\beta \left(\frac{B C_N^2}{\alpha} \right)^\alpha \left(\frac{Q(N)}{\sqrt{C_N^2}} \right)^{\alpha\beta} \right)^{1/(\alpha+\beta)}. \quad (2.112)$$

As a consistency check, the exact spectrum of the harmonic oscillator (2.26) is recovered when $\alpha = \beta = 2$. This procedure for solving the compact equations is general and can sometimes yield analytical solutions, as in our example; otherwise, the equations can be solved numerically. A key advantage of the ET is that its equations and solutions can be computed for an arbitrary number of particles N , since N is a simple parameter in our equations, which is particularly useful in the large- N approach to quantum chromodynamics [43, 44].

The variational nature of the method can also be demonstrated. Following the recipe described in Sec. 2.3, we define two functions

β	Accurate	ET	IET
-1	-0.26675	-0.12500 [53]	-0.28125 [5.4]
-0.5	-0.59173	-0.49139 [17]	-0.59977 [1.4]
0.1	1.88019	1.91406 [1.8]	1.87743 [0.15]
0.5	2.91654	3.08203 [5.7]	2.90211 [0.49]
1	3.86309	4.08852 [5.8]	3.84130 [0.56]
2	5.19615	5.19615 [0]	5.19615 [0]
3	6.15591	5.68394 [7.7]	6.22479 [1.1]

Table 2.1: Bosonic ground state energies for the Hamiltonian (2.109) with $N = 3$, $\alpha = 2$, and $A = B = 0.5$, for various values of β (arbitrary units). The results from the ET and IET with (2.114) are compared with more accurate ones [45], obtained with an hyperspherical expansion. The relative errors in % are indicated in square brackets. For $\beta = 2$, the ET and IET yield the exact result, as expected.

$$b^T(p) = Ap^{\alpha/2} \text{ and } b^V(r) = \text{sgn}(\beta)Br^{\beta/2}. \quad (2.113)$$

Analysis of their concavity shows that for $\alpha, \beta < 2$, the b functions are concave, leading to a lower bound. For $\alpha, \beta > 2$, the b functions are convex, leading to an upper bound. If α or $\beta = 2$, the function is neither convex nor concave. Finally, if $\alpha < 2$ and $\beta > 2$ (or vice versa), the variational character of the ET is indeterminate.

Next, we apply the IET by computing the parameter ϕ via (2.98). The solution \tilde{r}_0 of the ET for purely orbital motion is required, corresponding to the solution (2.111) with $Q(N)$ replaced by λ . Substituting this result into (2.98), and after some simplification, yields [39]

$$\phi = \sqrt{\alpha + \beta}, \quad (2.114)$$

which is independent of the quantum numbers of the system. Specifically, $\alpha = \beta = 2$ leads to $\phi = 2$, corresponding to the original ET, which provides the exact solution for the harmonic oscillator. The IET spectrum is then obtained from (2.112) with Q replaced by Q_ϕ .

A comparison between the ET, IET, and accurate results from [45] is shown in Table 2.1. Except for the Coulomb potential ($\beta = -1$), the ET already provides quite accurate results, with a relative error of around 5% or less. However, the IET significantly improves accuracy, reducing the relative error to less than 1% for some values of β . The predicted variational nature is also verified throughout, although it is lost for the IET results.

In addition to the spectrum, the ET can also approximate eigenfunctions and thus observables. More information about eigenfunction approximation can be found in Appendix A. Results on the accuracy of the approximation for some observables are available in [36] for two-body potentials and in [41] for three-body potentials.

β	$m = 0.2$				$m = 5$			
	Accurate	ET	IET	(ϕ_a, ϕ_b)	Accurate	ET	IET	(ϕ_a, ϕ_b)
-1	-0.1398	-0.0645 [54]	-0.1316 [5.9]	(1.07,1.14)	-0.3848	-0.1797 [53]	-0.3029 [21]	(1.05,1.64)
0.1	1.9452	1.9804 [1.8]	1.9489 [0.2]	(1.55,1.53)	1.8486	1.8820 [1.8]	1.8568 [0.4]	(1.48,1.77)
1	4.9392	5.2278 [5.8]	4.9687 [0.6]	(1.79,1.77)	3.4379	3.6386 [5.8]	3.4753 [1.1]	(1.74,1.88)
2	7.5730	7.5730 [0]	7.5730 [0]	(2,2)	4.3729	4.3729 [0]	4.3729 [0]	(2,2)
3	9.7389	8.9925 [7.7]	9.6703 [0.7]	(2.16,2.20)	5.0166	4.6320 [7.7]	4.9693 [0.9]	(2.20,2.15)

Table 2.2: Bosonic ground state energies of Hamiltonian (2.115) for several values of m and β . The results from the ET [23] (upper bound for $\beta < 2$ and lower bound for $\beta > 2$) and the IET [39] with (ϕ_a, ϕ_b) are compared with more accurate ones [45], obtained with an hyperspherical expansion. The relative errors in % are indicated between square brackets. In the case of $\beta = 2$, the ET and IET give the exact result as expected. Results for $m = 1$ are given in Table 2.1.

2.5.2 Results for different particles

The treatment of systems with different particles allows for the inclusion of more diverse systems. A power-law potential, as previously discussed, can be studied. Consider the three-body Hamiltonian

$$H = \sum_{i=1}^2 \frac{p_i^2}{2} + \frac{p_3^2}{2m} + \frac{1}{2} \text{sgn}(\beta) \sum_{i < j=2}^3 r_{ij}^\beta. \quad (2.115)$$

Solving the compact equations (2.87) does not yield an analytical solution; however, a numerical solution is always possible. The improvement procedure must also be applied numerically. The variational character analysis is identical to the case of identical particles. A comparison between the ET [23], IET [39], and more accurate results [45] is shown in Tab. 2.2. The conclusions are similar to the previous case. The accuracy obtained by the ET bounds is better than 8%, except for the Coulomb case. Except for one instance, the Coulomb interaction with $m = 5$, the improvement is again quite significant with the IET, even if its magnitude is somewhat unpredictable.

Consider now a more physically relevant system. Atoms can be modelled as systems with N_e electrons of mass m_e and electric charge e , along with a nucleus of mass m_N and electric charge Ze , with Z being the atomic number. The atomic Hamiltonian is then given by

$$H = \sum_{i=1}^{N_e} \frac{p_i^2}{2m_e} + \frac{p_N^2}{2m_N} + \sum_{i < j=2}^{N_e} k \frac{e^2}{r_{ij}} - \sum_{i=1}^{N_e} k \frac{Ze^2}{r_{iN}}, \quad (2.116)$$

where $k = 1/(4\pi\epsilon_0)$ and ϵ_0 is the vacuum permittivity. This Hamiltonian (2.116) includes the main contributions to the binding energy in an atom. Thus, the approximate results are compared with experimental data on ionisation energies [46], which are very close to the eigenvalues of (2.116). In natural units, $\epsilon_0 = 1$, such that $k = 1/(4\pi)$, and the elementary electric charge e is related to the fine-structure constant α via $e = \sqrt{4\pi\alpha} \approx 0.3$. The electron mass is $m_e \approx 0.511$ MeV and the proton/neutron mass is $m_p = m_n \approx 938$ MeV, making the eigenvalue of H expressed in units MeV.

	Exp.	ET	IET	(ϕ_a, ϕ_b)
${}^4\text{He}$	79	33	47	(1.21, 1.78)
${}^6\text{Li}^+$	198	85	123	(1.18, 1.77)
${}^6\text{Li}$	203	66	95	(1.03, 1.99)
${}^{12}\text{C}^{4+}$	882	386	568	(1.16, 1.77)
${}^{12}\text{C}$	1030	321	496	(0.96, 2.10)
${}^{16}\text{O}^{6+}$	1611	707	1047	(1.15, 1.77)
${}^{16}\text{O}$	2044	672	1062	(0.94, 2.14)

Table 2.3: Fermionic ground state binding energies (in eV) of Hamiltonian (2.116) for selected atoms with two or more electrons. Results from the ET and the IET with (ϕ_a, ϕ_b) are compared with the experimental values [46]. Error on the experimental values are not written since it is considerably lower than the error of the ET result.

Since electrons are spin-1/2 fermions, they exhibit two-fold degeneracy, which prevents more than two fermions from occupying identical states. The calculation of the global quantum number $Q(N)$, as defined by (2.27), becomes increasingly complex. The derivation of the global quantum number for the fermionic ground state (FGS) is presented in Appendix A, with the final result provided by (A.22). The computation of the modified global quantum number Q_ϕ for the FGS is detailed in Appendix A.4.1. Solving the compact equations (2.87) does not yield an analytical solution; however, a numerical solution is always possible. The improvement procedure must also be applied numerically. Because of the mixing between attractive and repulsive potentials, the variational character of the method cannot be determined. The comparison with experimental values is provided in Table 2.3. As expected, the ET results are not very accurate. This has already been observed in the case of identical particles with the Coulomb potential. However, unlike the previous case, the IET does not significantly improve accuracy. From various accuracy tests conducted in [42], we concluded that

- The presence of a divergence, such as in the Coulomb potential, reduces the accuracy of the ET.
- The absence of a variational character, caused by the mix of attractive and repulsive potentials, diminishes the effectiveness of the IET.

These two factors together explain the poor accuracy of the method for atomic systems.

To conclude this chapter, the challenge of solving the many-body Schrödinger equation (2.1) was introduced, and various resolution methods for approximating its eigensolutions were presented. First, the many-body harmonic oscillator (2.2) was discussed, along with its exact solutions, which rely on a diagonalisation procedure. While results for systems of identical particles (2.26) were

already known, this work extends the analysis to systems with distinct particles, notably providing the spectra (2.39) and (2.41) for two and three different sets of identical particles, respectively.

Following this, the ET, an approximation method for solving the many-body equation (2.1), was introduced. Within the ET, the approximate eigensolutions are obtained by minimising the energy of an auxiliary Hamiltonian (2.44), which is a harmonic oscillator Hamiltonian, with respect to auxiliary parameters. For identical particles, it was previously known that the eigensolutions could be derived by solving a set of three compact equations (2.71). With the now-known eigenvalue of the harmonic oscillator for systems of distinct particles, the ET has been generalised, resulting in a new set of compact equations (2.84), (2.85), (2.86), which is a novel contribution of this work.

An improvement procedure for the ET, known as the IET, introduces a parameter ϕ that modifies the global quantum number (2.27) according to (2.89). This parameter is determined by coupling the ET with the DOS method, leading to the equation (2.98). Similarly to the ET, the IET has now been generalised to systems with different particles, in particular those with a single distinct particle, as demonstrated by equations (2.108).

This generalisation of the ET and IET to include systems with different particles enables the study of a wider range of physical systems. Results for such systems are presented in Tables 2.2 and 2.3.

Bibliography

- [1] Cooper, F., Khare, A. & Sukhatme, U. Supersymmetry and quantum mechanics. *Phys. Rep.* **251**, 267 (1995).
- [2] Nunberg, P., Prospero, D. & Pace, E. An application of a new harmonic-oscillator basis to the calculation of trinucleon ground-state observables. *Nucl. Phys. A* **285**, 58 (1977).
- [3] Suzuki, Y. & Varga, K. *Stochastic Variational Approach to Quantum-Mechanical Few-Body Problems* (Springer, Berlin, 1998).
- [4] Krivec, R. Hyperspherical-harmonics methods for few-body problems. *Few-Body Syst.* **25**, 199 (1998).
- [5] Baye, D. The Lagrange-mesh method. *Phys. Rep.* **565**, 1 (2015).
- [6] Godfrey, S. & Isgur, N. Mesons in a relativized quark model with chromodynamics. *Phys. Rev. D* **32**, 189 (1985).
- [7] Capstick, S. & Isgur, N. Baryons in a relativized quark model with chromodynamics. *Phys. Rev. D* **34**, 2809 (1986).
- [8] Semay, C. Three theorems of quantum mechanics and their classical counterparts. *Eur. J. Phys.* **39**, 055401 (2018).
- [9] Calogero, F. Ground State of a One-Dimensional N -Body System. *J. Math. Phys.* **10**, 2197 (1969).
- [10] Silvestre-Brac, B., Semay, C., Buisseret, F. & Brau, F. The quantum \mathcal{N} -body problem and the auxiliary field method. *J. Math. Phys.* **51**, 032104 (2010).
- [11] Willemyns, C. T. & Semay, C. Some specific solutions to the translation-invariant N -body harmonic oscillator hamiltonian. *J. Phys. Commun.* **5**, 115002 (2021).
- [12] Yáñez, R. J., Van Assche, W. & Dehesa, J. S. Position and momentum information entropies of the D -dimensional harmonic oscillator and hydrogen atom. *Phys. Rev. A* **50**, 3065 (1994).
- [13] Takahashi, T. T., Matsufuru, H., Nemoto, Y. & Suganuma, H. Three-quark potential in $SU(3)$ lattice QCD. *Phys. Rev. Lett.* **86**, 18 (2001).
- [14] Silvestre-Brac, B., Semay, C., Narodetskii, I. M. & Veselov, A. I. The baryonic Y-shape confining potential energy and its approximants. *Eur. Phys. J. C* **32**, 385 (2004).
- [15] Gattobigio, M., Kievsky, A. & Viviani, M. Spectra of helium clusters with up to six atoms using soft-core potentials. *Phys. Rev. A* **84**, 052503 (2011).
- [16] Ishikawa, S. Three-body potentials in α -particle model of light nuclei. *Few-Body Syst.* **58**, 37 (2017).
- [17] Ferraris, M., Giannini, M., Pizzo, M., Santopinto, E. & Tiator, L. A three-body force model for the baryon spectrum. *Phys. Lett. B* **364**, 231 (1995).

-
- [18] Dmitrašinović, V. Cubic casimir operator of $SU_C(3)$ and confinement in the nonrelativistic quark model. *Phys. Lett. B* **499**, 135 (2001).
- [19] Pepin, S. & Stancu, F. Three-body confinement force in hadron spectroscopy. *Phys. Rev. D* **65**, 054032 (2002).
- [20] Desplanques, B. *et al.* The baryonic spectrum in a constituent quark model including a three-body force. *Z. Physik A* **343**, 331 (1992).
- [21] Buisseret, F., Willemyns, C. T. & Semay, C. Many-quark interactions: large- N scaling and contribution to baryon masses. *Universe* **8**, 311 (2022).
- [22] Hall, R. L. & Schwesinger, B. The complete exact solution to the translation-invariant N -body harmonic oscillator problem. *J. Math. Phys.* **20**, 2481 (1979).
- [23] Semay, C., Cimino, L. & Willemyns, C. Envelope theory for systems with different particles. *Few Body-Syst.* **61**, 19 (2020).
- [24] Dirac, P. A. M. *Lectures on Quantum Mechanics* (Belter Graduate School of Sciences, Yeshiva University, New York, 1964).
- [25] Zwiebach, B. *A first course in string theory (2nd ed.)* (Cambridge University Press, Cambridge, 2009).
- [26] Semay, C. & Sicorello, G. Many-body forces with the envelope theory. *Few Body-Syst.* **59**, 119 (2018).
- [27] Lucha, W. Relativistic virial theorems. *Mod. Phys. Lett. A* **05**, 2473 (1990).
- [28] Hall, R. L. Energy trajectories for the N -boson problem by the method of potential envelopes. *Phys. Rev. D* **22**, 2062 (1980).
- [29] Hall, R. L. A geometrical theory of energy trajectories in quantum mechanics. *J. Math. Phys.* **24**, 324 (1983).
- [30] Semay, C. General comparison theorem for eigenvalues of a certain class of hamiltonians. *Phys. Rev. A* **83**, 024101 (2011).
- [31] Semay, C. & Cimino, L. Tests of the envelope theory in one dimension. *Few-Body Syst.* **60**, 64 (2019).
- [32] Cimino, L. & Semay, C. Compact equations for the envelope theory. *Braz. J. Phys.* **52**, 45 (2022).
- [33] Semay, C. An upper bound for asymmetrical spinless salpeter equations. *Phys. Lett. A* **376**, 2217 (2012).
- [34] Semay, C. & Roland, C. Approximate solutions for N -body hamiltonians with identical particles in D dimensions. *Results Phys.* **3**, 231 (2013).
- [35] Lobashev, A. A. & Trunov, N. N. A universal effective quantum number for centrally symmetric problems. *J. Phys. A: Math. Theor.* **42**, 345202 (2009).

- [36] Semay, C. Numerical tests of the envelope theory for few-boson systems. *Few-Body Syst.* **56**, 149 (2015).
- [37] Olsson, M. G. Universal behavior in excited heavy-light and light-light mesons. *Phys. Rev. D* **55**, 5479 (1997).
- [38] Semay, C. Improvement of the envelope theory with the dominantly orbital state method. *Eur. Phys. J. Plus* **130**, 156 (2015).
- [39] Chevalier, C., Willemyns, C. T., Cimino, L. & Semay, C. Improvement of the envelope theory for systems with different particles. *Few-Body Syst.* **63**, 40 (2022).
- [40] Makarov, D. N. Coupled harmonic oscillators and their quantum entanglement. *Phys. Rev. E* **97**, 042203 (2018).
- [41] Cimino, L., Tourbez, C., Chevalier, C., Lacroix, G. & Semay, C. Tests of the envelope theory for three-body forces. *Few-Body Syst.* **65**, 20 (2024).
- [42] Cimino, L., Chevalier, C., Carlier, E. & Viseur, J. Accuracy tests of the envelope theory. *Results Phys.* **58**, 107470 (2024).
- [43] Buisseret, F. & Semay, C. Light baryon masses in different large- N_c limits. *Phys. Rev. D* **82**, 056008 (2010).
- [44] Buisseret, F., Matagne, N. & Semay, C. Spin contribution to light baryons in different large- N limits. *Phys. Rev. D* **85**, 036010 (2012).
- [45] Basdevant, J. L., Martin, A. & Richard, J. M. Improved bounds on many-body hamiltonians: (II). Baryons from mesons in the quark model. *Nucl. Phys. B* **343**, 69 (1990).
- [46] Kramida, A., Yu. Ralchenko, Reader, J. & NIST ASD Team. NIST Atomic Spectra Database (ver. 5.11), [Online]. <https://physics.nist.gov/asd> (2023).

A massive particle is often characterised by its mass m , spin s , and projection along the z -axis $\mu = \{-s, -s + 1, \dots, s - 1, s\}$. Let us denote the state of the particle by $|s \mu\rangle$ for the moment. The coupling of two spins s_1 and s_2 yields a total spin S , determined by the usual rule $|s_1 - s_2| \leq S \leq s_1 + s_2$. The two-body state is expressed as

$$|S M; s_1 s_2\rangle = \sum_{\mu_1, \mu_2} (s_1 \mu_1 s_2 \mu_2 |S M) |s_1 \mu_1\rangle \otimes |s_2 \mu_2\rangle, \quad (3.1)$$

where $(s_1 \mu_1 s_2 \mu_2 |S M)$ is a Clebsch-Gordan coefficient. This approach can be extended to the coupling of three or more massive particles. The purpose of this discussion is to remind that the methodology for treating massive particles is well-established in quantum mechanics.

Consider now a massless particle, such as a photon or, for our interest, a gluon. Unlike massive particles, massless particles exhibit only two projections of spin, $\pm s$; intermediate projections are not observed. This property can be understood classically from the two polarisations of light, which is explained by the gauge symmetry of Maxwell's equations. The coupling of two massless particles is then non-trivial and differs from the coupling of two massive particles. Nonetheless, such couplings are essential in the study of exotic hadrons, such as glueballs or, in our interest, hybrid baryons. Therefore, it is necessary to develop a technique for the coupling of angular momenta that is valid for both massive and massless particles. This endeavour was initiated by Jacob and Wick in their seminal paper [1], where they developed the helicity formalism, which serves as a foundation for describing one- and two-body states, both massive and massless. In Sec. 3.1, the characterisation of particles is discussed, and the helicity formalism is developed for describing one-body states. Subsequently, in Sec. 3.2, the formalism is extended to two-body states, and the correct coupling of angular momenta is derived. Finally, the helicity formalism is applied to hybrid baryons in Sec. 3.3. Natural units $c = \hbar = 1$ will be used in all equations.

3.1 One-body states

Before diving into the helicity formalism, we must address how to correctly characterise a particle. Specifically, we require that all inertial observers agree

on the nature of the particle. For instance, velocity is not a suitable quantum number, as it can be altered by a boost or a spatial rotation. However, the rest mass is a Lorentz invariant, as every physics student knows, and thus is an appropriate choice for characterising a particle.

To identify other Lorentz invariants that will be useful for our discussion, it is necessary to study the Poincaré group, which is the isometry group of Minkowski spacetime. For a detailed review of the group and its algebra, particularly the commutation relations of the generators, the interested reader can refer to Appendix B. In summary, the study of this group reveals that all particles can be characterised by their mass m , as expected, and momentum \mathbf{p} . Moreover, massive particles can be further characterised by their spin s and projection along the z -axis μ , whereas massless particles are characterised by a helicity quantum number λ , which can be interpreted as the projection of angular momentum along the direction of motion.

3.1.1 Massive particles and canonical states

Saying that a massive particle has all the above characteristics means that the one-body state describing it, denoted $|m; p \theta \phi; s \mu\rangle_c$ or $|m; \mathbf{p}; s \mu\rangle_c$ for short, must be an eigenstate of the corresponding operators

$$\begin{aligned}
 P^2 |m; \mathbf{p}; s \mu\rangle_c &= m^2 |m; \mathbf{p}; s \mu\rangle_c, \\
 J^2 |m; \mathbf{p}; s \mu\rangle_c &= s(s+1) |m; \mathbf{p}; s \mu\rangle_c, \\
 P_0 |m; \mathbf{p}; s \mu\rangle_c &= (p^2 + m^2)^{1/2} |m; \mathbf{p}; s \mu\rangle_c, \\
 P_1 |m; \mathbf{p}; s \mu\rangle_c &= p \sin \theta \cos \phi |m; \mathbf{p}; s \mu\rangle_c, \\
 P_2 |m; \mathbf{p}; s \mu\rangle_c &= p \sin \theta \sin \phi |m; \mathbf{p}; s \mu\rangle_c, \\
 P_3 |m; \mathbf{p}; s \mu\rangle_c &= p \cos \theta |m; \mathbf{p}; s \mu\rangle_c, \\
 J_3 |m; \mathbf{p}; s \mu\rangle_c &= \mu |m; \mathbf{p}; s \mu\rangle_c,
 \end{aligned} \tag{3.2}$$

where $p = |\mathbf{p}|$ and (θ, ϕ) are the polar and azimuthal angles of \mathbf{p} . The above operators are defined in more detail in Appendix B, but we recall that $P_{\mu=\{0,1,2,3\}}$ are the momentum operators, $P^2 = P_\mu P^\mu$ is the squared momentum operator, $J_{i=\{1,2,3\}}$ are the angular momentum operators, and $J^2 = J_i J^i$ is the squared angular momentum operator. Since the state $|m; \mathbf{p}; s \mu\rangle_c$ is an eigenstate of the J_3 operator¹, i.e. the projection of the spin along the z -axis, it is referred to as a *canonical state* and represents the usual states of (non-relativistic) quantum mechanics.

Orthonormality and completeness relations

The canonical states $|m; p \theta \phi; s \mu\rangle_c$ are orthonormal

$$\begin{aligned}
 {}_c \langle m; p \theta \phi; s \mu | m; p' \theta' \phi'; s' \mu' \rangle_c &= 2w(p) \delta(p - p') \\
 &\quad \times \delta(\phi - \phi') \delta(\cos \theta - \cos \theta') \delta_{\mu \mu'},
 \end{aligned} \tag{3.3}$$

¹Technically speaking, the canonical state is not an eigenstate of J^2 and J_3 because it is not at rest. Rather, it is an eigenstate of the Pauli-Lubanski (PL) operator W^2 and the third component of the PL vector W_3 (see Appendix B). However, since the eigenvalues of W^2 and W_3 are related to s and μ , respectively, we simplify the definition of the canonical states.

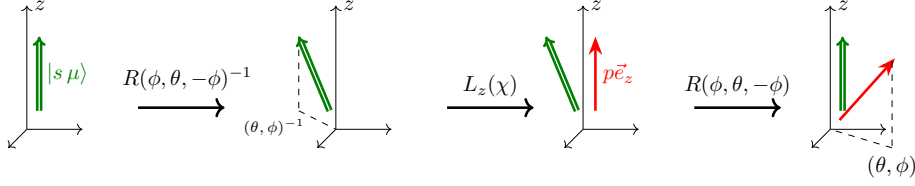


Figure 3.1: Graphical illustration of the construction (3.6) for massive canonical states. The double green arrow represents the spin projection, and the red arrow the particle's momentum.

and form a complete set for all allowed values of μ and momentum \mathbf{p}

$$\sum_{\mu=-s}^s \int \frac{d\mathbf{p}}{2w(p)} |m; \mathbf{p}; s \mu\rangle_c \langle m; \mathbf{p}; s \mu| = \mathbf{1}. \quad (3.4)$$

The factors $w(p) = (p^2 + m^2)^{1/2}$ ensure that the above relations are Lorentz invariant [2].

Reference state

The canonical state $|m; \mathbf{p}; s \mu\rangle_c$ can be constructed from a state $|m; \bar{\mathbf{p}}; s \mu\rangle$ with a reference four-momentum $\bar{\mathbf{p}}$, typically taken as the rest state $\bar{\mathbf{p}} = (m, 0, 0, 0)$. The construction is achieved by means of Lorentz boosts in the z -direction, denoted $L_z(\chi)$ with χ being the rapidity, and rotations, denoted

$$R(\alpha, \beta, \gamma) = \exp(-i\alpha J_3) \exp(-i\beta J_2) \exp(-i\gamma J_3), \quad (3.5)$$

with (α, β, γ) representing the Euler angles. Interested readers can refer to Appendix B.2 for more information about the rotation formalism. More explicitly [3]

$$|m; p \theta \phi; s \mu\rangle_c = U(R(\phi, \theta, \gamma) L_z(\chi) R^{-1}(\phi, \theta, \gamma)) |m; \bar{\mathbf{p}}; s \mu\rangle. \quad (3.6)$$

In the above equation, the notation $U(\cdot)$ specifies the representation of the Poincaré group under which the particle transforms [2, 4], i.e. the value of m and s , but readers unfamiliar with this notation should not be concerned. A graphical illustration of the transformation (3.6) is presented in Fig. 3.1.

The transformations are considered active. First, an inverse rotation of angles (ϕ, θ, γ) is applied on the rest state (the choice for the angle γ will be explained later). Since the particle is at rest, the rotation does not modify the momentum but rotates the spin projection axis. Then, a Lorentz boost of rapidity

$$\chi = \cosh^{-1} \left(\frac{\sqrt{p^2 + m^2}}{m} \right), \quad (3.7)$$

is applied in the z -direction, giving the particle a momentum magnitude p in this direction [5]. The spin is not affected by the boost. Finally, a second rotation with the same angles (ϕ, θ, γ) is applied so that the particle's momentum has the polar angles (θ, ϕ) . The spin projection axis is reset to the z -axis again.

Coming back to the angles of the rotation, the last angle γ is arbitrary, but two conventions are often used: either $\gamma = 0$ [5] or $\gamma = -\phi$ [1]. In both conventions, the angle γ is not an independent variable. For canonical states, all conventions are equivalent. Indeed, since rotations around the z -axis commute with boosts in the z -direction (see (B.3)), the two rotations of angle γ in (3.6) cancel out. However, as we shall see, this is not the case for helicity states.

3.1.2 Massless particles and helicity states

Since massless particles cannot be characterised by spin, but rather by helicity λ , they cannot be described by a canonical state. Instead, they are described by a state denoted $|0; p \theta \phi; s \lambda\rangle$ or $|0; \mathbf{p}; s \lambda\rangle$ for short, which is an eigenstate of the operators

$$\begin{aligned} P^2 |0; \mathbf{p}; s \lambda\rangle &= 0 |0; \mathbf{p}; s \lambda\rangle, \\ P_0 |0; \mathbf{p}; s \lambda\rangle &= p |0; \mathbf{p}; s \lambda\rangle, \\ P_1 |0; \mathbf{p}; s \lambda\rangle &= p \sin \theta \cos \phi |0; \mathbf{p}; s \lambda\rangle, \\ P_2 |0; \mathbf{p}; s \lambda\rangle &= p \sin \theta \sin \phi |0; \mathbf{p}; s \lambda\rangle, \\ P_3 |0; \mathbf{p}; s \lambda\rangle &= p \cos \theta |0; \mathbf{p}; s \lambda\rangle, \\ \Lambda |0; \mathbf{p}; s \lambda\rangle &= \lambda |0; \mathbf{p}; s \lambda\rangle, \end{aligned} \tag{3.8}$$

where Λ is the helicity operator (B.8). The label s in the state notation is not the eigenvalue of J^2 but the “spin” corresponding to a projection λ . For gluons or photons, $s = 1$. These states are referred to as the *helicity states* since they are eigenstates of Λ . They follow similar orthogonality and completeness relations as canonical states, but with $\mu \rightarrow \lambda$.

Reference state

As with the canonical state, the helicity state can be constructed from a reference state $|0; \bar{p}; s \lambda\rangle$, where the reference four-momentum is typically taken as $\bar{p} = (\kappa, 0, 0, \kappa)$, where κ is an arbitrary positive energy, say 1 eV [4]. Note that since the momentum’s direction is chosen as the z -axis, the helicity operator Λ coincides with J_3 . In other words, $J_3 |0; \bar{p}; s \lambda\rangle = \lambda |0; \bar{p}; s \lambda\rangle$. More explicitly [3]

$$|0; p \theta \phi; s \lambda\rangle = U(R(\phi, \theta, \gamma)L_z(\chi)) |0; \bar{p}; s \lambda\rangle. \tag{3.9}$$

The construction is similar to (3.6), except that the first (inverse) rotation is missing. A graphical illustration of the transformation (3.9) is presented in Fig. 3.2. First, a Lorentz boost of rapidity

$$\chi = \cosh^{-1} \left(\frac{p^2 + 1}{2p} \right), \tag{3.10}$$

is applied in the z -direction, giving the particle a momentum magnitude p in this direction [6]. The helicity is not affected by the boost since it is a Lorentz invariant for massless particles. Then, a rotation with angles (ϕ, θ, γ) is applied so that the particle’s momentum has the polar angles (θ, ϕ) . The rotation by angle γ does not affect the system since the motion is along the z -axis. The

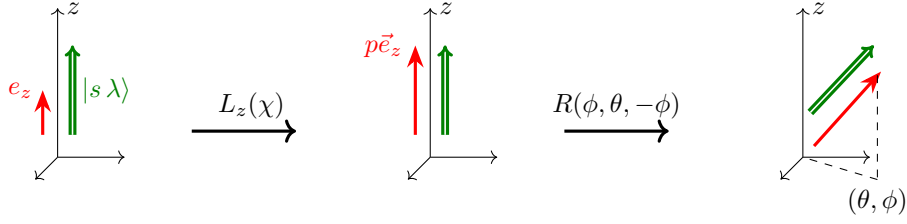


Figure 3.2: Graphical illustration of the construction (3.9) for massless helicity states. The double green arrow represents the spin projection, and the red arrow the particle’s momentum.

helicity is also “rotated” so that it remains the projection of angular momentum along the momentum direction.

We still have an arbitrary choice for the final angle γ . However, the choice between the conventions 0 and $-\phi$ will change the state. Indeed, considering (B.3), it is straightforward to show the relation between the two conventions

$$\begin{aligned}
 |0; p \theta \phi; s \lambda\rangle_{\gamma=-\phi} &= U(e^{-i\phi J_3} e^{-i\theta J_2} e^{i\phi J_3} L_z(\chi)) |0; \bar{p}; s \lambda\rangle \\
 &= U(e^{-i\phi J_3} e^{-i\theta J_2} L_z(\chi)) e^{i\phi \lambda} |0; \bar{p}; s \lambda\rangle \\
 &= e^{i\phi \lambda} |0; p \theta \phi; s \lambda\rangle_{\gamma=0}.
 \end{aligned} \tag{3.11}$$

In the following discussion, the convention $-\phi$ will be used, which is the convention in [1]. It is crucial to remain consistent with the chosen convention throughout the following derivations.

3.1.3 Massive particles and helicity states

Up to now, massive particles have been described by canonical states, which are eigenstates of J_3 , following the construction (3.6). However, the construction of helicity states (3.9) can also be applied to the reference state for massive particles

$$|m; p \theta \phi; s \lambda\rangle = U(R(\phi, \theta, -\phi) L_z(\chi)) |m; \bar{p}; s \lambda\rangle. \tag{3.12}$$

Since the initial rotation is missing, the spin is not projected along the z -axis, but along the direction of momentum, as depicted in Fig. 3.3. Thus, the one-body state for massive particles, $|m; \mathbf{p}; s \lambda\rangle$, becomes an eigenstate of the helicity operator. Consequently, the state $|m; \mathbf{p}; s \lambda\rangle$ is referred to as the helicity state for massive particles.

Even though helicity is not a Lorentz invariant for massive particles, the helicity basis permits the treatment of both massive and massless particles within the same formalism, whereas canonical states are only valid for massive particles. Furthermore, helicity states exhibit interesting properties compared to canonical states, as reviewed below. Notably, choosing the direction of motion as the quantisation axis for spin is less arbitrary than using the conventional z -axis.

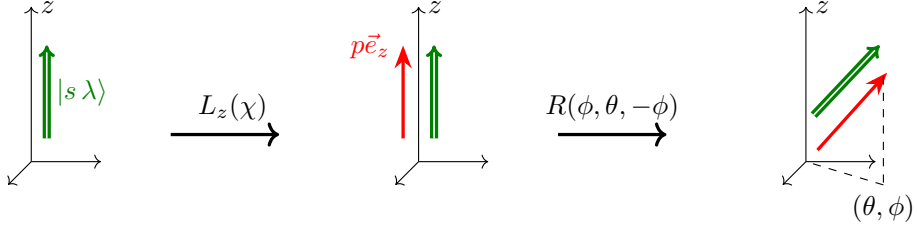


Figure 3.3: Graphical illustration of the construction (3.12) for massive helicity states. The double green arrow represents the spin projection, and the red arrow the particle's momentum.

Invariance under rotation

Consider the action of an arbitrary rotation $R(\alpha, \beta, \gamma)$ on the helicity state $|m; \mathbf{p}; s \lambda\rangle$. Intuitively, the momentum's angles (θ, ϕ) will be rotated, but the helicity should remain unchanged. Starting from (3.12)

$$\begin{aligned} U(R(\alpha, \beta, \gamma)) |m; p \theta \phi; s \lambda\rangle &= U(R(\alpha, \beta, \gamma) R(\phi, \theta, -\phi) L_z(\chi)) |m; \bar{p}; s \lambda\rangle \\ &= U(e^{-i\phi' J_3} e^{-i\theta' J_2} e^{-i\gamma' J_3} L_z(\chi)) |m; \bar{p}; s \lambda\rangle, \end{aligned} \quad (3.13)$$

where ϕ', θ' and γ' are chosen so that $R(\phi', \theta', \gamma') = R(\alpha, \beta, \gamma) R(\phi, \theta, -\phi)$ is a new rotation. Using (B.3), we get

$$U(R(\alpha, \beta, \gamma)) |m; p \theta \phi; s \lambda\rangle = U(e^{-i\phi' J_3} e^{-i\theta' J_2} L_z(\chi)) e^{-i\gamma' \lambda} |m; \bar{p}; s \lambda\rangle. \quad (3.14)$$

Inserting the identity $\mathbb{1} = \exp(i\phi' J_3) \exp(-i\phi' J_3)$ in the above equation yields

$$\begin{aligned} U(R(\alpha, \beta, \gamma)) |m; p \theta \phi; s \lambda\rangle &= e^{-i\gamma' \lambda} U(e^{-i\phi' J_3} e^{-i\theta' J_2} e^{i\phi' J_3} e^{-i\phi' J_3} L_z(\chi)) |m; \bar{p}; s \lambda\rangle \\ &= e^{-i(\gamma' + \phi') \lambda} U(e^{-i\phi' J_3} e^{-i\theta' J_2} e^{i\phi' J_3} L_z(\chi)) |m; \bar{p}; s \lambda\rangle \\ &= e^{-i(\gamma' + \phi') \lambda} U(R(\phi', \theta', -\phi') L_z(\chi)) |m; \bar{p}; s \lambda\rangle \\ &= e^{-i(\gamma' + \phi') \lambda} |m; p \theta' \phi'; s \lambda\rangle. \end{aligned} \quad (3.15)$$

The phase factor $e^{-i(\gamma' + \phi') \lambda}$ ensures that the state, initially in the $-\phi$ convention, stays in the same convention. Since the helicity λ is preserved by the rotation, the relation (3.15) is often referred to as the helicity rotational invariance.

Note that this result is identical for massless helicity states $|0; p \theta \phi; s \lambda\rangle$ because the massless reference state $|0; \bar{p}; s \lambda\rangle$ is also an eigenstate of J_3 .

Invariance under Lorentz boost and Wigner rotation

Consider now a Lorentz boost $L_{\hat{p}}$ in the direction of the momentum, denoted \hat{p} . Any boost $L_{\hat{r}}$ applied in a direction \hat{r} with polar angles (β, α) can be decomposed as [3]

$$L_{\hat{r}} = R(\alpha, \beta, \gamma) L_z R^{-1}(\alpha, \beta, \gamma), \quad (3.16)$$

where γ is arbitrary. Intuitively, the momentum magnitude will change but not the helicity. Starting again from (3.12), and using (3.16), one can show

$$\begin{aligned} U(L_{\hat{r}}(\chi')) |m; \mathbf{p} \theta \phi; s \lambda\rangle & \\ &= U(L_{\hat{r}}(\chi')) R(\phi, \theta, -\phi) L_z(\chi) |m; \bar{\mathbf{p}}; s \lambda\rangle \\ &= U(R(\phi, \theta, -\phi) L_z(\chi') R^{-1}(\phi, \theta, -\phi) R(\phi, \theta, -\phi) L_z(\chi)) |m; \bar{\mathbf{p}}; s \lambda\rangle \quad (3.17) \\ &= U(R(\phi, \theta, -\phi) L_z(\chi') L_z(\chi)) |m; \bar{\mathbf{p}}; s \lambda\rangle \\ &= |m; \mathbf{p}' \theta \phi; s \lambda\rangle, \end{aligned}$$

with $\mathbf{p}' = L_z(\chi') \mathbf{p}$ being the momentum of the particle after the second boost. Since the helicity is preserved, this property is referred to as the helicity boost invariance. Note that this property is only valid if the boost does not switch the sign of \mathbf{p} . As for the rotational invariance, this property is also valid for massless states.

The action of a boost in an arbitrary direction (θ', ϕ') can also be studied. It can be shown that the resultant state is given by a rotation [5, 7]

$$U(L) |m; \mathbf{p}; s \lambda\rangle = \sum_{\lambda'} D_{\lambda' \lambda}^s(\alpha_W, \beta_W, \gamma_W) |m; \mathbf{p}'; s \lambda'\rangle, \quad (3.18)$$

where $(\alpha_W, \beta_W, \gamma_W)$ are the angles of the so-called *Wigner rotation*, and $D_{\lambda' \lambda}^s$ are the Wigner D -matrices (B.10). As expected, the helicity for a massive particle is not invariant under all transformations of the Poincaré group. However, similar computations for massless particles show that helicity is indeed conserved by an arbitrary boost [6].

Change of basis

Since canonical and helicity states form a complete basis for describing massive particles, it should be possible to transform from one basis to the other. Comparing (3.6) and (3.12), we can derive the change of basis relationship as follows

$$\begin{aligned} |m; \mathbf{p}; s \lambda\rangle &= U(R(\phi, \theta, -\phi) L_z(\chi)) |m; \bar{\mathbf{p}}; s \lambda\rangle \\ &= U(R(\phi, \theta, -\phi) L_z(\chi) R^{-1}(\phi, \theta, -\phi) R(\phi, \theta, -\phi)) |m; \bar{\mathbf{p}}; s \lambda\rangle \\ &= U(R(\phi, \theta, -\phi) L_z(\chi) R^{-1}(\phi, \theta, -\phi)) \\ &\quad \times \sum_{\mu=-s}^s D_{\mu \lambda}^s(\phi, \theta, -\phi) |m; \bar{\mathbf{p}}; s \mu\rangle \quad (3.19) \\ &= \sum_{\mu=-s}^s D_{\mu \lambda}^s(\phi, \theta, -\phi) |m; \mathbf{p}; s \mu\rangle_c, \end{aligned}$$

where we used relation (B.11) in the third line.

3.1.4 Parity and opposite momentum states

Given the parity P is an element of the Poincaré group and switches the sign of the spatial coordinates, $P\mathbf{r} = -\mathbf{r}$, parity will switch the sign of momentum but not of angular momentum, implying the helicity is switched. Let us study the action of the parity operator \hat{P} on the helicity states. Useful commutation relations are [3]

$$[P, R(\alpha, \beta, \gamma)] = 0 \text{ and } P L_{\hat{r}}(\chi) = L_{-\hat{r}}(\chi) P, \quad (3.20)$$

the last equation meaning that the parity switches the direction \hat{r} of a boost.

Parity on massive states

We begin the discussion with the simpler massive case. Since the reference state $|m; \bar{\mathbf{p}}; s \lambda\rangle$ is chosen at rest, it is an eigenstate of the parity operator [4]

$$\hat{P} |m; \bar{\mathbf{p}}; s \lambda\rangle = \eta |m; \bar{\mathbf{p}}; s \lambda\rangle, \quad (3.21)$$

with $\eta = \pm 1$ being the intrinsic parity of the particle. Conventionally, quarks have $\eta = 1$ and antiquarks have $\eta = -1$. Starting from (3.12), the action of the parity operator is given by

$$\begin{aligned} \hat{P} |m; \mathbf{p} \theta \phi; s \lambda\rangle &= \hat{P} U(R(\phi, \theta, -\phi) L_z(\chi)) |m; \bar{\mathbf{p}}; s \lambda\rangle \\ &= \eta U(R(\phi, \theta, -\phi) L_{-z}(\chi)) |m; \bar{\mathbf{p}}; s \lambda\rangle. \end{aligned} \quad (3.22)$$

Expressing the boost L_{-z} in terms of L_z via (3.16), and inserting the identity $1 = \exp(-2i\pi J_2) \exp(2i\pi J_2)$ on the right side, we obtain

$$\begin{aligned} \hat{P} |m; \mathbf{p} \theta \phi; s \lambda\rangle &= \eta U(R(\phi, \theta, -\phi) e^{-i\pi J_2} L_z(\chi) e^{i\pi J_2} e^{-2i\pi J_2} e^{2i\pi J_2}) |m; \bar{\mathbf{p}}; s \lambda\rangle \\ &= \eta (-1)^{2s} U(R(\phi, \theta, -\phi) e^{-i\pi J_2} L_z(\chi) e^{-i\pi J_2}) |m; \bar{\mathbf{p}}; s \lambda\rangle \\ &= \eta (-1)^{3s-\lambda} U(R(\phi, \theta, -\phi) e^{-i\pi J_2} L_z(\chi)) |m; \bar{\mathbf{p}}; s - \lambda\rangle \\ &= \eta (-1)^{s+\lambda} U(R(\phi, \theta, -\phi) e^{-i\pi J_2} L_z(\chi)) |m; \bar{\mathbf{p}}; s - \lambda\rangle. \end{aligned} \quad (3.23)$$

On the second line, the action of the 2π rotation gives rise to a factor $(-1)^{2s}$. This factor originates from the fact that for fermions, a complete rotation is identified to minus the identity. This property is sometimes referred to as the projective representation of $SO(3)$ [4]. On the third line, the action of a rotation of angle π around the y -axis is given by (B.11) and (B.20). Finally, the last line is obtained from the fact that $2(s \pm \lambda)$ is always an even integer.

By defining a helicity state of opposite momentum as

$$|m; -\mathbf{p}; s \lambda\rangle = (-1)^{s-\lambda} U(R(\phi, \theta, -\phi) e^{-i\pi J_2} L_z(\chi)) |m; \bar{\mathbf{p}}; s \lambda\rangle, \quad (3.24)$$

the action of the parity operator becomes

$$\hat{P} |m; \mathbf{p}; s \lambda\rangle = \eta (-1)^{2s} |m; -\mathbf{p}; s - \lambda\rangle. \quad (3.25)$$

Massive one-body states are not eigenstates of the parity operator, as expected intuitively. The factor $(-1)^{s-\lambda}$ in (3.24) is added for convenience. Indeed, in the limit $\mathbf{p} \rightarrow \mathbf{0}$, the opposite momentum state reduces to

$$\begin{aligned}
|m; -\mathbf{p}; s \lambda\rangle &\rightarrow (-1)^{s-\lambda} U(R(0, \pi, 0) L_z(0)) |m; \bar{\mathbf{p}}; s \lambda\rangle \\
&= (-1)^{s-\lambda} \sum_{\lambda'} (-1)^{s+\lambda'} \delta_{-\lambda \lambda'} |m; \bar{\mathbf{p}}; s \lambda'\rangle \\
&= |m; \bar{\mathbf{p}}; s - \lambda\rangle.
\end{aligned} \tag{3.26}$$

This convention is the same as in [1], but other conventions exist for states with opposite momentum.

Parity on massless states

The massless case is subtler because the reference state $|0; \bar{\mathbf{p}}; s \lambda\rangle$ is not at rest, but rather moving along the z -axis. Hence, the action of the parity operator will switch the sign of the reference four-momentum and helicity [4]

$$\hat{P} |0; \bar{\mathbf{p}}; s \lambda\rangle = \eta e^{-i\pi J_2} |0; \bar{\mathbf{p}}; s - \lambda\rangle, \tag{3.27}$$

where η is the intrinsic parity. Gluons are characterised by $\eta = -1$ [8]. Starting from (3.9), similar calculations as for the massive case yield

$$\hat{P} |0; p \theta \phi; s \lambda\rangle = \eta U(R(\phi, \theta, -\phi) e^{-i\pi J_2} L_z(\chi)) |0; \bar{\mathbf{p}}; s - \lambda\rangle. \tag{3.28}$$

Hence, the action of the parity operator on massless states seems different from the one on massive states. However, we know that massless particles only have two helicities $\lambda = \pm s$. Thus, the phase factor $(-1)^{s+\lambda}$ is either equal to 1 for $\lambda = -s$, or $(-1)^{2s}$ for $\lambda = s$. For bosons, such as gluons, $(-1)^{2s} = 1$ and so the massive formula yields the same result as for massless particles. This feature will be often present in other derivations: results for massive and massless states often coincide. The definition for a state with opposite momentum can be reused for massless particles following similar arguments.

3.2 Two-body states

Let us proceed to the description of two-body systems. Building on the previous section, two-body states can be expressed in the canonical basis for massive particles or the helicity basis for both massive and massless particles. As canonical states correspond to the usual states in quantum mechanics, we will first develop the concepts around two-body helicity states. Given that most results are valid for both massive and massless states, the notation for a helicity state is simplified to $|\mathbf{p}; s \lambda\rangle$, and for a reference state to $|\bar{\mathbf{p}}; s \lambda\rangle$.

3.2.1 Two-body helicity states

Consider two particles with masses m_1 and m_2 , spins s_1 and s_2 , helicities λ_1 and λ_2 , and momenta \mathbf{p}_1 and \mathbf{p}_2 . The two-body helicity state is constructed as follows

$$|\mathbf{p}_1 \mathbf{p}_2; s_1 \lambda_1 s_2 \lambda_2\rangle = |\mathbf{p}_1; s_1 \lambda_1\rangle \otimes |\mathbf{p}_2; s_2 \lambda_2\rangle. \tag{3.29}$$

The system's total energy is $W = w_1(p_1) + w_2(p_2)$, where $w_i(p_i) = (m_i^2 + \mathbf{p}_i^2)^{1/2}$. To describe physical states using the helicity formalism, we boost the state (3.29) to the centre of mass (CM) frame, where $\mathbf{P} = \mathbf{p}_1 + \mathbf{p}_2 = \mathbf{0}$, using (3.24)

$$\begin{aligned}
|\mathbf{p}; s_1 \lambda_1 s_2 \lambda_2\rangle &= |\mathbf{p}; s_1 \lambda_1\rangle \otimes |-\mathbf{p}; s_2 \lambda_2\rangle \\
&= U(R(\phi, \theta, -\phi)) [U(L_z(\chi)) |\bar{p}; s_1 \lambda_1\rangle \\
&\quad \otimes (-1)^{s_2 - \lambda_2} U(R(0, \pi, 0) L_z(\chi)) |\bar{p}; s_2 \lambda_2\rangle] \\
&\equiv U(R(\phi, \theta, -\phi)) |p_z; s_1 \lambda_1 s_2 \lambda_2\rangle,
\end{aligned} \tag{3.30}$$

where \mathbf{p} is the relative momentum between the two particles, and $|p_z; s_1 \lambda_1 s_2 \lambda_2\rangle$ is a two-body state with relative motion in the z -direction. The Lorentz-invariant normalisation of the two-body state (3.30) is given by [2]

$$\begin{aligned}
\langle p' \theta' \phi'; s_1 \lambda'_1 s_2 \lambda'_2 | p \theta \phi; s_1 \lambda_1 s_2 \lambda_2 \rangle \\
&= \frac{4W}{p} \delta(W - W') \delta(\phi - \phi') \delta(\cos \theta - \cos \theta') \delta_{\lambda_1 \lambda'_1} \delta_{\lambda_2 \lambda'_2}, \\
&= \frac{4w_1(p)w_2(p)}{p^2} \delta(p - p') \delta(\phi - \phi') \delta(\cos \theta - \cos \theta') \delta_{\lambda_1 \lambda'_1} \delta_{\lambda_2 \lambda'_2},
\end{aligned} \tag{3.31}$$

and forms a complete set for all allowed values of λ_1, λ_2 and \mathbf{p} .

3.2.2 Helicity angular momentum states

The two-body helicity state $|\mathbf{p}; s_1 \lambda_1 s_2 \lambda_2\rangle$ has a well-defined relative momentum \mathbf{p} , making it an eigenstate of the operators P_μ . However, it does not possess a total angular momentum J or projection M because it is not an eigenstate of the operators J^2 and J_3 . Since the two-body state is described in the CM frame, where it is at rest, it should be possible to assign a total angular momentum to the system. The following state

$$\begin{aligned}
|p; J M; s_1 \lambda_1 s_2 \lambda_2\rangle &= C_J \int d \cos \theta d \phi \\
&\quad \times D_{M \lambda_1 - \lambda_2}^{J*}(\phi, \theta - \phi) |p \theta \phi; s_1 \lambda_1 s_2 \lambda_2\rangle,
\end{aligned} \tag{3.32}$$

where C_J is a normalisation factor (to be specified later), is a two-body helicity state with total angular momentum J and projection M [1]. Intuitively, this involves integrating over all angles (θ, ϕ) of the momentum and weighting with a Wigner D -matrix instead of spherical harmonics.

Instead of proving that the state (3.32) is an eigenstate of J^2 and J_3 , we can demonstrate that it behaves correctly under rotation, as described by (B.11). Starting from (3.32) and (3.30), we show that

$$\begin{aligned}
&U(R(\alpha, \beta, \gamma)) |p; J M; s_1 \lambda_1 s_2 \lambda_2\rangle \\
&= C_J \int d \cos \theta d \phi D_{M \lambda_1 - \lambda_2}^{J*}(\phi, \theta - \phi) U(R(\alpha, \beta, \gamma)) \\
&\quad \times R(\phi, \theta, -\phi) |p_z; s_1 \lambda_1 s_2 \lambda_2\rangle \\
&= C_J \int d \cos \theta d \phi D_{M \lambda_1 - \lambda_2}^{J*}(\phi, \theta - \phi) U(R(\alpha', \beta', \gamma')) |p_z; s_1 \lambda_1 s_2 \lambda_2\rangle,
\end{aligned} \tag{3.33}$$

where $R(\alpha', \beta', \gamma') = R(\alpha, \beta, \gamma) R(\phi, \theta, -\phi)$ is a new rotation. Using the addition theorem of two Wigner D -matrices (B.13), the transformed state is

$$\begin{aligned}
& U(R(\alpha, \beta, \gamma)) |p; J M; s_1 \lambda_1 s_2 \lambda_2\rangle \\
&= C_J \int d \cos \theta d \phi \sum_{M'} (D_{M M'}^{J*}(\alpha, \beta, \gamma))^{-1} D_{M' \lambda_1 - \lambda_2}^{J*}(\alpha', \beta', \gamma') \\
&\quad \times U(R(\alpha', \beta', \gamma')) |p_z; s_1 \lambda_1 s_2 \lambda_2\rangle \\
&= C_J \int d \cos \theta d \phi \sum_{M'} D_{M' M}^J(\alpha, \beta, \gamma) D_{M' \lambda_1 - \lambda_2}^{J*}(\alpha', \beta', \gamma') \\
&\quad \times U(R(\alpha', \beta', \gamma')) |p_z; s_1 \lambda_1 s_2 \lambda_2\rangle,
\end{aligned} \tag{3.34}$$

where we used the unitarity of the Wigner D -matrices (B.14) in the second line. The integration covers all the domain of the angles (θ, ϕ) , corresponding to the 2-sphere. Thus, the measure $d \cos \theta d \phi$ can be changed to $d \cos \beta' d \alpha'$, keeping the integral invariant (the interested reader can look in [9] for more information about the invariant or Haar measure). Thanks to this change, the definition of the angular momentum state (3.32) is recovered², leading to our final result

$$\begin{aligned}
& U(R(\alpha, \beta, \gamma)) |p; J M; s_1 \lambda_1 s_2 \lambda_2\rangle \\
&= \sum_{M'=-J}^J D_{M' M}^J(\alpha, \beta, \gamma) |p; J M'; s_1 \lambda_1 s_2 \lambda_2\rangle,
\end{aligned} \tag{3.35}$$

which is the correct behaviour (B.11) of a state with angular momentum J . From the properties of the Wigner D -matrices, the construction (3.32) yields an important selection rule for the following discussion

$$J \geq |\lambda_1 - \lambda_2|. \tag{3.36}$$

Finally, note that relation (3.32) can be inverted as follows

$$\begin{aligned}
|p \theta \phi; s_1 \lambda_1 s_2 \lambda_2\rangle &= \sum_{J=|\lambda_1 - \lambda_2|}^{\infty} \sum_{M=-J}^J C_J \\
&\quad \times D_{M \lambda_1 - \lambda_2}^J(\phi, \theta - \phi) |p; J M; s_1 \lambda_1 s_2 \lambda_2\rangle.
\end{aligned} \tag{3.37}$$

This relation can be verified by substituting (3.32) and using the completeness relations of Wigner D -matrices (B.12b). The explicit demonstration is not shown here, as the above relation will not be needed in our discussion, but can be found in [2].

Normalisation

The normalisation factor C_J in (3.32) is chosen to ensure that the angular momentum state $|p; J M; s_1 \lambda_1 s_2 \lambda_2\rangle$ has a standard Lorentz-invariant normalisation [2]

²Note that we must ensure the last angle $\gamma' = -\alpha'$ to stay in the $-\phi$ convention. This requirement leads to a phase that can be absorbed into the normalisation factor C_J .

$$\begin{aligned}
& \langle p'; J' M'; s_1 \lambda'_1 s_2 \lambda'_2 | p; J M; s_1 \lambda_1 s_2 \lambda_2 \rangle \\
&= \frac{4W}{p} \delta(W - W') \delta_{J J'} \delta_{M M'} \delta_{\lambda_1 \lambda'_1} \delta_{\lambda_2 \lambda'_2} \\
&= \frac{4w_1(p)w_2(p)}{p^2} \delta(p - p') \delta_{J J'} \delta_{M M'} \delta_{\lambda_1 \lambda'_1} \delta_{\lambda_2 \lambda'_2}.
\end{aligned} \tag{3.38}$$

Using the orthonormality relation of Wigner D -matrices (B.12a) and of two-body helicity states (3.31), the computation yields [1]

$$C_J = \sqrt{\frac{2J+1}{4\pi}}. \tag{3.39}$$

Parity

To compute the action of the parity operator on the state $|p; J M; s_1 \lambda_1 s_2 \lambda_2\rangle$, we start by considering its known action on the state $|\mathbf{p}; s \lambda\rangle$ given by (3.23). We need to determine its action on the opposite momentum state $|\mathbf{-p}; s \lambda\rangle$. Similar derivations to (3.23) lead to

$$\hat{P} |\mathbf{-p}; s \lambda\rangle = \eta(-1)^{2s} |\mathbf{p}; s - \lambda\rangle. \tag{3.40}$$

Then, the action of the parity operator on (3.32) is given by

$$\begin{aligned}
\hat{P} |p; J M; s_1 \lambda_1 s_2 \lambda_2\rangle &= \eta_1 \eta_2 (-1)^{2(s_1+s_2)} C_J \int d \cos \theta d \phi \\
&\times D_{M \lambda_1 - \lambda_2}^{J*}(\phi, \theta, -\phi) |\mathbf{-p}; s_1 - \lambda_1\rangle \otimes |\mathbf{p}; s_2 - \lambda_2\rangle.
\end{aligned} \tag{3.41}$$

In the above equation, the momenta's sign in the tensor product are opposite to the ones in the definition (3.32). After lengthy computations [1, 3], one can show

$$\hat{P} |p; J M; s_1 \lambda_1 s_2 \lambda_2\rangle = \eta_1 \eta_2 (-1)^{J-s_1-s_2} |p; J M; s_1 - \lambda_1 s_2 - \lambda_2\rangle. \tag{3.42}$$

We conclude that the two-body helicity state is not an eigenstate of the parity operator. However, to describe hadronic states within the helicity formalism, since the strong interaction is invariant under the action of parity, hadronic states should be eigenstates of \hat{P} . Using the following linear combination [10]

$$|H_{\pm}; J^P; \lambda_1 \lambda_2\rangle = \frac{1}{\sqrt{2}} [|p; J M; s_1 \lambda_1 s_2 \lambda_2\rangle \pm |p; J M; s_1 - \lambda_1 s_2 - \lambda_2\rangle], \tag{3.43}$$

the state $|H_{\pm}; J^P; \lambda_1 \lambda_2\rangle$ becomes an eigenstate of the parity operator with an eigenvalue

$$P = \pm \eta_1 \eta_2 (-1)^{J-s_1-s_2}. \tag{3.44}$$

Only the relative sign of λ_1 and λ_2 is relevant.

Symmetry

For systems of two identical particles, where $m_1 = m_2 = m$ and $s_1 = s_2 = s$, the wavefunction must be (anti)symmetric under the exchange of the particles. The action of the permutation operator \hat{P}_{12} between the two particles on the state $|p; JM; s_1 \lambda_1 s_2 \lambda_2\rangle$ yields

$$\hat{P}_{12} |p; JM; s \lambda_1 s \lambda_2\rangle = (-1)^{J-2s} |p; JM; s \lambda_2 s \lambda_1\rangle. \quad (3.45)$$

A demonstration of the above formula can be found in [1]. To impose the correct symmetry, the symmetriser operator (up to a normalisation factor)

$$\hat{\mathcal{S}} = 1 + (-1)^{2s} \hat{P}_{12}, \quad (3.46)$$

can be applied on the helicity state $|p; JM; s \lambda_1 s \lambda_2\rangle$. For bosons (s integer), $\hat{\mathcal{S}}$ corresponds to the symmetriser, whereas for fermions (s half integer) $\hat{\mathcal{S}}$ is the antisymmetriser. Its action on the angular momentum helicity states is then

$$\hat{\mathcal{S}} |p; JM; s \lambda_1 s \lambda_2\rangle = |p; JM; s \lambda_1 s \lambda_2\rangle + (-1)^J |p; JM; s \lambda_2 s \lambda_1\rangle. \quad (3.47)$$

Thus, the two-body states of bosons are characterised by even J , and the two-body states of fermions are characterised by odd J .

3.2.3 Two-body canonical states

After deriving the two-body helicity states, let us move on to the two-body canonical states. We recall that only massive particles can be described by canonical states. The discussion begins by constructing a two-body state in the CM frame, similar to the helicity states defined earlier

$$\begin{aligned} |p; s_1 \mu_1 s_2 \mu_2\rangle_c &= U(R(\phi, \theta, -\phi) L_z(\chi) R^{-1}(\phi, \theta, -\phi)) |\bar{p}; s_1 \mu_1\rangle \\ &\quad \otimes U(R(\pi + \phi, \pi - \theta, -(\pi + \phi))) \\ &\quad \times L_z(\chi) R^{-1}(\pi + \phi, \pi - \theta, -(\pi + \phi)) |\bar{p}; s_2 \mu_2\rangle. \end{aligned} \quad (3.48)$$

Since the set of all canonical basis states forms a complete set for describing two-body systems, it is possible to transform from one basis to the other using the following relation

$$\begin{aligned} |p; s_1 \lambda_1 s_2 \lambda_2\rangle &= \sum_{\mu_1=-s_1}^{s_1} \sum_{\mu_2=-s_2}^{s_2} D_{\mu_1 \lambda_1}^{s_1}(\phi, \theta, -\phi) \\ &\quad \times D_{\mu_2 -\lambda_2}^{s_2}(\phi, \theta, -\phi) |p; s_1 \mu_1 s_2 \mu_2\rangle_c. \end{aligned} \quad (3.49)$$

The demonstration is completely analogous to the change of basis between one-body states (3.19). Then, a total angular momentum J is provided through intermediate spin and orbital angular momentum [3]

$$\begin{aligned} |p; JM; LS; \lambda_1 \lambda_2\rangle &= \sum_{\mu_L, \mu_S, \mu_1, \mu_2} (L \mu_L S \mu_S | JM)(s_1 \mu_1 s_2 \mu_2 | S \mu_S) \\ &\quad \times \int d \cos \theta d \phi Y_m^l(\theta, \phi) |p \theta \phi; s_1 \mu_1 s_2 \mu_2\rangle_c, \end{aligned} \quad (3.50)$$

where $(abcd|ef)$ is a Clebsch-Gordan coefficient and $Y_m^l(\theta, \phi)$ is a spherical harmonic. Since this construction involves the orbital angular momentum L , it is often used in non-relativistic treatments.

Since the helicity and canonical bases form complete sets for describing a two-body system with total angular momentum J , it is possible to transform from one basis to another by means of the following transformation [1]

$$|p; JM; s_1 \lambda_1 s_2 \lambda_2\rangle = \sum_S \sum_L \sqrt{\frac{2L+1}{2J+1}} (s_1 \lambda_1 s_2 - \lambda_2 | S \lambda_1 - \lambda_2) \times (L 0 S \lambda_1 - \lambda_2 | J \lambda_1 - \lambda_2) |p; JM; L S; \lambda_1 \lambda_2\rangle, \quad (3.51)$$

where the first sum runs over all values $|s_1 - s_2| \leq S \leq s_1 + s_2$, and the second sum over all values $|J - S| \leq L \leq J + S$.

3.3 Application of the helicity formalism to hybrid baryons

As explained in Chapter 1, a hybrid baryon can be visualised as a four-body system consisting of three massive quarks and a massless gluon, in a constituent approach. Although extending the helicity formalism to more than two particles is possible [7, 11, 12], it presents a significant challenge worthy of a separate thesis. In order to keep the helicity treatment manageable, the hybrid baryon is reduced to a two-body system composed of a gluon and a core containing the three quarks (the quark core model will be explained in more detail in Chapter 4). This simplification allows for the computation of a complete basis of helicity states describing hybrid baryons. Given that the strong interaction is invariant under rotations and parity, hadronic states must be described by states with well-defined J^P quantum numbers, namely, helicity states (3.43). Since the two particles are distinct, there is no need to symmetrise the wavefunction. The total angular momentum J_C of the quark core, composed of massive particles, can be computed in the usual manner.

Before computing the helicity states, it is beneficial to revisit our main objective. Our primary challenge is to accurately couple the spin of the quark core with the helicity of the gluon, which can be achieved using the helicity basis. However, helicity states are not the states of non-relativistic quantum mechanics, which are the canonical states as previously discussed. Nevertheless, it is possible to change the basis thanks to relation (3.51). By knowing the action of the Hamiltonian on canonical states, we can determine the mean value of the Hamiltonian between helicity states. This procedure has already been applied in [10] for studying two-gluon glueballs in a constituent approach, where the helicity formalism is essential. The results for the glueball spectrum in [10] were comparable to those obtained via lattice QCD [13, 14, 15], validating the approach. Furthermore, it was demonstrated in [10] that if the gluon is assumed to have spin rather than helicity, meaning it possesses a third projection $\lambda = 0$, the glueball spectrum is significantly altered. New states emerge that are absent in the lattice QCD predictions, underscoring the importance of accurately incorporating the gluon's helicity in the computations.

In our initial approach, we assume no excitation among the quarks, i.e. $L_C = 0$. Consequently, the allowed total angular momenta for the quark core are $J_C = 1/2$ and $3/2$. The parity of the core is given by $\eta_C = (-1)^{L_C} = 1$. Let us now specify the helicity states describing hybrid baryons for these two values of J_C . Recall that gluons are characterised by $\lambda_g = \pm 1$ and $\eta_g = -1$.

3.3.1 Quark core with $J_C = 1/2$

For a quark core with spin $J_C = 1/2$, the allowed quark core helicities are $\lambda_C = \pm 1/2$. Thus, the hybrid baryon is described by a set of four states $|H_{\pm}; J^P; \lambda_1 \lambda_2\rangle$. Recalling the selection rule on angular momentum (3.36) and the formula for the parity of a helicity state (3.44), it is possible to compute the allowed J^P quantum numbers for each helicity state

$$\left| H_+; J^P; \frac{1}{2} 1 \right\rangle \text{ with } J = k + \frac{1}{2} \text{ and } P = (-1)^k \Rightarrow \frac{1^+}{2}, \frac{3^-}{2}, \frac{5^+}{2}, \dots \quad (3.52a)$$

$$\left| H_-; J^P; \frac{1}{2} 1 \right\rangle \text{ with } J = k + \frac{1}{2} \text{ and } P = -(-1)^k \Rightarrow \frac{1^-}{2}, \frac{3^+}{2}, \frac{5^-}{2}, \dots \quad (3.52b)$$

$$\left| H_+; J^P; -\frac{1}{2} 1 \right\rangle \text{ with } J = k + \frac{3}{2} \text{ and } P = -(-1)^k \Rightarrow \frac{3^-}{2}, \frac{5^+}{2}, \dots \quad (3.52c)$$

$$\left| H_-; J^P; -\frac{1}{2} 1 \right\rangle \text{ with } J = k + \frac{3}{2} \text{ and } P = (-1)^k \Rightarrow \frac{3^+}{2}, \frac{5^-}{2}, \dots \quad (3.52d)$$

where k is a positive integer. Next, the change of basis (3.51) is applied to the above helicity states. To simplify the notation, we express a canonical state using spectroscopic notation $|^{2S+1}L_J\rangle$

$$\begin{aligned} \left| H_+; J^P; \frac{1}{2} 1 \right\rangle &= \sqrt{\frac{2}{3}} |^2k+1_J\rangle - \sqrt{\frac{k+2}{6(2k+1)}} |^4k+1_J\rangle \\ &\quad + \sqrt{\frac{k}{2(2k+1)}} |^4k-1_J\rangle, \end{aligned} \quad (3.53a)$$

$$\begin{aligned} \left| H_-; J^P; \frac{1}{2} 1 \right\rangle &= \sqrt{\frac{2}{3}} |^2k_J\rangle + \sqrt{\frac{k}{6(2k+3)}} |^4k_J\rangle \\ &\quad - \sqrt{\frac{k+2}{2(2k+3)}} |^4k+2_J\rangle, \end{aligned} \quad (3.53b)$$

$$\left| H_+; J^P; -\frac{1}{2} 1 \right\rangle = \sqrt{\frac{3(k+1)}{2(2k+3)}} |^4k+2_J\rangle + \sqrt{\frac{k+3}{2(2k+3)}} |^4k_J\rangle, \quad (3.53c)$$

$$\left| H_-; J^P; -\frac{1}{2} 1 \right\rangle = \sqrt{\frac{k+1}{2(2k+5)}} |^4k+3_J\rangle + \sqrt{\frac{3(k+3)}{2(2k+5)}} |^4k+1_J\rangle. \quad (3.53d)$$

One can verify the orthonormality of the helicity states as a proof check of the computations. Since canonical states are eigenstates of the squared total

\hat{Q}	\mathbf{J}^2	\mathbf{L}^2	\mathbf{S}^2	$\mathbf{L} \cdot \mathbf{S}$
$ H_+; J^P; \frac{1}{2}1\rangle$	$J(J+1)$	$J(J+1) + 5/4$	$7/4$	$-3/2$
$ H_-; J^P; \frac{1}{2}1\rangle$	$J(J+1)$	$J(J+1) + 5/4$	$7/4$	$-3/2$
$ H_+; J^P; -\frac{1}{2}1\rangle$	$J(J+1)$	$J(J+1) - 3/4$	$15/4$	$-3/2$
$ H_-; J^P; -\frac{1}{2}1\rangle$	$J(J+1)$	$J(J+1) - 3/4$	$15/4$	$-3/2$

Table 3.1: Mean values of different operators \hat{Q} for the helicity states (3.52).

angular momentum operator \mathbf{J}^2 , the squared orbital angular momentum \mathbf{L}^2 , and the squared total spin \mathbf{S}^2 , it is possible to compute the mean value of these operators between the helicity states. The results are presented in Table 3.1. One can check that $\langle \mathbf{J}^2 \rangle = \langle \mathbf{L}^2 \rangle + \langle \mathbf{S}^2 \rangle + 2 \langle \mathbf{L} \cdot \mathbf{S} \rangle$.

3.3.2 Quark core with $J_C = 3/2$

For a quark core with spin $J_C = 3/2$, the allowed quark core helicities are $\lambda_C = \pm 1/2, \pm 3/2$, leading to eight hybrid baryon states $|H_{\pm}; J^P; \lambda_1 \lambda_2\rangle$. By recalling the selection rule on angular momentum (3.36) and the parity formula for a helicity state (3.44), we can compute the allowed J^P quantum numbers for each helicity state as follows

$$\left| H_+; J^P; \frac{1}{2}1 \right\rangle \text{ with } J = k + \frac{1}{2} \text{ and } P = -(-1)^k \Rightarrow \frac{1}{2}^-, \frac{3}{2}^+, \frac{5}{2}^-, \dots \quad (3.54a)$$

$$\left| H_-; J^P; \frac{1}{2}1 \right\rangle \text{ with } J = k + \frac{1}{2} \text{ and } P = (-1)^k \Rightarrow \frac{1}{2}^+, \frac{3}{2}^-, \frac{5}{2}^+, \dots \quad (3.54b)$$

$$\left| H_+; J^P; \frac{3}{2}1 \right\rangle \text{ with } J = k + \frac{1}{2} \text{ and } P = -(-1)^k \Rightarrow \frac{1}{2}^-, \frac{3}{2}^+, \frac{5}{2}^-, \dots \quad (3.54c)$$

$$\left| H_-; J^P; \frac{3}{2}1 \right\rangle \text{ with } J = k + \frac{1}{2} \text{ and } P = (-1)^k \Rightarrow \frac{1}{2}^+, \frac{3}{2}^-, \frac{5}{2}^+, \dots \quad (3.54d)$$

$$\left| H_+; J^P; -\frac{1}{2}1 \right\rangle \text{ with } J = k + \frac{3}{2} \text{ and } P = (-1)^k \Rightarrow \frac{3}{2}^+, \frac{5}{2}^-, \dots \quad (3.54e)$$

$$\left| H_-; J^P; -\frac{1}{2}1 \right\rangle \text{ with } J = k + \frac{3}{2} \text{ and } P = -(-1)^k \Rightarrow \frac{3}{2}^-, \frac{5}{2}^+, \dots \quad (3.54f)$$

$$\left| H_+; J^P; -\frac{3}{2}1 \right\rangle \text{ with } J = k + \frac{5}{2} \text{ and } P = -(-1)^k \Rightarrow \frac{5}{2}^-, \dots \quad (3.54g)$$

$$\left| H_-; J^P; -\frac{3}{2}1 \right\rangle \text{ with } J = k + \frac{5}{2} \text{ and } P = (-1)^k \Rightarrow \frac{5}{2}^+, \dots \quad (3.54h)$$

where k is a positive integer. Next, we apply the change of basis (3.51) to the above helicity states

$$\left| H_+; J^P; \frac{1}{2}1 \right\rangle = \sqrt{\frac{3(k+3)(k+2)}{20(2k+3)(2k+1)}} |^6 k+2_J\rangle - \sqrt{\frac{4(k+2)}{5(2k+3)}} |^4 k+2_J\rangle$$

$$\begin{aligned}
 & -\sqrt{\frac{3k(k+2)}{10(2k+3)(2k-1)}} |{}^6k_J\rangle + \sqrt{\frac{4k}{15(2k+3)}} |{}^4k_J\rangle \\
 & + \frac{\sqrt{6}}{6} |{}^2k_J\rangle + \sqrt{\frac{3k(k-1)}{4(2k+1)(2k-1)}} |{}^6k-2_J\rangle, \quad (3.55a)
 \end{aligned}$$

$$\begin{aligned}
 |H_-; J^P; \frac{1}{2}1\rangle & = \sqrt{\frac{3(k+3)(k+2)}{4(2k+5)(2k+3)}} |{}^6k+3_J\rangle - \sqrt{\frac{4(k+2)}{15(2k+1)}} |{}^4k+1_J\rangle \\
 & + \sqrt{\frac{4k}{5(2k+1)}} |{}^4k-1_J\rangle + \sqrt{\frac{3k(k-1)}{20(2k+3)(2k+1)}} |{}^6k-1_J\rangle \\
 & + \frac{\sqrt{6}}{6} |{}^2k+1_J\rangle - \sqrt{\frac{3k(k+2)}{10(2k+5)(2k+1)}} |{}^6k+1_J\rangle, \quad (3.55b)
 \end{aligned}$$

$$\begin{aligned}
 |H_+; J^P; \frac{3}{2}1\rangle & = \sqrt{\frac{3(k+2)}{5(2k+3)}} |{}^4k+2_J\rangle + \sqrt{\frac{(k+3)(k+2)}{20(2k+3)(2k+1)}} |{}^6k+2_J\rangle \\
 & - \sqrt{\frac{k}{5(2k+3)}} |{}^4k_J\rangle - \sqrt{\frac{k(k+2)}{10(2k+3)(2k-1)}} |{}^6k_J\rangle \\
 & + \frac{\sqrt{2}}{2} |{}^2k_J\rangle + \sqrt{\frac{k(k-1)}{4(2k+1)(2k-1)}} |{}^6k-2_J\rangle, \quad (3.55c)
 \end{aligned}$$

$$\begin{aligned}
 |H_-; J^P; \frac{3}{2}1\rangle & = \sqrt{\frac{3k}{5(2k+1)}} |{}^4k-1_J\rangle - \sqrt{\frac{k(k-1)}{20(2k+3)(2k+1)}} |{}^6k-1_J\rangle \\
 & - \sqrt{\frac{k+2}{5(2k+1)}} |{}^4k+1_J\rangle - \sqrt{\frac{(k+3)(k+2)}{4(2k+5)(2k+3)}} |{}^6k+3_J\rangle \\
 & - \frac{\sqrt{2}}{2} |{}^2k+1_J\rangle + \sqrt{\frac{k(k+2)}{10(2k+5)(2k+1)}} |{}^6k+1_J\rangle, \quad (3.55d)
 \end{aligned}$$

$$\begin{aligned}
 |H_+; J^P; -\frac{1}{2}1\rangle & = \sqrt{\frac{k+1}{5(2k+5)}} |{}^4k+3_J\rangle - \sqrt{\frac{27(k+4)(k+1)}{20(2k+5)(2k+3)}} |{}^6k+3_J\rangle \\
 & + \sqrt{\frac{3(k+3)}{5(2k+5)}} |{}^4k+1_J\rangle + \sqrt{\frac{3k(k+3)}{4(2k+3)(2k+1)}} |{}^6k-1_J\rangle \\
 & + \sqrt{\frac{3}{10}} \frac{k-2}{\sqrt{(2k+5)(2k+1)}} |{}^6k+1_J\rangle, \quad (3.55e)
 \end{aligned}$$

$$\begin{aligned}
 |H_-; J^P; -\frac{1}{2}1\rangle & = \sqrt{\frac{3(k+1)}{5(2k+3)}} |{}^4k+2_J\rangle - \sqrt{\frac{3(k+4)(k+1)}{4(2k+7)(2k+5)}} |{}^6k+4_J\rangle \\
 & - \sqrt{\frac{3}{10}} \frac{k+6}{\sqrt{(2k+7)(2k+3)}} |{}^6k+2_J\rangle + \sqrt{\frac{k+3}{5(2k+3)}} |{}^4k_J\rangle \\
 & + \sqrt{\frac{27k(k+3)}{20(2k+5)(2k+3)}} |{}^6k_J\rangle, \quad (3.55f)
 \end{aligned}$$

$$\begin{aligned}
 |H_+; J^P; -\frac{3}{2}1\rangle & = \sqrt{\frac{5(k+2)(k+1)}{4(2k+7)(2k+5)}} |{}^6k+4_J\rangle + \sqrt{\frac{5(k+5)(k+1)}{2(2k+7)(2k+3)}} |{}^6k+2_J\rangle \\
 & + \sqrt{\frac{(k+5)(k+4)}{4(2k+5)(2k+3)}} |{}^6k_J\rangle, \quad (3.55g)
 \end{aligned}$$

\hat{Q}	J^2	L^2	S^2	$L \cdot S$
$ H_+; J^P; \frac{1}{2}1\rangle$	$J(J+1)$	$J(J+1) + 17/4$	$19/4$	$-9/2$
$ H_-; J^P; \frac{1}{2}1\rangle$	$J(J+1)$	$J(J+1) + 17/4$	$19/4$	$-9/2$
$ H_+; J^P; \frac{3}{2}1\rangle$	$J(J+1)$	$J(J+1) + 9/4$	$11/4$	$-5/2$
$ H_-; J^P; \frac{3}{2}1\rangle$	$J(J+1)$	$J(J+1) + 9/4$	$11/4$	$-5/2$
$ H_+; J^P; -\frac{1}{2}1\rangle$	$J(J+1)$	$J(J+1) + 9/4$	$27/4$	$-9/2$
$ H_-; J^P; -\frac{1}{2}1\rangle$	$J(J+1)$	$J(J+1) + 9/4$	$27/4$	$-9/2$
$ H_+; J^P; -\frac{3}{2}1\rangle$	$J(J+1)$	$J(J+1) - 15/4$	$35/4$	$-5/2$
$ H_-; J^P; -\frac{3}{2}1\rangle$	$J(J+1)$	$J(J+1) - 15/4$	$35/4$	$-5/2$

Table 3.2: Mean values of different operators \hat{Q} for the helicity states (3.54).

$$\begin{aligned}
|H_-; J^P; -\frac{3}{2}1\rangle &= \sqrt{\frac{(k+1)(k+2)}{4(2k+7)(2k+9)}} |{}^6k+5_J\rangle + \sqrt{\frac{5(k+1)(k+5)}{2(2k+5)(2k+9)}} |{}^6k+3_J\rangle \\
&+ \sqrt{\frac{5(k+4)(k+5)}{4(2k+5)(2k+7)}} |{}^6k+1_J\rangle. \tag{3.55h}
\end{aligned}$$

All the states are orthonormal as expected. Similar to the previous case, the mean value of the operators J^2 , L^2 , and S^2 can be computed between the above eigenstates. The results are presented in Table 3.2.

3.3.3 Physical states

Assuming there is no excitation in the quark core, the sets of helicity states (3.52) and (3.54) describe a hybrid baryon with total angular momentum J and parity P in a quark core model. By the symmetry of strong interaction, states with different J^P quantum numbers cannot mix with each other. Similarly, states with different quark core spin J_C cannot mix either (see the orthonormality relation (3.38)). However, states with the same J^P and J_C quantum numbers may mix through the action of the Hamiltonian. In particular, they may mix through the operator L^2 , which is hidden in the kinetic term of the Hamiltonian. In the study of two-gluon glueballs [10], it was shown that there is no such mixing and the matrix elements of L^2 are diagonal. However, nothing guarantees it will be the same case for hybrid baryons. Thus, let us compute the matrix elements of L^2 for the helicity states giving fixed values of J^P .

Before moving on, we simplify the notation by writing a helicity state (3.43) as $|J^P; J_C; \alpha\rangle$, where α is a set of quantum numbers differentiating the states with the same value J^P and J_C . The matrix elements of L^2 are noted

$$w_{\alpha\beta} = \langle J^P; J_C; \alpha | L^2 | J^P; J_C; \beta \rangle. \tag{3.56}$$

Let us also define an effective orbital angular momentum l_{eff} between the quark core and the gluon, so that the eigenvalues of L^2 are written as $l_{\text{eff}}(l_{\text{eff}} + 1)$.

$$J^P = \frac{1}{2}^+$$

Only the state (3.52a) can produce a $J^P = 1/2^+$ state for $J_C = 1/2$. Obviously, no mixing occurs since there is a single state and the mean value of \mathbf{L}^2 is given by $w_{11} = 2$, corresponding to $l_{\text{eff}} = 1$. For $J_C = 3/2$, the two states (3.54b) and (3.54d) intervene. The \mathbf{L}^2 matrix elements are

$$w_{\alpha\beta} = \begin{pmatrix} 5 & -\sqrt{3} \\ -\sqrt{3} & 3 \end{pmatrix}. \quad (3.57)$$

Thus, mixing occurs between these two states. The eigenvalues of the above matrix are equal to 6 and 2, corresponding to $l_{\text{eff}} = 2$ and 1 respectively, and the diagonalised basis, denoted as $|J^{PC}; J_C; l_{\text{eff}}\rangle$, is given by

$$\left| \frac{1}{2}^+ ; \frac{3}{2}; 2 \right\rangle = -\sqrt{\frac{1}{2}} |^2 1_J\rangle + \sqrt{\frac{1}{10}} |^4 1_J\rangle - \sqrt{\frac{2}{5}} |^6 3_J\rangle, \quad (3.58a)$$

$$\left| \frac{1}{2}^+ ; \frac{3}{2}; 1 \right\rangle = -\sqrt{\frac{1}{6}} |^2 1_J\rangle - \sqrt{\frac{5}{6}} |^4 1_J\rangle. \quad (3.58b)$$

Note that the three states giving rise to $1/2^+$ quantum numbers are characterised by integer l_{eff} . This property will also appear in the subsequent cases. Let us note that this property is not observed for two-gluon glueballs [10].

$$J^P = \frac{1}{2}^-$$

Only the state (3.52b) can produce a $J^P = 1/2^-$ state for $J_C = 1/2$. Obviously, no mixing occurs since there is a single state and the mean value of \mathbf{L}^2 is given by $w_{11} = 2$, corresponding to $l_{\text{eff}} = 1$. For $J_C = 3/2$, the two states (3.54a) and (3.54c) intervene. The \mathbf{L}^2 matrix elements are the same as (3.57). The diagonalised basis is given by

$$\left| \frac{1}{2}^- ; \frac{3}{2}; 2 \right\rangle = \sqrt{\frac{9}{10}} |^4 2_J\rangle - \sqrt{\frac{1}{10}} |^6 2_J\rangle, \quad (3.59a)$$

$$\left| \frac{1}{2}^- ; \frac{3}{2}; 1 \right\rangle = \sqrt{\frac{2}{3}} |^2 0_J\rangle + \sqrt{\frac{1}{30}} |^4 2_J\rangle + \sqrt{\frac{3}{10}} |^6 2_J\rangle. \quad (3.59b)$$

$$J^P = \frac{3}{2}^+$$

The states (3.52b) and (3.52d) give rise to $J^P = 3/2^+$ states for $J_C = 1/2$. Interestingly, the matrix elements of \mathbf{L}^2 are the same as the ones for $J_C = 3/2$ states in the previous case (3.57). The diagonalised basis is given by

$$\left| \frac{3}{2}^+ ; \frac{1}{2}; 2 \right\rangle = -\sqrt{\frac{1}{2}} |^2 1_J\rangle + \sqrt{\frac{1}{10}} |^4 1_J\rangle + \sqrt{\frac{2}{5}} |^4 3_J\rangle, \quad (3.60a)$$

$$\left| \frac{3}{2}^+ ; \frac{1}{2}; 1 \right\rangle = \sqrt{\frac{1}{6}} |^2 1_J\rangle + \sqrt{\frac{5}{6}} |^4 1_J\rangle. \quad (3.60b)$$

For the $J_C = 3/2$ states, three states (3.54a), (3.54c) and (3.54e) produce $J^P = 3/2^+$ with

$$w_{\alpha\beta} = \begin{pmatrix} 8 & -2\sqrt{3} & -2\sqrt{3} \\ -2\sqrt{3} & 6 & 0 \\ -2\sqrt{3} & 0 & 6 \end{pmatrix}. \quad (3.61)$$

The eigenvalues are equal to 12, 6 and 2, and the diagonalised basis is given by

$$\left| \frac{3^+}{2}; \frac{3}{2}; 3 \right\rangle = \sqrt{\frac{4}{5}} |^4 3_J\rangle - \sqrt{\frac{1}{5}} |^6 3_J\rangle, \quad (3.62a)$$

$$\begin{aligned} \left| \frac{3^+}{2}; \frac{3}{2}; 2 \right\rangle &= -\frac{1}{2} |^2 1_J\rangle + \frac{2\sqrt{2}}{5} |^4 1_J\rangle - \frac{\sqrt{2}}{5} |^4 3_J\rangle \\ &\quad - \frac{\sqrt{3}}{10} |^6 1_J\rangle - \frac{2\sqrt{2}}{5} |^6 3_J\rangle, \end{aligned} \quad (3.62b)$$

$$\left| \frac{3^+}{2}; \frac{3}{2}; 1 \right\rangle = \sqrt{\frac{5}{12}} |^2 1_J\rangle + \sqrt{\frac{2}{15}} |^4 1_J\rangle - \sqrt{\frac{9}{20}} |^6 1_J\rangle. \quad (3.62c)$$

$J^P = \frac{3}{2}^-$

The states (3.52a) and (3.52c) give rise to $J^P = 3/2^-$ states for $J_C = 1/2$. The L^2 matrix elements are the same as (3.57) and the diagonalised basis is given by

$$\left| \frac{3^-}{2}; \frac{1}{2}; 2 \right\rangle = -\sqrt{\frac{1}{2}} |^2 2_J\rangle + \sqrt{\frac{1}{2}} |^4 2_J\rangle, \quad (3.63a)$$

$$\left| \frac{3^-}{2}; \frac{1}{2}; 1 \right\rangle = \sqrt{\frac{1}{6}} |^2 2_J\rangle + \sqrt{\frac{2}{3}} |^4 0_J\rangle + \sqrt{\frac{1}{6}} |^4 2_J\rangle, \quad (3.63b)$$

For the $J_C = 3/2$ states, three states (3.54b), (3.54d) and (3.54f) produce $J^P = 3/2^-$ with the matrix elements of L^2 given by (3.61). The diagonalised basis is given by

$$\left| \frac{3^-}{2}; \frac{3}{2}; 3 \right\rangle = -\sqrt{\frac{2}{5}} |^2 2_J\rangle + \frac{2}{5} |^4 2_J\rangle - \frac{1}{5} \sqrt{\frac{2}{7}} |^6 2_J\rangle - \sqrt{\frac{3}{7}} |^6 4_J\rangle, \quad (3.64a)$$

$$\left| \frac{3^-}{2}; \frac{3}{2}; 2 \right\rangle = \frac{1}{2} |^2 2_J\rangle + \sqrt{\frac{2}{5}} |^4 2_J\rangle - \frac{1}{2} \sqrt{\frac{7}{5}} |^6 2_J\rangle, \quad (3.64b)$$

$$\left| \frac{3^-}{2}; \frac{3}{2}; 1 \right\rangle = -\frac{1}{2\sqrt{15}} |^2 2_J\rangle + \sqrt{\frac{2}{3}} |^4 0_J\rangle - \frac{2}{5} \sqrt{\frac{2}{3}} |^4 2_J\rangle - \frac{\sqrt{21}}{10} |^6 2_J\rangle. \quad (3.64c)$$

$J^P = \frac{5}{2}^+, \frac{7}{2}^-, \dots$

Consider now states with $J \geq 5/2$ and alternating parity starting from $P = 1$. For $J_C = 1/2$, states (3.52a) and (3.52c) intervene. The L^2 matrix elements are

$$w_{\alpha\beta} = \begin{pmatrix} k^2 + 6k + 10 & -\sqrt{(k+4)(k+2)} \\ -\sqrt{(k+4)(k+2)} & (k+4)(k+2) \end{pmatrix}, \quad (3.65)$$

where k is a positive integer. The eigenvalues are $(k+2)(k+3)$ and $(k+3)(k+2)$ and the diagonalised basis is

$$\begin{aligned} \left| J^P \geq \frac{5^+}{2}; \frac{1}{2}; k+2 \right\rangle &= \sqrt{\frac{k+2}{3(k+3)}} |^2k+3_J\rangle + \sqrt{\frac{(k+2)(k+4)}{3(k+3)(2k+5)}} |^4k+3_J\rangle \\ &\quad + \sqrt{\frac{k+3}{2k+5}} |^4k+1_J\rangle, \end{aligned} \quad (3.66a)$$

$$\left| J^P \geq \frac{5^+}{2}; \frac{1}{2}; k+3 \right\rangle = \sqrt{\frac{2k+5}{3(k+3)}} |^4k+3_J\rangle - \sqrt{\frac{k+4}{3(k+3)}} |^2k+3_J\rangle. \quad (3.66b)$$

For $J_C = 3/2$, the states (3.54b), (3.54d), (3.54f) and (3.54h) intervene. The L^2 matrix elements are

$$\begin{pmatrix} k^2 + 6k + 13 & -\sqrt{3}(k+3) & -2\sqrt{(k+4)(k+2)} & 0 \\ -\sqrt{3}(k+3) & k^2 + 6k + 11 & 0 & 0 \\ -2\sqrt{(k+4)(k+2)} & 0 & k^2 + 6k + 11 & -\sqrt{3(k+5)(k+1)} \\ 0 & 0 & -\sqrt{3(k+5)(k+1)} & (k+5)(k+1) \end{pmatrix}, \quad (3.67)$$

with the eigenvalues $(k+1)(k+2)$, $(k+2)(k+3)$, $(k+3)(k+4)$ and $(k+4)(k+5)$ and the diagonalised basis

$$\left| J^P \geq \frac{5^+}{2}; \frac{3}{2}; k+1 \right\rangle = \sqrt{\frac{3(k+1)}{5(k+2)}} |^4k+1_J\rangle + \sqrt{\frac{2k+7}{5(k+2)}} |^6k+1_J\rangle, \quad (3.68a)$$

$$\begin{aligned} \left| J^P \geq \frac{5^+}{2}; \frac{3}{2}; k+2 \right\rangle &= \frac{k+2}{\sqrt{6(2k+7)(k+3)}} |^2k+3_J\rangle \\ &\quad - \sqrt{\frac{(2k+7)(k+3)}{5(2k+5)(k+2)}} |^4k+1_J\rangle \\ &\quad + (k+2) \sqrt{\frac{16(k+4)}{15(2k+7)(2k+5)(k+3)}} |^4k+3_J\rangle \\ &\quad + \sqrt{\frac{3(k+3)(k+1)}{5(2k+5)(k+2)}} |^6k+1_J\rangle \\ &\quad + \sqrt{\frac{3(2k+9)(k+4)(k+2)}{10(2k+7)(2k+5)(k+3)}} |^6k+3_J\rangle, \end{aligned} \quad (3.68b)$$

$$\begin{aligned} \left| J^P \geq \frac{5^+}{2}; \frac{3}{2}; k+3 \right\rangle &= -\sqrt{\frac{2k+5}{6(k+3)}} |^2k+3_J\rangle - \frac{k+7}{\sqrt{15(k+4)(k+3)}} |^4k+3_J\rangle \\ &\quad + \sqrt{\frac{3(2k+9)(k+2)}{10(k+4)(k+3)}} |^6k+3_J\rangle, \end{aligned} \quad (3.68c)$$

$$\begin{aligned}
\left| J^P \geq \frac{5^+}{2}; \frac{3}{2}; k+4 \right\rangle &= \sqrt{\frac{k+5}{2(2k+7)}} |^2k+3_J\rangle - \sqrt{\frac{(2k+5)(k+5)}{5(2k+7)(k+4)}} |^4k+3_J\rangle \\
&+ \sqrt{\frac{(2k+5)(k+5)(k+2)}{10(2k+9)(2k+7)(k+4)}} |^6k+3_J\rangle \\
&+ \sqrt{\frac{k+4}{2k+9}} |^6k+5_J\rangle. \tag{3.68d}
\end{aligned}$$

$$J^P = \frac{5^-}{2}, \frac{7^+}{2}, \dots$$

Consider now states with $J \geq 5/2$ and alternating parity starting from $P = -1$. For $J_C = 1/2$, states (3.52b) and (3.52d) intervene. The L^2 matrix elements are the same as (3.65). The eigenvalues are $(k+2)(k+3)$ and $(k+3)(k+4)$, where k is a positive integer, and the diagonalised basis is

$$\left| J^P \geq \frac{5^-}{2}; \frac{1}{2}; k+2 \right\rangle = \sqrt{\frac{k+2}{3(k+3)}} |^2k+2_J\rangle + \sqrt{\frac{2k+7}{3(k+3)}} |^4k+2_J\rangle, \tag{3.69a}$$

$$\begin{aligned}
\left| J^P \geq \frac{5^-}{2}; \frac{1}{2}; k+3 \right\rangle &= -\sqrt{\frac{k+4}{3(k+3)}} |^2k+2_J\rangle + \sqrt{\frac{k+3}{2k+7}} |^4k+4_J\rangle \\
&+ \sqrt{\frac{(k+4)(k+2)}{3(2k+7)(k+3)}} |^4k+2_J\rangle. \tag{3.69b}
\end{aligned}$$

For $J_C = 3/2$, the states (3.54a), (3.54c), (3.54e) and (3.54g) intervene. The L^2 matrix elements are the same as (3.67), with the eigenvalues $(k+1)(k+2)$, $(k+2)(k+3)$, $(k+3)(k+4)$ and $(k+4)(k+5)$ and the diagonalised basis

$$\begin{aligned}
\left| J^P \geq \frac{5^-}{2}; \frac{3}{2}; k+1 \right\rangle &= \sqrt{\frac{k+1}{2(2k+5)}} |^2k+2_J\rangle + \sqrt{\frac{k+2}{2k+3}} |^6k_J\rangle \\
&+ \sqrt{\frac{(2k+7)(k+1)}{5(2k+5)(k+2)}} |^4k+2_J\rangle \\
&+ \sqrt{\frac{(2k+7)(k+4)(k+1)}{10(2k+5)(2k+3)(k+2)}} |^6k+2_J\rangle, \tag{3.70a}
\end{aligned}$$

$$\begin{aligned}
\left| J^P \geq \frac{5^-}{2}; \frac{3}{2}; k+2 \right\rangle &= -\sqrt{\frac{2k+7}{6(k+3)}} |^2k+2_J\rangle + \frac{k-1}{\sqrt{15(k+3)(k+2)}} |^4k+2_J\rangle \\
&+ \sqrt{\frac{3(2k+3)(k+4)}{10(k+3)(k+2)}} |^6k+2_J\rangle, \tag{3.70b}
\end{aligned}$$

$$\begin{aligned}
\left| J^P \geq \frac{5^-}{2}; \frac{3}{2}; k+3 \right\rangle &= -(k+4) \sqrt{\frac{16(k+2)}{15(2k+7)(2k+5)(k+3)}} |^4k+2_J\rangle \\
&+ \frac{k+4}{\sqrt{6(2k+5)(k+3)}} |^2k+2_J\rangle \\
&+ \sqrt{\frac{(2k+5)(k+3)}{5(2k+7)(k+4)}} |^4k+4_J\rangle \\
&+ \sqrt{\frac{3(2k+3)(k+4)(k+2)}{10(2k+7)(2k+5)(k+3)}} |^6k+2_J\rangle
\end{aligned}$$

$$+ \sqrt{\frac{3(k+5)(k+3)}{5(2k+7)(k+4)}} |{}^6k+4_J\rangle, \quad (3.70c)$$

$$\left| J^P \geq \frac{5^-}{2}; \frac{3}{2}; k+4 \right\rangle = -\sqrt{\frac{3(k+5)}{5(k+4)}} |{}^4k+4_J\rangle + \sqrt{\frac{2k+5}{5(k+4)}} |{}^6k+4_J\rangle. \quad (3.70d)$$

In all these cases, it is always possible to define an integer value for l_{eff} .

To conclude this chapter, the helicity formalism for one- and two-body states has been reviewed. It was demonstrated that the helicity basis can describe both massless and massive particles through equations (3.9) and (3.12), respectively. In particular, a two-body helicity state with well-defined total angular momentum J and parity P was constructed using equations (3.32) and (3.43). Building on this, the helicity basis for hybrid baryons in a quark core model was computed. In this model, the hybrid baryon is treated as an effective two-body system, with a quark core possessing an angular momentum $J_C = 1/2$ or $3/2$, and a gluon with helicity ± 1 . For $J_C = 1/2$, the hybrid baryon is characterised by the four helicity states (3.52), while for $J_C = 3/2$, it is described by eight helicity states (3.54). Each helicity state was then decomposed into canonical states, corresponding to the familiar quantum mechanical states, using equation (3.51). The decomposition was performed using the Mathematica software [16, 17], with the results provided in (3.53) and (3.55) for $J_C = 1/2$ and $3/2$, respectively.

These decompositions enabled the calculation of matrix elements for various operators, such as \mathbf{L}^2 . Notably, it was observed that the matrix elements of \mathbf{L}^2 between states with the same J^P and J_C quantum numbers are non-diagonal. Consequently, the matrix elements were diagonalised, leading to the identification of the physical states presented in Sec. 3.3.3.

Bibliography

- [1] Jacob, M. & Wick, G. C. On the general theory of collisions for particles with spin. *Ann. Phys.* **7**, 404 (1959).
- [2] Martin, A. D. & Spearman, T. D. *Elementary Particle Theory* (North-Holland Publishing Company, Amsterdam, 1970).
- [3] Chung, S.-U. Spin formalisms. <https://suchung.web.cern.ch/spinfmt1.pdf> (2014). CERN Yellow Report.
- [4] Weinberg, S. *The Quantum Theory of Fields. Volume I: Foundations* (Cambridge University Press, Cambridge, 2005).
- [5] Giebink, D. R. Relativity and spin in one-, two-, and three-body systems. *Phys. Rev. C* **32**, 502 (1985).
- [6] Lindner, N. H., Peres, A. & Terno, D. R. Wigner's little group and Berry's phases for massless particles. *J. Phys. A: Math. Gen.* **36**, L449 (2003).
- [7] Wick, G. C. Angular momentum states for three relativistic particles. *Ann. Phys.* **18**, 65 (1962).
- [8] Navas, S. *et al.* Review of particle physics. *Phys. Rev. D* **110**, 030001 (2024).
- [9] Tung, W.-K. *Group Theory in Physics* (World Scientific, Singapore, 1985).
- [10] Mathieu, V., Buisseret, F. & Semay, C. Gluons in glueballs: Spin or helicity? *Phys. Rev. D* **77**, 114022 (2008).
- [11] Berman, S. M. & Jacob, M. Systematics of angular and polarization distributions in three-body decays. *Phys. Rev.* **139**, B1023 (1965).
- [12] Werle, J. A simple representation for relativistic many-particle systems. *Nucl. Phys.* **44**, 579 (1963).
- [13] Morningstar, C. J. & Peardon, M. Glueball spectrum from an anisotropic lattice study. *Phys. Rev. D* **60**, 034509 (1999).
- [14] Chen, Y. *et al.* Glueball spectrum and matrix elements on anisotropic lattices. *Phys. Rev. D* **73**, 014516 (2006).
- [15] Meyer, H. B. & Teper, M. J. Glueball Regge trajectories and the pomeron: a lattice study. *Phys. Lett. B* **605**, 344 (2005).
- [16] Wolfram Research, Inc. Mathematica, Version 14.1. <https://www.wolfram.com/mathematica>. Champaign, IL, 2024.
- [17] Gómez Muñoz, J. L. & Delgado, F. QUANTUM: A Wolfram *Mathematica* add-on for Dirac bra-ket notation, non-commutative algebra, and simulation of quantum computing circuits. *J. Phys.: Conf. Ser.* **698**, 012019 (2016).

Hybrid baryons in a constituent approach 4

As discussed in the Introduction and Chapter 1, Quantum Chromodynamics (QCD) allows the existence of states beyond ordinary hadrons (baryons and mesons), such as the hybrid states. In these states, the gluonic field is in an excited state, and the quark content forms a colour octet state. It has been demonstrated in [1, 2] that for hybrid mesons, the excited gluonic field can be equivalently represented as a constituent gluon¹. Assuming this equivalence also holds for hybrid baryons, these can be modelled as a system comprising three quarks and a constituent gluon. Consequently, in the constituent approach of QCD, a hybrid baryon is described by the following generic Hamiltonian, where the natural units $\hbar = c = 1$ are used

$$H_{\text{HB}} = \sum_{i=1}^3 T_q(p_i) + T_g(p_g) + \sum_{i < j=2}^3 V_{qq}(r_{ij}) + \sum_{i=1}^3 V_{qg}(r_{ig}), \quad (4.1)$$

where $T(p_i)$ represents the kinetic energy, which depends on the modulus of the momentum $p_i = |\mathbf{p}_i|$, and $V(r_{ij})$ denotes the potential, which is a function of the distance between the particles $r_{ij} = |\mathbf{r}_i - \mathbf{r}_j|$. The characteristics of these potentials are elaborated in subsequent sections. The resolution of the associated four-body Schrödinger-like equation will also be discussed later.

The adoption of a constituent approach for gluons may appear controversial. Pioneering research into glueballs, which are purely gluonic states, can be found in [3, 4]. In these studies, glueballs are treated as bound states of constituent gluons, but the properties of the gluons (such as mass and spin) vary. In the approach of the first study [3], gluons are massless particles that acquire a constituent mass when confined within a hadron. Conversely, in the second study [4], gluons are inherently massive particles. Although it is clear that a massless gluon has a helicity degree of freedom, with two spin projections ± 1 , it is not clear if it is the same when they are confined within a hadron. A study in [5] concluded that the spectrum of two-gluon glueballs in a constituent approach aligns well with lattice QCD results if gluons have a helicity degree of freedom. This conclusion is confirmed in [6], where an effective potential was derived from

¹The term “constituent” is used here to differentiate this gluon from virtual gluons, which mediate the strong interaction between colour sources.

the available lattice QCD data and was compatible with the potential used in [5]. Therefore, this methodology will be applied to our study of hybrid baryons. Before detailing the model for hybrid baryons, the kinetic energy of all particles is chosen to be semi-relativistic

$$T_i(p_i) = \sqrt{p_i^2 + m_i^2}, \quad (4.2)$$

where m_i is the mass of the particle in the model. This kinematics is essential for the gluon, as it is massless, and for light quarks (u, d, s), since the constituent approach yields accurate results with this choice of kinematics [7, 8]. For heavy quarks (c, b), the non-relativistic kinematics $m_i + p^2/(2m_i)$ could be used, but we maintain the semi-relativistic form for consistency.

Following the discussion in Chapter 1, the short-range interaction between quarks and gluons is chosen from one-gluon exchange (OGE) processes, while the confinement is reproduced by flux tubes. In Sec. 4.1, various configurations of the flux tubes in hybrid baryons are presented, along with the quark core model. The interaction within the core is discussed in Sec. 4.2, followed by the core-gluon interaction in Sec. 4.3. Finally, the spectrum for heavy hybrid baryons is presented in Sec. 4.4.

4.1 Flux tubes for hybrid baryons

The confinement mechanism inside a baryon was discussed in Sec. 1.3. It was shown that confinement can be reproduced by the formation of strings, or flux tubes, by each quark, which are then neutralised at a single point, forming a Y -junction (see, for instance, Fig. 1.6). Let us extend this concept to hybrid baryons. Since a gluon is a colour octet particle, a generalisation of the potential V_Y , as given by (1.56), to non-fundamental flux tubes is required. A popular choice is the Casimir scaling hypothesis [9, 10], which posits that a coloured source produces a flux tube proportional to the value of its $SU(3)$ quadratic Casimir F^2 . The values of the quadratic Casimir for various representations of $SU(3)$ are listed in Table 1.2.

Following the approach of [11], a possible flux tube configuration for hybrid baryons is illustrated in Fig. 4.1a. Two quarks, labelled q_1 and q_2 , produce a fundamental string that connects at a point \mathbf{u} . This resulting string can be in either the $\mathbf{\bar{3}}$ or the $\mathbf{6}$ representation of $SU(3)$, and it connects at a point \mathbf{t} with the string of the third quark, labelled q_3 , to form a vertex neutralised by an octet $\mathbf{8}$ string, produced by the gluon. The corresponding potential is given by

$$V = \sigma \min_{\mathbf{u}, \mathbf{t}} \left\{ \frac{4}{3} [|\mathbf{r}_1 - \mathbf{u}| + |\mathbf{r}_2 - \mathbf{u}| + |\mathbf{r}_3 - \mathbf{t}|] + F^2 |\mathbf{u} - \mathbf{t}| + 3|\mathbf{t} - \mathbf{r}_g| \right\}, \quad (4.3)$$

with σ being the string tension, and F^2 being the quadratic Casimir of the intermediate string. This configuration involves several complications

1. The presence of two junctions $\mathbf{u}(\mathbf{r}_1, \mathbf{r}_2, \mathbf{r}_3, \mathbf{r}_g)$ and $\mathbf{t}(\mathbf{r}_1, \mathbf{r}_2, \mathbf{r}_3, \mathbf{r}_g)$ leading to an over complicated four-body interaction.
2. The intermediate string between \mathbf{u} and \mathbf{t} can exist in two colour representations $\mathbf{\bar{3}}$ or $\mathbf{6}$, leading to possible couplings.

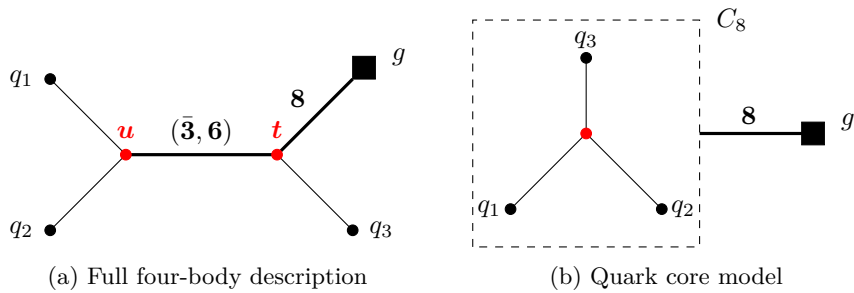


Figure 4.1: Flux-tube models for a hybrid baryon. Black dots represent quarks, and the black rectangle represents the gluon. The red dots mark the connection of flux tubes. Fundamental flux tubes are depicted as simple lines, and other flux tubes as thick lines with the representation indicated above.

3. There is no reason to assume that only quarks q_1 and q_2 connect at u , leading to flip flopping between different configurations.

Therefore, instead of considering the full four-body configuration, we employ a quark core model. In this model, the three quarks interact first to form a colour octet core C_8 , which then interacts with the gluon to neutralise their colour. A representation of the quark core model is provided in Fig. 4.1b. This model simplifies the hybrid baryon to an effective two-body system, which is easier to handle in terms of flux tubes and allows the direct use of the two-body helicity formalism, in line with [5]. The helicity states for a hybrid baryon in a quark core model have already been computed in Sec. 3.3. This model is similar to the quark-diquark description of baryon in which two quarks form a cluster interacting with the third one. This model has a long history but it is still quite popular nowadays [12, 13, 14]. This description is interesting to study the internal structure of baryons, but it is also used to compute properties of multi-quark systems as tetraquarks [15] and pentaquarks [16]. The quark-diquark structure in a baryon is favoured by the presence of two heavy quarks forming a very tight cluster in its ground state which interacts with a third quark lighter than the other ones [12, 13]. Recent computations using the envelope theory (see Chapter 2), an approximation method for solving the many-body Schrödinger equation, corroborate these conclusions [17]. Therefore, heavy quarks will be considered initially to favour the formation of the quark core. Only excitation between the core and the gluon will be considered.

By employing the quark core model, the study of hybrid baryons can be divided into two parts. The first part involves describing the quark core itself, which is a three-body system and shares similarities with the structure of baryons. The second part concerns the coupling between the core and the gluon, which is a two-body system. Let us first examine the dynamics of the quark core.

4.2 Quark core Hamiltonian

As discussed in Sec. 1.3, a popular choice for the quark-antiquark interaction is the Cornell potential

m_c	1.320 GeV	A	0.203 GeV ²
m_b	4.731 GeV	B	0.437
		f	1.086

Table 4.1: Parameters for the Cornell potential (4.4) from [18, 19].

$$V_{q\bar{q}}(r) = -\frac{A}{r} + B r, \quad (4.4)$$

where we recall that the Coulomb term originates from OGE processes, and the linear term from the flux tube model. The parameters $A = \frac{4}{3}\alpha_s$ and $B = \frac{4}{3}\sigma$, which are linked to the strong coupling constant α_s and the string tension σ respectively, are model-dependent. Since we are dealing with heavy quarks, we propose to use the parameters from the Fulcher model [18], which reproduces the centre of gravity of heavy mesons for both non-relativistic and semi-relativistic kinematics. The parameters for semi-relativistic kinematics are presented in Table 4.1.

A generalisation of this potential to baryons, and three-quark systems in general, has also been discussed in Sec. 1.3, leading to the three-quark potential

$$V_{qqq} = \frac{3}{4} \sum_{i < j=2}^3 \left[A \frac{F(i) \cdot F(j)}{r_{ij}} + \frac{f}{2} B F^2(i) r_{ij} \right], \quad (4.5)$$

where $r_{ij} = |\mathbf{r}_i - \mathbf{r}_j|$, $F^2(i)$ is the $SU(3)$ quadratic Casimir associated with the i th particle, and

$$F(i) \cdot F(j) = \frac{1}{2} [(F(i) + F(j))^2 - F(i)^2 - F(j)^2]. \quad (4.6)$$

The constant 3/4 is added so that the potential reduces correctly to (4.4) when mesons are considered. Finally, the Y -junction potential V_Y , as given by (1.56), is replaced by the Δ potential (1.59), where $f \approx 1.086$ is a constant added to better reproduce the Y -junction [19], as explained in Chapter 1.

Let us now compute the value of the different colour operators in (4.5). First, since only quarks, that is fundamental colour sources, are present, the quadratic Casimir takes the value $F^2(i) = 4/3$ for all three particles. Next, we have to compute the value of the colour operator $(F(i) + F(j))^2$ in (4.6), which is the quadratic Casimir associated with the quark pair $q_i q_j$. For ordinary baryons, each quark pair must be in the $\bar{\mathbf{3}}$ representation, so that the baryon is in a colour singlet state. Thus, the colour factor (4.6) is equal to $-2/3$ for every pair, leading to the baryon Hamiltonian for three quarks with the same mass m_q

$$H_B = \sum_{i=1}^3 \sqrt{p_i^2 + m_q^2} + \frac{1}{2} \sum_{i < j=2}^3 \left[-\frac{A}{r_{ij}} + f B r_{ij} \right]. \quad (4.7)$$

The computation of (4.6) for hybrid baryons is subtler. Indeed, the quark core must be in a colour octet $\mathbf{8}$ state, implying a quark pair can be in both the

$\bar{\mathbf{3}}$ and $\mathbf{6}$ representation. To compute the value of $(F(i) + F(j))^2$, the colour wavefunction of the quark core must be written explicitly.

4.2.1 Wavefunction of the quark core

Since the quark core is in a colour octet configuration, its colour wavefunction, denoted $|\phi\rangle$, has a mixed symmetry under the exchange of quarks. Explicit expressions of mixed symmetric three-body wavefunctions can be found in [20], but they are not needed for our computations. We also assume there is no excitation between the quarks ($L = 0$), implying its spatial wavefunction $|\psi\rangle$ is symmetric. To determine the spin and flavour symmetry, it is necessary to further detail the quark content of the quark core.

Three identical quarks

For a quark core made of three identical quarks qqq , with $q = \{c, b\}$ being a heavy quark, the flavour wavefunction $|\xi\rangle$ is symmetric. Since quarks are fermions, the total wavefunction $|\Psi\rangle$ must be completely antisymmetric. Thus, the spin wavefunction $|\chi\rangle$ must have a mixed symmetry so that, when combined with the mixed symmetry of the colour wavefunction, a completely antisymmetric spin-colour wavefunction is formed. The mixed symmetry of the colour wavefunction, and the assumption that the quark core is in its ground state, imposes that the quark core can only have a spin $J_C = 1/2$. More explicitly [20]

$$|\Psi\rangle_{qqq} = \frac{1}{\sqrt{2}} |\psi^S\rangle \otimes |\xi^S\rangle (|\chi^{MS}\rangle \otimes |\phi^{MA}\rangle - |\chi^{MA}\rangle \otimes |\phi^{MS}\rangle). \quad (4.8)$$

Since the three quarks are identical, the mean value of the colour operator $(F(i) + F(j))^2$ between the above eigenstate takes the same value for every pair. It is easier to compute $(F(1) + F(2))^2$ since we know the symmetry between the first two quarks. For the mixed symmetric (MS) wavefunction, the quark pair q_1q_2 is in the $\mathbf{6}$ representation, whereas it is in the $\bar{\mathbf{3}}$ representation for the mixed antisymmetric (MA) wavefunction. Therefore, from the values in Table 1.2, we obtain

$$\begin{aligned} & (F(1) + F(2))^2 |\Psi\rangle_{qqq} \\ &= \frac{1}{\sqrt{2}} |\psi^S\rangle \otimes |\xi^S\rangle (F(1) + F(2))^2 \\ & \quad \times (|\chi^{MS}\rangle \otimes |\phi^{MA}\rangle - |\chi^{MA}\rangle \otimes |\phi^{MS}\rangle) \\ &= \frac{1}{\sqrt{2}} |\psi^S\rangle \otimes |\xi^S\rangle \left(|\chi^{MS}\rangle \otimes \frac{4}{3} |\phi^{MA}\rangle - |\chi^{MA}\rangle \otimes \frac{10}{3} |\phi^{MS}\rangle \right), \end{aligned} \quad (4.9)$$

so that

$${}_{qqq} \langle \Psi | (F(i) + F(j))^2 | \Psi \rangle_{qqq} = \frac{7}{3} \forall i, j. \quad (4.10)$$

Substituting this value in (4.6) leads to

$${}_{qqq} \langle \Psi | (F(i) + F(j))^2 | \Psi \rangle_{qqq} = \frac{1}{2} \left[\frac{7}{3} - \frac{4}{3} - \frac{4}{3} \right] = -\frac{1}{6} \forall i, j, \quad (4.11)$$

implying the OGE interaction between the quarks in a core is attractive but is four times weaker than the interaction inside a baryon. Since the linear attraction between the quarks is the same in a baryon and a quark core, we can expect that the weakening of the Coulomb repulsion leads to the quark core mass m_C being greater than that of a baryon m_B .

Two identical quarks

Consider now a quark core made of two identical quarks qqq' , with $q, q' = \{c, b\}$ and $q' \neq q$. Since the total wavefunction must be antisymmetric only with respect to the first two particles, the symmetries will be determined for these two particles. The flavour wavefunction is symmetric. The spin wavefunction is either antisymmetric ($S_{qq} = 0$) and must be combined with the mixed symmetric (MS) colour wavefunction $|\phi^{MS}\rangle$, or symmetric ($S_{qq} = 1$) and must be combined with the mixed antisymmetric (MA) colour wavefunction $|\phi^{MA}\rangle$. In the first case, the total spin of the quark core is $J_C = 1/2$, and in the second case it can be $J_C = 1/2$ or $3/2$.

Turning to the colour operator $F(i) \cdot F(j)$, since the third quark is different, we have $\langle F(1) \cdot F(2) \rangle \neq \langle F(1) \cdot F(3) \rangle = \langle F(2) \cdot F(3) \rangle$. The mean value of the operator $F(1) \cdot F(2)$ is easier to compute because it is associated with the identical particles, for which we know the symmetry. Specifically,

$$\langle \phi^{MS} | F(1) \cdot F(2) | \phi^{MS} \rangle = \frac{1}{3} \text{ and } \langle \phi^{MA} | F(1) \cdot F(2) | \phi^{MA} \rangle = -\frac{2}{3}. \quad (4.12)$$

Note that for the MS colour wavefunction, the interaction term is repulsive. The computation of the mean value of $F(2) \cdot F(3)$ is more challenging because we do not know the symmetry between the second and third particles. One approach is to rewrite the colour wavefunction from the (12) coupling to the (23) coupling. Schematically, we can write

$$((12)^{c_{12}3})_M^C = \sum_{c_{23}} C_{c_{23}}^{C,M} (1(23)^{c_{23}})_M^C, \quad (4.13)$$

where the notation indicates that the quarks (ij) couple to form a colour c_{ij} . The total colour state is C and its projection² is M . In particular, we consider only the octet state $C = \mathbf{8}$. Since the colour operator (4.6) does not depend on the projection of the colour, we choose to work with the wavefunctions

$$\begin{aligned} |\phi^{MS}\rangle &= ((12)^{\mathbf{6}3})^{\mathbf{8}} = \frac{1}{\sqrt{6}}[(RB + BR)R - 2RRB], \\ |\phi^{MA}\rangle &= ((12)^{\mathbf{3}3})^{\mathbf{8}} = \frac{2}{\sqrt{6}}(RB - BR)R. \end{aligned} \quad (4.14)$$

In the sum in (4.13), only states with the same total colour C and projection M contribute. Computations show

²By projection, we mean all the possible wavefunctions with a given symmetry associated to the colour state C .

$$\begin{aligned} |\phi^{MS}\rangle &= -\frac{1}{2}(1(23)^6)^{\mathbf{8}} - \frac{\sqrt{3}}{2}(1(23)^{\bar{3}})^{\mathbf{8}}, \\ |\phi^{MA}\rangle &= \frac{\sqrt{3}}{2}(1(23)^6)^{\mathbf{8}} - \frac{1}{2}(1(23)^{\bar{3}})^{\mathbf{8}}. \end{aligned} \quad (4.15)$$

Knowing the symmetry of the pair (23), the mean value of $F(2) \cdot F(3)$ can be computed

$$\langle \phi^{MS} | F(2) \cdot F(3) | \phi^{MS} \rangle = -\frac{5}{12} \text{ and } \langle \phi^{MA} | F(2) \cdot F(3) | \phi^{MA} \rangle = \frac{1}{12}. \quad (4.16)$$

This time, it is the MA wavefunction that provides a repulsive interaction. These systems will not be considered in the following discussion, but their study is foreseen in the near future.

4.2.2 Spectrum of the quark core

Thanks to the knowledge of the value of the colour operator in equation (4.6), the Hamiltonian of a quark core can be expressed. Focusing only on systems with three identical quarks for simplicity, the Hamiltonian reads

$$H_C = \sum_{i=1}^3 \sqrt{p_i^2 + m_q^2} + \frac{1}{2} \sum_{i<j=2}^3 \left[-\frac{A}{4r_{ij}} + f B r_{ij} \right], \quad (4.17)$$

where the mass and parameters are given in Table 4.1. The next step is to compute the eigensolutions of the corresponding three-body Schrödinger equation. Two methods are proposed for this purpose.

Envelope theory

The envelope theory (ET) is an approximation method for solving the N -body Schrödinger equation, as presented in Chapter 2. Although the method is not the most accurate, it can provide simple and analytical results for the energy and wavefunction. More importantly, the method treats the number of particles N as a parameter, making it well-suited for large- N systems. To illustrate the method, the spectrum of the Hamiltonian (4.17) for an N -body system, with the semi-relativistic kinematics replaced by non-relativistic kinematics, is computed. The resolution of the ET equations (2.71) on the system

$$T(p) = m + \frac{p^2}{2m} \text{ and } V(r) = -\frac{\alpha}{r} + \beta r, \quad (4.18)$$

leads to the approximate spectrum

$$r_0 = \sqrt{\frac{\alpha}{3\beta}} F_+(Y), \quad (4.19a)$$

$$\begin{aligned} M_{\text{ET}} &= N m + \frac{N(N-1)}{2} \frac{\sqrt{3\alpha\beta}}{2} \left[F_+(Y) - \frac{1}{F_+(Y)} \right] \\ \text{with } Y &= \frac{2Q(N)^2}{mN(N-1)^2} \sqrt{\frac{27\beta}{\alpha^3}}, \end{aligned} \quad (4.19b)$$

	ET				OBE			
	m_B	m_C	Δ	r_0	m_B	m_C	Δ	a
<i>ccc</i>	5.032	5.231	0.199	2.58	4.822	5.119	0.297	2.100
<i>bbb</i>	14.664	14.983	0.319	1.69	14.401	14.894	0.493	1.374

Table 4.2: Eigenvalues of Hamiltonian (4.7), m_B , and Hamiltonian (4.17), m_C , with the mass gap $\Delta = m_C - m_B$, computed with the ET and OBE (in GeV). The OBE mass is computed with $\mathcal{N}_{\max} = 16$. For (4.17), the ET parameter $r_0^2 = \langle \mathbf{r}^2 \rangle$ and the OBE variational parameter a , computed at $\mathcal{N}_{\max} = 0$, are also provided (in GeV^{-1}).

where r_0 is an intermediate parameter of the ET linked to the mean value of $\langle \mathbf{r}^2 \rangle$ (2.53), $Q(N)$ is a global quantum number given by (2.27), and

$$F_+(Y) \equiv \left(Y + \sqrt{Y^2 + 1} \right)^{1/3} - \left(Y - \sqrt{Y^2 + 1} \right)^{-1/3}, \quad (4.20)$$

is the only positive real solution of the cubic equation $x^3 + 3x - 2Y = 0$ [21]. Following the recipe in Sec. 2.3, it can be shown that the approximate spectrum is an upper bound. For semi-relativistic kinematics, the equations (2.71) yield no analytical results, but they can be solved numerically. The approximate spectrum is also an upper bound. In particular, for $N = 3$, the ground state energy for heavy quarks is given in Table 4.2. It is also interesting to compute the gap between the mass of the quark core and the mass of the ordinary baryon with the same quark content, that is, the eigenvalue of (4.7). The mass gap is also given in Table 4.2.

Additionally, the ET provides an approximation for the quark core wavefunction. Following the details in Appendix A, the ground state wavefunction is given by (A.15)

$$\psi_{\text{ET}} = \left(\frac{\lambda_1^2}{\pi} \right)^{3/4} e^{-\lambda_1^2 x_1^2/2} \left(\frac{\lambda_2^2}{\pi} \right)^{3/4} e^{-\lambda_2^2 x_2^2/2}, \quad (4.21)$$

where λ_i is a parameter given by (A.39), and \mathbf{x}_i is the Jacobi variable (2.3). In particular, λ_i only depends on the parameter r_0 which is derived during the computation of the spectrum and is given in Table 4.2.

Oscillator bases expansion

The oscillator bases expansion (OBE) is an accurate numerical technique for solving the three-body Schrödinger equation, particularly suited for handling semi-relativistic kinematics. Interested readers can find more information about the method in [22, 23, 24, 25]. As the name implies, the method relies on expanding the three-body wavefunction ψ into harmonic oscillator wavefunctions, denoted φ_{n_l} . More explicitly,

$$\psi_{\text{OBE}} = \sum_{\mathcal{N}} \sum_s d_s(\mathcal{N}) [\varphi_{n_1 l_1}(\lambda_1 \mathbf{x}_1) \varphi_{n_2 l_2}(\lambda_2 \mathbf{x}_2)]^L, \quad (4.22)$$

where $[\varphi_{n_1 l_1}(\lambda_1 \mathbf{x}_1) \varphi_{n_2 l_2}(\lambda_2 \mathbf{x}_2)]^L$ denotes a three-body oscillator wavefunction with a given total angular momentum L and symmetry (if applicable). Some examples of symmetric three-body wavefunctions are given in Appendix A. The second sum over s runs over all the oscillator states with the same number of quanta $\mathcal{N} = 2(n_1 + n_2) + l_1 + l_2$, and the first sum over \mathcal{N} runs, theoretically, from 0 to infinity. In practice, the first sum is truncated to a certain value \mathcal{N}_{\max} . The number of quanta is linked to the global quantum number Q , given by (2.27), by the relation $Q(3) = \mathcal{N} + 3$. The parameters λ_i are given by

$$\lambda_1 = \frac{1}{a} \text{ and } \lambda_2 = \frac{2}{\sqrt{3}} \frac{1}{a}, \quad (4.23)$$

where a is a variational parameter determined by minimising the matrix elements of the Hamiltonian. The above relation is only valid for three identical particles [24, 25]. Since the OBE is a variational method, its eigenvalues are always upper bounds. Results for the Hamiltonians H_B and H_C are given in Table 4.2, where the ground state has been computed with $\mathcal{N}_{\max} = 16$ [26]. The exactitude of the last digit is guaranteed.

Since both the ET and OBE yield upper bounds, a comparison between the two methods shows that the OBE is more accurate. Therefore, its results will be used in the following discussion. Note that the ET remains a useful tool when the number of particles is large, as for instance in the large- N_c approach of QCD in which a baryon contains N_c quarks.

Currently, no experimental data exists on triply charmed or bottom baryons that would enable a direct verification of the accuracy of our model and computational tools [27]. However, predictions from lattice QCD (LQCD) calculations [28], non-relativistic quark models [29, 30, 31], and Regge phenomenology [32] suggest mass ranges of 4700–4800 MeV for ccc baryons and 14000–15000 MeV for bbb baryons. The baryon masses, m_B , calculated in our model fall within these predicted ranges.

4.3 Core-gluon interaction

The core-gluon interaction is inherently more complex due to the intricate structure of the system. Nevertheless, according to the Casimir scaling hypothesis [10], the strong interaction depends solely on the color charge of the sources. Since the quark core is in a colour octet state, the core-gluon interaction is expected to be analogous to the gluon-gluon interaction, for which potentials are available. Specifically, we utilise the potential from [5], which was used in the study of two-gluon glueballs

$$V_{gg} = A'r - \frac{B'}{r}. \quad (4.24)$$

The form of this potential is similar to the Fulcher potential (4.4), except that the parameters A' and B' differ. Since $\langle F^2 \rangle = 3$ for a colour octet state, and $\langle F(g) \cdot F(g) \rangle = -3$ for a two-gluon glueball, the gluon-gluon potential is linked to the quark-antiquark potential by $V_{gg} = \frac{9}{4} V_{q\bar{q}}$. The parameters A' and B' from [5] are provided in Table 4.3, as well as the values in Table 4.1 multiplied by 9/4. As we can see, the set of parameters in [5] is not exactly the same as in [18]. It might seem strange that different values for the string tension and

	gluon-gluon	$q\bar{q}$
m_g	0	
A'	0.416 GeV ²	0.457 GeV ²
B'	1.350	0.983

Table 4.3: Parameters for the glueball and hybrid baryon Hamiltonians [5]. Corresponding parameters for the $q\bar{q}$ systems taken from Table 4.1 are also indicated.

the strong coupling constant are assigned according to the particles, quarks or gluons, considered. We preferred to keep different sets of parameters because it is difficult to find common values that give good results for all systems, taking into account the simplicity of the models.

However, the quark core is not a point-like particle like the gluon; it has spatial extension. Consequently, the interaction between two point-like sources must be convoluted with the density of the extended source as per the formula [13]

$$\tilde{V}(\mathbf{R}) = \int d\mathbf{r} \rho(\mathbf{r}) V(|\mathbf{R} + \mathbf{r}|), \quad (4.25)$$

where $\rho(\mathbf{r})$ represents the normalised³ colour density (i.e., the density of quarks). A natural definition for a normalised N -body density is [33]

$$\rho(\mathbf{r}) = \frac{1}{N} \sum_{i=1}^N \int \cdots \int \prod_{i=1}^N d\mathbf{r}_i |\psi|^2 \delta(\mathbf{r} - \mathbf{r}_i), \quad (4.26)$$

where $\psi = \psi(\mathbf{r}_1, \dots, \mathbf{r}_N)$ is the N -body wave function. In our approach, the quark core wavefunction is approximated by (4.22). Although this could lead to overly complex expressions for the quark density, computations reveal that the probability of the first component of the expansion (the product of two ground states of oscillator functions in Jacobi coordinates) accounts for more than 90% of the wave function for ground state cores. Using a trial state reduced to this unique component, the masses are reproduced with a relative error of 0.1%. We thus use this approximation to compute the density of the core, which then takes the simple form

$$\rho(\mathbf{r}) = \frac{\lambda^3}{\pi^{3/2}} e^{-\lambda^2 r^2} \text{ with } \lambda = \sqrt{3}/a. \quad (4.27)$$

If the ET was used instead of the OBE, the structure of the quark density would be identical since the ET also approximates the ground state wavefunction as the product of two ground states of oscillator functions in Jacobi coordinates (4.21). The variational parameter a in (4.27) is computed with $\mathcal{N}_{\max} = 0$, as reported in Table 4.2.

The computation of the convoluted potential is then analytical [26] and the core-gluon Hamiltonian, or the hybrid baryon Hamiltonian, reads

³Our choice of normalisation is $\int d\mathbf{r} \rho(\mathbf{r}) = 1$. The density is sometimes normalised to N .

$$\begin{aligned}
H_{\text{HB}} = & \sqrt{p^2 + m_C^2} + \sqrt{p^2 + m_g^2} \\
& + B' \left[\frac{e^{-\lambda^2 r^2}}{\sqrt{\pi\lambda}} + \left(r + \frac{1}{2\lambda^2 r} \right) \text{erf}(\lambda r) \right] - A' \frac{\text{erf}(\lambda r)}{r},
\end{aligned} \tag{4.28}$$

where m_C is the quark core mass given in Table 4.2, and $\text{erf}(x)$ denotes the error function. The next step is to solve the corresponding two-body Schrödinger equation.

4.4 Spectrum of heavy hybrid baryons

The eigenvalues of the Hamiltonian (4.28) can be computed using the ET through equations (2.88), but a more accurate method for two-body systems, the Lagrange-mesh (LM) method, is preferred. For two-body systems, the LM method is more accurate and easier to use than the OBE. Note that the LM method has not been generalised to three-body systems with semi-relativistic kinematics. The LM method, as detailed in [34], is well-suited for handling semi-relativistic kinematics and systems with spin, as discussed in [35]. Although hybrid baryons must be described by helicity states due to their unique properties, these helicity states can be expanded into ordinary canonical states (see Chapter 3).

For a hybrid baryon composed of three identical quarks in their ground states, the quark core spin is $J_C = 1/2$, as detailed in Sec. 4.2. Thus, the associated helicity states are given by (3.52). When computing the spectrum, the matrix elements of \mathbf{L}^2 , the squared orbital angular momentum operator, must be evaluated. However, as shown in Sec. 3.3.3, the helicity states mix through this operator. It was noted that all the eigenvalues took the form $l_{\text{eff}}(l_{\text{eff}} + 1)$, where l_{eff} is an effective angular momentum between the quark core and the gluon. The matrix elements can be diagonalised, allowing the LM method to be used with the diagonalised basis. This diagonalisation process was performed in Sec. 3.3.3. Alternatively, the LM method can be adapted to account for coupled channels, as explained in Appendix C. Both approaches to account for the mixing of states yield the same spectrum.

Similar to the quark core, it is insightful to compute the mass gap between the hybrid baryon and the corresponding ordinary baryon. The spectrum of heavy hybrid baryons for the lowest J^P states is presented in Table 4.4 [26]. The exactitude of the last digit is guaranteed.

The main results from Table 4.4 are

- The hierarchy of states is similar for both *cccg* and *bbbg* states.
- The common value $l_{\text{eff}} = 1$ for $1/2^\pm$ and $3/2^\pm$ (see Sec. 3.3.3) states causes their degeneracy.
- The lowest states have $1/2^\pm$ and $3/2^\pm$, and have a common mass around 1.8 GeV above the one of the ground state baryon.
- As in the case of *gg* systems, no states with $l_{\text{eff}} = 0$ exist [5].

J^P	(n, l)	$cccg$	$bbbg$
$1/2^\pm$	(0,1)	1.842	1.784
$3/2^\pm$	(0,1)	1.842	1.784
$1/2^-$	(1,0)	2.131	2.013
$3/2^\pm$	(0,2)	2.350	2.336
$1/2^+$	(1,1)	2.552	2.469
$3/2^\pm$	(1,1)	2.552	2.469
$3/2^\pm$	(1,2)	2.938	2.880

Table 4.4: Mass gap $m_{HB} - m_B$ in GeV for the lowest $J = 1/2$ and $J = 3/2$ $cccg$ and $bbbg$ hybrid baryons for a gluon with a helicity [26]. The radial and orbital quantum numbers of the pair are denoted (n, l) .

As discussed in the Introduction, hybrid baryon spectra have been computed using various models in the light quark sector, but comparing our results for heavy sectors with those from the light sector, which are the targets of future experiments, remains challenging. For example, the LQCD study [36] with $m_\pi = 396$ MeV only presents positive parity spectra, showing that $1/2^+$ and $3/2^+$ hybrid baryons have similar masses, with hybrid- Δ around 1.5 GeV above the baryon Δ . Some similarities exist, but extending our model to the light sector is necessary for reliable comparisons. Note that the interactions considered here are purely central; spin-dependent contributions could lift some degeneracies, as seen with light $J_B^{P_B} = 1/2^+$ and $3/2^+$ baryons, which are degenerate with our Hamiltonian (4.7).

Eventually, similar computations for the hybrid baryon spectrum have been realised for a gluon with a spin degree of freedom, that is, with an additional 0 projection. The structure of the spin-orbital wavefunctions is, of course, different, but the value of the parameters in (4.24) also differs, as explained in [5]. The resultant spectrum is given in [26] and is quite different from the one in Table 4.4, which further emphasises the importance of correctly including the helicity of the gluon.

To conclude this final chapter, the interaction between quarks and the gluon in hybrid baryons was discussed. First, the quark core model, in which the three quarks form a core that interacts with the gluon, was justified. The quark core spectrum was then computed using a Cornell-inspired potential (4.5) for three-quark systems. The colour operators in (4.5) were evaluated for both a baryon, representing a colour singlet state, and a quark core, representing a colour octet state, leading to the Hamiltonians (4.7) and (4.17) for the baryon and quark core, respectively. Semi-relativistic kinematics were considered in these calculations. The eigenvalues of these Hamiltonians were computed using two distinct methods: the ET and the EOB methods. The results for triply charmed (ccc) and bottom (bbb) systems are summarised in Table 4.2.

The core-gluon interaction was then examined. Based on the Casimir scaling

hypothesis, the core-gluon interaction was modelled similarly to the gluon-gluon interaction (4.24) convoluted with the quark density (4.25) to account for the spatial extension of the quark core. The resulting Hamiltonian is given by (4.28), and its eigensolutions were computed using the LM method. The mean values of the Hamiltonian were evaluated between the helicity states derived in Chapter 3, with the mixing from the \mathbf{L}^2 operator taken into consideration. Results for the mass gap between hybrid baryons and their corresponding baryons, with the same quark content, are presented in Table 4.4.

Bibliography

- [1] Buisseret, F. & Semay, C. Two- and three-body descriptions of hybrid mesons. *Phys. Rev. D* **74**, 114018 (2006).
- [2] Buisseret, F., Semay, C., Mathieu, V. & Silvestre-Brac, B. Excited flux tube from $q\bar{q}g$ hybrid mesons. *Eur. Phys. J. A* **32**, 123 (2007).
- [3] Barnes, T. A transverse gluonium potential model with Breit-fermi hyperfine effects. *Z. Phys. C - Particles and Fields* **10**, 275 (1981).
- [4] Cornwall, J. M. & Soni, A. Glueballs as bound states of massive gluons. *Phys. Lett. B* **120**, 431 (1983).
- [5] Mathieu, V., Buisseret, F. & Semay, C. Gluons in glueballs: Spin or helicity? *Phys. Rev. D* **77**, 114022 (2008).
- [6] Buisseret, F. Effective potential between two transverse gluons from lattice QCD. *Phys. Rev. D* **79**, 037503 (2009).
- [7] Godfrey, S. & Isgur, N. Mesons in a relativized quark model with chromodynamics. *Phys. Rev. D* **32**, 189 (1985).
- [8] Capstick, S. & Isgur, N. Baryons in a relativized quark model with chromodynamics. *Phys. Rev. D* **34**, 2809 (1986).
- [9] Bali, G. S. Casimir scaling of SU(3) static potentials. *Phys. Rev. D* **62**, 114503 (2000).
- [10] Semay, C. About the Casimir scaling hypothesis. *Eur. Phys. J. A* **22**, 353 (2004).
- [11] Deng, C., Ping, J., Yang, Y. & Wang, F. Baryonia and near-threshold enhancements. *Phys. Rev. D* **88**, 074007 (2013).
- [12] Fleck, S., Silvestre-Brac, B. & Richard, J. M. Search for diquark clustering in baryons. *Phys. Rev. D* **38**, 1519 (1988).
- [13] Giannuzzi, F. Doubly heavy baryons in a Salpeter model with AdS/QCD inspired potential. *Phys. Rev. D* **79**, 094002 (2009).
- [14] Torcato, A., Arriaga, A., Eichmann, G. & Peña, M. T. Heavy baryon spectroscopy in a quark-diquark approach. *Few-Body Syst.* **64**, 45 (2023).
- [15] Carlucci, M. V., Giannuzzi, F., Nardulli, G., Pellicoro, M. & Stramaglia, S. AdS-QCD quark-antiquark potential, meson spectrum and tetraquarks. *Eur. Phys. J. C* **57**, 569 (2008).
- [16] Giannuzzi, F. Heavy pentaquark spectroscopy in the diquark model. *Phys. Rev. D* **99**, 094006 (2019).
- [17] Tourbez, C., Cimino, L. & Semay, C. Modèle de baryon en structure quark-diquark (2024). Report of an “Introduction to Scientific Research” project.
- [18] Fulcher, L. P. Matrix representation of the nonlocal kinetic energy operator, the spinless Salpeter equation and the Cornell potential. *Phys. Rev. D* **50**, 447 (1994).

- [19] Silvestre-Brac, B., Semay, C., Narodetskii, I. M. & Veselov, A. I. The baryonic Y-shape confining potential energy and its approximants. *Eur. Phys. J. C* **32**, 385 (2004).
- [20] Close, F. E. *An Introduction to Quarks and Partons* (Academic Press, London, 1979).
- [21] Silvestre-Brac, B., Semay, C. & Buisseret, F. Semirelativistic hamiltonians and the auxiliary field method. *Int. J. Mod. Phys. A* **24**, 4695 (2009).
- [22] Nunberg, P., Prosperi, D. & Pace, E. An application of a new harmonic-oscillator basis to the calculation of trinucleon ground-state observables. *Nucl. Phys. A* **285**, 58 (1977).
- [23] Silvestre-Brac, B. Spectrum and static properties of heavy baryons. *Few-Body Syst.* **20**, 1 (1996).
- [24] Silvestre-Brac, B., Bonnaz, R., Semay, C. & Brau, F. Quantum three body problems using harmonic oscillator bases with different sizes. <https://arxiv.org/abs/2003.11028> (2000). Internal Report ISN 00.66.
- [25] Chevalier, C. & Youcef Khodja, S. Three-body forces in oscillator bases expansion. *Few-Body Syst.* **65**, 86 (2024).
- [26] Cimino, L., Willemyns, C. T. & Semay, C. Quark core-gluon model for heavy hybrid baryons. *Phys. Rev. D* **110**, 034032 (2024).
- [27] Navas, S. *et al.* Review of particle physics. *Phys. Rev. D* **110**, 030001 (2024).
- [28] Brown, Z. S., Detmold, W., Meinel, S. & Orginos, K. Charmed bottom baryon spectroscopy from lattice QCD. *Phys. Rev. D* **90**, 094507 (2014).
- [29] Liu, M.-S., Lü, Q.-F. & Zhong, X.-H. Triply charmed and bottom baryons in a constituent quark model. *Phys. Rev. D* **101**, 074031 (2020).
- [30] Kakadiya, A., Shah, Z. & Rai, A. K. Spectroscopy of Ω_{ccc} and Ω_{bbb} baryons. *Int. J. Mod. Phys. A* **37**, 2250225 (2022).
- [31] Ortiz-Pacheco, E. & Bijker, R. Masses and radiative decay widths of S - and P -wave singly, doubly, and triply heavy charm and bottom baryons. *Phys. Rev. D* **108**, 054014 (2023).
- [32] Wei, K.-W., Chen, B., Liu, N., Wang, Q.-Q. & Guo, X.-H. Spectroscopy of singly, doubly, and triply bottom baryons. *Phys. Rev. D* **95**, 116005 (2017).
- [33] Nazarov, V. U. Time-dependent effective potential and exchange kernel of homogeneous electron gas. *Phys. Rev. B* **87**, 165125 (2013).
- [34] Baye, D. The Lagrange-mesh method. *Phys. Rep.* **565**, 1 (2015).
- [35] Semay, C., Baye, D., Hesse, M. & Silvestre-Brac, B. Semirelativistic Lagrange mesh calculations. *Phys. Rev. E* **64**, 016703 (2001).
- [36] Dudek, J. J. & Edwards, R. G. Hybrid baryons in QCD. *Phys. Rev. D* **85**, 054016 (2012).

Conclusions and prospects

This thesis must now draw to a close. Before presenting the main contributions of this four-year endeavour, as well as some prospects, it is essential to review the context in which this work was undertaken.

The study of hybrid baryons is part of the broader research into exotic hadrons. According to the fundamental theory of Quantum Chromodynamics (QCD), these particles should exist, yet there is scant experimental data available to confirm their presence [1, 2]. Investigating these exotic states serves as a valuable probe for testing the properties of QCD beyond ordinary matter and can assist experimentalists in their identification. Theoretical studies on hybrid hadrons have utilised various QCD approaches, particularly lattice QCD [3]. However, only recently have experimental efforts begun to search for hybrid baryons at the CEBAF Large Acceptance Spectrometer (CLAS12) in Experimental Hall B at Jefferson Lab [4]. As of 2024, the experiment has been delayed, but the first data are anticipated to be available in the coming years [5]. Identifying hybrid baryons is challenging, as ordinary and hybrid baryons can be characterised by the same J^P quantum numbers. Consequently, hybrid baryons are expected to appear as an overpopulation relative to some models of baryon excitation. Given their potential detection in the near future, a comprehensive understanding of these objects is crucial for their accurate identification.

This thesis represents a modest contribution to the understanding of hybrid baryons. Compared to previous studies, our work is distinguished by its semi-relativistic potential approach and the proper inclusion of gluon helicity. As detailed in the preceding chapters, only the spectrum of heavy hybrid baryons was computed.

1 Contributions of this work

This thesis can be divided into two parts. The first part was devoted to the study of the many-body Schrödinger equation and the development of an approximation method, called the envelope theory (ET), as discussed in Chapter 2. Although the Schrödinger equation appeared in the constituent approach of QCD, the ET was not directly used to compute the spectrum of hybrid baryons. However, as we shall explain in the prospects, the ET will prove to be a useful tool in the extension of our model. The second part focused on hybrid

baryons themselves, with the construction of a semi-relativistic potential model in Chapter 4, supported by the computation of the helicity states in Chapter 3.

The ET was originally developed for systems with identical particles, where the method's utility for hadronic physics was demonstrated. For the treatment of hybrid baryons, the method had to be extended to systems with different particles. Although some preliminary work with different particles was performed [6, 7], a correct extension of the method had yet to be achieved. This initial work began during my Master's thesis, back in 2019-2020. In this work, the eigenvalue of the many-body harmonic oscillator (2.2) for a system of $N_a + 1$ and $N_a + N_b$ particles was computed, as given by (2.39). The next step was to extend the compact equations (2.71), but unfortunately, no extensions were determined. Nonetheless, the approximate spectrum of some systems could be computed using the minimisation equations (2.50). Some of these results were presented in Sec. 2.5. The findings of this work are summarised in [8]. This paper is not the first one I worked on with the ET. Back in 2018-2019, I familiarised myself with ET by working on an extension to a one-dimensional system, leading to my first paper [9].

Returning to the extension of the ET to systems with different particles, the discovery of the decomposition (2.35) of the harmonic oscillator Hamiltonian was a crucial element in determining the compact equations of the ET for a system of $N_a + N_b$ particles. The first year of my thesis was dedicated to deriving these compact equations, resulting in the set of equations (2.84), (2.85), and (2.86). The procedure for finding the compact equations for systems with different particles was presented in [10].

In [8], a preliminary extension of the improved ET (IET), presented in Sec. 2.4, was used by maintaining the same value of the parameter ϕ found for a system of all identical particles, as given by (2.98). However, this extension lacked formal justification. With the determination of the compact equations, an extension of the ET improvement procedure could be realised. The primary work and computations were conducted by my colleague Cyrille Chevalier during his Master's thesis for a system of $N_a + 1$ particles only, leading to the equations (2.108). His work was presented in [11]. Thanks to the efforts detailed in [8, 10, 11], a proper extension of the ET to systems with $N_a + 1$ particles, which is the system of interest for hybrid baryons, was achieved.

The ET, being a simple and user-friendly method, has facilitated numerous projects with students. Notably, two projects funded by a Research Initiation Grant from the University of Mons were realised. The first project, in 2022, focused on assessing the accuracy of the ET. Indeed, the accuracy of the method cannot be predicted, except, when it is relevant, its variational character. For instance, previous computations with identical particles had already indicated that the spectrum for the Coulomb potential is not accurate. This conclusion was also confirmed for systems with different particles. However, the IET significantly improved the accuracy in the case of identical particles. Nevertheless, the study of atomic systems revealed that the improvement procedure did not consistently enhance accuracy. The main objective of the project was to test a variety of potentials for systems with identical particles to identify qualitative features that might explain the method's lack of accuracy. The ET results were compared to more accurate ones obtained using a numerical method based on

the expansion in oscillator bases (EOB), developed by Cyrille, to whom I am still indebted. These features are presented in Sec. 2.5 and led to a publication [12].

The second project, conducted in 2023, focused on extending the IET to K -body forces for systems with identical particles. This work was not included in this thesis as it had no direct implications for hybrid baryons. The project concluded that, although the IET can be extended to K -body systems, its impact is minimal and sometimes results in less accurate outcomes compared to the original ET. A limitation of the improvement procedure was thus identified. Nonetheless, the project extended beyond its initial scope by computing observables within the ET. Specifically, symmetric three-body states were computed. They are presented in Appendix A. The results of this project led to a publication [13].

Once the extension of the ET to systems with different particles was achieved, the study of hybrid baryons could commence. Before explicitly formulating the Hamiltonian of a hybrid baryon, it was necessary to compute the helicity states of the exotic state to correctly account for the helicity of the gluon. As explained in Chapter 4, a quark core model was utilised to directly apply the well-established two-body helicity formalism.

After familiarising myself with the original paper by Jacob and Wick on the helicity formalism [14], as well as the study [15] on two-gluon glueballs in a constituent approach, the helicity states of the hybrid baryons were derived for a quark core with spin $J_C = 1/2$ and $J_C = 3/2$, leading to equations (3.52) and (3.54), respectively. The decomposition of these helicity states into canonical states, given by (3.51), is an essential step for using the helicity states in a constituent approach, as shown in [15].

This decomposition was performed using the software Mathematica [16] and resulted in relations (3.53) and (3.55). Thanks to these relations, the matrix elements of various operators, such as the squared orbital angular momentum \mathbf{L}^2 , could be computed. These computations were also carried out in Mathematica with the aid of the QUANTUM library [17]. The matrix elements of the operator \mathbf{L}^2 were found to be non-diagonal, as detailed in Sec. 3.3.3, indicating that helicity states mix through this operator. This feature had not been observed for two-gluon glueballs in [15].

Eventually, the dynamics of hybrid baryons can be specified. Given that the quark core model shares similarities with the quark-diquark model of baryons, a preliminary study on this approach was conducted. This study took place during an ‘‘Introduction to Scientific Research’’ project undertaken by a first-year Master’s student, Clara Tourbez. The aim of this study was twofold: first, to better understand the regime in which a diquark, and by extension a quark core, is formed; and second, to explore potential models for describing three-quark and quark-diquark systems. This were conducted with a semi-relativistic kinematics.

The conclusion of the study [18] revealed that the presence of heavy quarks, as well as the absence of orbital excitation between them, favoured the formation of a diquark. These results are in good agreement with a non-relativistic kinematics [19]. Consequently, the same configuration was adopted for our model of hybrid baryons. It was also shown that the Cornell potential (4.4), with

parameters taken from [20], leads to results that align well with those found in the literature.

Following this preliminary work, the potential between the three quarks is established as (4.5). The next step involved computing the values of the different colour operators for a colour octet quark core. Some preliminary knowledge of $SU(3)$ group theory was clearly beneficial. The computations were performed for two configurations: three identical quarks and two identical quarks, although only the first configuration was used for the spectrum. The results are presented in Sec. 4.4.

With the quark core Hamiltonian (4.17) known, its eigenvalues could be computed. Thanks to the EOB method, the mass of the quark core and the mass gap with the corresponding baryons $\Delta = m_C - m_B$ were computed. These results are presented in Table 4.2.

The core-gluon interaction then had to be determined. Assuming the universality of the interaction between two colour octet sources, the core-gluon potential was chosen to be the same as that for a gluon-gluon potential, as in [15]. The spatial extension of the quark core was included by convoluting the gluon-gluon potential with the quark density. This same approach was used for the quark-diquark potential in [18, 21]. By approximating the wavefunction of the quark core as a product of Gaussian functions, the convolution could be performed analytically, leading to the hybrid baryon Hamiltonian (4.28).

Finally, the spectrum of hybrid baryons could be obtained by computing the eigenvalues of (4.28). The Lagrange-mesh (LM) method was used since it is an accurate and easy-to-use method for two-body systems. The LM method is initially developed for particles with spin but, thanks to the relations (3.53) and (3.55), it can be extended to particles with helicity.

One last problem remained: the mixing of states through the \mathbf{L}^2 operator. The first approach to this problem involved diagonalising the matrix elements of \mathbf{L}^2 , which was performed in Sec. 3.3.3, and then using the diagonalised basis in the LM method. The second approach involved adapting the LM method to include coupled channels, as presented in Appendix C. Computations revealed that both approaches are equivalent. Ultimately, the spectrum of heavy hybrid baryons in our model was computed and is presented in Table 4.4. All these results on hybrid baryons are compiled in a final paper [22].

2 Future works

Although this thesis is now completed, research on hybrid baryons continues. As mentioned at the beginning of this conclusion, this work is just a small part of the broader study of hybrid baryons and serves as a proof of concept for future work and extensions.

Firstly, some work remains on the ET. As mentioned, the extension of the IET was only performed for systems with $N_a + 1$ particles. A generalisation of the formulae to $N_a + N_b$ particles is theoretically possible, although the computations will be cumbersome. Since the energy of the harmonic oscillator for three different particles is available (2.41), the compact equations for this configuration could be determined. These extensions will allow the treatment of new exotic hadrons or the improvement of existing models. Finally, in line

with the philosophy of [12], new accuracy tests could be performed, particularly by including different particles and examining the impact of the mass ratio. Further tests could help us understand why the improvement procedure for K -body forces does not work as intended. However, all these extensions, while interesting in themselves, are not directly useful for the study of hybrid baryons.

Regarding hybrid baryons, our model can be improved in several ways. For heavy hybrid baryons, we propose the following directions

- Computation of the spectrum for bbc and ccb hybrid baryons. The resolution of (4.17) would not pose a problem, as the EOB technique can handle three-body systems with different particles. However, the convolution step would be more challenging since the quark density has a different structure.
- Inclusion of spin effects between the quarks and the gluon will help to break the observed degeneracy in Table 4.4. Since we are using heavy quarks, it is expected that these effects will not significantly impact the spectrum, allowing for a perturbative approach. The convolution of the potential is another difficulty, although preliminary work has already been performed in [18].
- Study of the impact of radial and orbital excitation within the quark core, which lead to more complicated quark density $\rho(\mathbf{r})$.
- Study of the impact of using parameters other than those from [15, 20] on the spectrum.
- Improving the dynamics of the model by studying the quark core in a quark-diquark approach. Such an extension requires knowledge of three-body helicity formalism. In this approach, we unfreeze the dynamics between the gluon and the core, but we also reduce some degrees of freedom within the quark core.

Obviously, heavy hybrid baryons are not expected to be the first ones detected. Hence, extending our model to light quarks is a clear priority from an experimental point of view. Two aspects of our model must be improved.

- It is necessary to use a universal potential model that can provide accurate spectra for both ordinary and exotic hadrons. The seminal works [23, 24] can serve as a good starting point. The semi-relativistic Hamiltonians developed in these papers include relativised potentials and sophisticated spin contributions. An improved version with a screening effect for linear confinement has been recently proposed [25]. Using Casimir scaling, a version for glueballs and hybrid hadrons could be tested.
- The formation of a diquark inside a baryon is favoured by a strong mass asymmetry between the quarks or the presence of high angular momentum [19]. This suggests that the formation of a compact three-quark cluster is likely not favoured in the ground states of light hybrid baryons. However, we believe this difficulty can be overcome by allowing the quark core to be in a superposition of different states with mixing controlled by the dynamics of the gluon. The coupling interaction could be computed

as a perturbation arising from the difference between the full four-body Hamiltonian and the quark-core gluon one.

An analytic scheme to study the phenomenology of hadrons, with a clear connection to QCD, can be obtained by starting from the large number of colours (N_c) limit of QCD [26, 27]. This approach is particularly fruitful in the light baryon sector. It can be combined with potential models to gain new insights into the structure of hadrons [28, 29, 30, 31]. Therefore, we plan to use a combined potential and large- N_c approach to study light hybrid baryons. This will allow us to track the properties of hybrid baryons from large values of N_c down to 3, the physical value. However, a difficulty arises because the colour wave function of the quark core has a mixed symmetry of the form $[21 \dots 1]$, in Young-Yamanouchi notation. This means it is, for instance, symmetrical under $1 \leftrightarrow 2$ and antisymmetrical under $1 \leftrightarrow 3, 4, \dots, N_c$. In the 't Hooft limit, it is not possible to build a totally antisymmetrical wave function above $N_c = 3$, since there are not enough spin-flavour quark states. However, the situation is different in the Veneziano limit with a large number of flavours (N_f) [32], where $N_c \rightarrow \infty$, $N_f \rightarrow \infty$, and the ratio N_c/N_f remains finite. Another difficulty is that the quark core then becomes an N_c -body system, and the hybrid baryon an $N_c + 1$ one. The corresponding many-body Schrödinger equations can be solved using the ET, whose main advantage is treating the number of particles as a simple parameter, making the ET a well-suited method for this project.

Finally, the approach of our model can be used to study other exotic hadrons, notably hybrid mesons $q\bar{q}g$. Some computations of the helicity states of hybrid mesons in a quark core model have already been performed [33].

3 Farewell

Having summarised the culmination of four years of research in just four pages, I am now at the conclusion of this thesis. Without reiterating what has been expressed in the Acknowledgements, I wish to extend my heartfelt thanks once again to everyone who has supported me throughout this journey — my supervisors, colleagues, friends, and family. Your encouragement and assistance have been invaluable.

To the diligent reader who has navigated through this manuscript, I extend a sincere thank you. This thesis marks the end of an intensive period of study and exploration into the intriguing realm of hadronic physics. Farewell!

Lorenzo Cimino
Mons, Belgium, 23rd September 2024

Bibliography

- [1] Navas, S. *et al.* Review of particle physics. *Phys. Rev. D* **110**, 030001 (2024).
- [2] Chen, H.-X., Chen, W., Liu, X., Liu, Y.-R. & Zhu, S.-L. An updated review of the new hadron states. *Rep. Prog. Phys.* **86**, 026201 (2023).
- [3] Dudek, J. J. & Edwards, R. G. Hybrid baryons in QCD. *Phys. Rev. D* **85**, 054016 (2012).
- [4] Burkert, V. *et al.* A search for hybrid baryons in Hall B with CLAS12. https://www.jlab.org/exp_prog/proposals/16/PR12-16-010.pdf (2016). Report of the 44th Program Advisory Committee (PAC44) Meeting.
- [5] Lanza, L. Search for hybrid baryons and KY electroproduction at CLAS12. <https://indico.jlab.org/event/729/contributions/14461/> (2024). Oral presentation during the NSTAR 2024 conference at York (UK).
- [6] Semay, C., Buisseret, F. & Stancu, F. Mass formula for strange baryons in large N_c QCD versus quark model. *Phys. Rev. D* **76**, 116005 (2007).
- [7] Semay, C., Buisseret, F. & Stancu, F. Charm and bottom baryon masses in the combined $1/N_c$ and $1/m_Q$ expansion versus the quark model. *Phys. Rev. D* **78**, 076003 (2008).
- [8] Semay, C., Cimino, L. & Willemyns, C. Envelope theory for systems with different particles. *Few-Body Syst.* **61**, 19 (2020).
- [9] Semay, C. & Cimino, L. Tests of the envelope theory in one dimension. *Few-Body Syst.* **60**, 64 (2019).
- [10] Cimino, L. & Semay, C. Compact equations for the envelope theory. *Braz. J. Phys.* **52**, 45 (2022).
- [11] Chevalier, C., Willemyns, C. T., Cimino, L. & Semay, C. Improvement of the envelope theory for systems with different particles. *Few-Body Syst.* **63**, 40 (2022).
- [12] Cimino, L., Chevalier, C., Carlier, E. & Viseur, J. Accuracy tests of the envelope theory. *Results Phys.* **58**, 107470 (2024).
- [13] Cimino, L., Tourbez, C., Chevalier, C., Lacroix, G. & Semay, C. Tests of the envelope theory for three-body forces. *Few-Body Syst.* **65**, 20 (2024).
- [14] Jacob, M. & Wick, G. C. On the general theory of collisions for particles with spin. *Ann. Phys.* **7**, 404 (1959).
- [15] Mathieu, V., Buisseret, F. & Semay, C. Gluons in glueballs: Spin or helicity? *Phys. Rev. D* **77**, 114022 (2008).
- [16] Wolfram Research, Inc. Mathematica, Version 14.1. <https://www.wolfram.com/mathematica>. Champaign, IL, 2024.

-
- [17] Gómez Muñoz, J. L. & Delgado, F. QUANTUM: A Wolfram *Mathematica* add-on for Dirac bra-ket notation, non-commutative algebra, and simulation of quantum computing circuits. *J. Phys.: Conf. Ser.* **698**, 012019 (2016).
- [18] Tourbez, C., Cimino, L. & Semay, C. Modèle de baryon en structure quark-diquark (2024). Report of an “Introduction to Scientific Research” project.
- [19] Fleck, S., Silvestre-Brac, B. & Richard, J. M. Search for diquark clustering in baryons. *Phys. Rev. D* **38**, 1519 (1988).
- [20] Fulcher, L. P. Matrix representation of the nonlocal kinetic energy operator, the spinless Salpeter equation and the Cornell potential. *Phys. Rev. D* **50**, 447 (1994).
- [21] Giannuzzi, F. Doubly heavy baryons in a Salpeter model with AdS/QCD inspired potential. *Phys. Rev. D* **79**, 094002 (2009).
- [22] Cimino, L., Willemyns, C. T. & Semay, C. Quark core-gluon model for heavy hybrid baryons. *Phys. Rev. D* **110**, 034032 (2024).
- [23] Godfrey, S. & Isgur, N. Mesons in a relativized quark model with chromodynamics. *Phys. Rev. D* **32**, 189 (1985).
- [24] Capstick, S. & Isgur, N. Baryons in a relativized quark model with chromodynamics. *Phys. Rev. D* **34**, 2809 (1986).
- [25] Weng, X.-Z., Deng, W.-Z. & Zhu, S.-L. Heavy baryons in the relativized quark model with chromodynamics. <https://arxiv.org/abs/2405.19039> (2024). ArXiv:2405.19039.
- [26] 't Hooft, G. A planar diagram theory for strong interactions. *Nucl. Phys. B* **72**, 461 (1974).
- [27] Witten, E. Baryons in the $1/N$ expansion. *Nucl. Phys. B* **160**, 57 (1979).
- [28] Buisseret, F. & Semay, C. Light baryon masses in different large- N_c limits. *Phys. Rev. D* **82**, 056008 (2010).
- [29] Buisseret, F., Matagne, N. & Semay, C. Spin contribution to light baryons in different large- N limits. *Phys. Rev. D* **85**, 036010 (2012).
- [30] Willemyns, C. & Schat, C. Operator analysis of effective spin-flavor interactions for $L = 1$ excited baryons. *Phys. Rev. D* **93**, 034007 (2016).
- [31] Buisseret, F., Willemyns, C. T. & Semay, C. Many-quark interactions: large- N scaling and contribution to baryon masses. *Universe* **8**, 311 (2022).
- [32] Veneziano, G. U(1) without instantons. *Nucl. Phys. B* **159**, 213 (1979).
- [33] Cimino, L. Helicity basis for hybrid mesons. Personal notes.

Wavefunction of the N -body harmonic oscillator

A

In this appendix, information about the wavefunctions of the many-body harmonic oscillator is provided. In particular, the bosonic and fermionic ground states are computed. Additionally, three-body states with given symmetry and angular momentum are explicitly detailed. Natural units $\hbar = c = 1$ are used.

A.1 One-body oscillator wavefunction

We begin the discussion by reviewing the one-body harmonic oscillator in D dimensions, described by the Hamiltonian $H = \mathbf{p}^2/(2m) + k\mathbf{r}^2$. Eigensolutions can be computed in Cartesian coordinates $\mathbf{r} = (r_1, \dots, r_D)$ and (hyper)spherical coordinates $\mathbf{r} = (r, \hat{\mathbf{r}})$. In Cartesian coordinates, the wavefunction is given by

$$\varphi_{\{\nu\}}(\lambda\mathbf{r}) = \prod_{i=1}^D \varphi_{\nu_i}(\lambda r_i) \quad (\text{A.1})$$

$$\text{with } \varphi_{\nu}(\lambda r) = \frac{1}{\sqrt{2^{\nu}\nu!}} \left(\frac{\lambda^2}{\pi}\right)^{1/4} e^{-\lambda^2 r^2/2} H_{\nu}(\lambda r),$$

where $\lambda^2 = \sqrt{2mk}$ and where $H_n(y)$ is a Hermite polynomial. The wavefunction is labelled by D quantum numbers $\{\nu\} = \{\nu_1, \dots, \nu_D\}$, but the eigenvalue depends only on their sum since $E = \sqrt{2k/m} \sum_i^D (\nu_i + 1/2)$. This leads to a degeneracy of the system that will be computed later. For $D \geq 2$, the harmonic oscillator can also be solved in (hyper)spherical coordinates, leading to the following expression of the wavefunction [1]

$$\varphi_{nl\{\mu\}}(\lambda\mathbf{r}) = \lambda^{D/2} \left[\frac{2n!}{\Gamma(n+l+D/2)} \right]^{1/2} \quad (\text{A.2})$$

$$\times (\lambda r)^l e^{-\lambda^2 r^2/2} L_n^{l+D/2-1}(\lambda^2 r^2) Y_{\{\mu\}}^l(\hat{\mathbf{r}}),$$

where $\lambda^2 = \sqrt{2mk}$, $\Gamma(n)$ is the Gamma function, $L_n^l(x)$ is a generalised Laguerre polynomial and $Y_{\{\mu\}}^l(\hat{\mathbf{x}})$ is a hyperspherical harmonic. The wavefunction

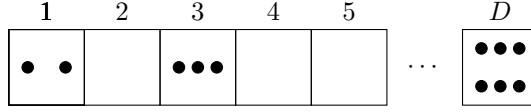


Figure A.1: A particular occupancy of \mathcal{N} particles in D boxes. An empty box correspond to a null quantum number.

is labelled by the principal quantum number n , the angular quantum number l , and a set of $D - 2$ magnetic quantum numbers $\{\mu\}$. However, the energy only depends on the first two, given by $E = \sqrt{2k/m} (2n + l + \frac{D}{2})$. A useful result for the following discussion is the expectation value of the observable \mathbf{r}^2 [2]

$$\langle \varphi_{nl} | \mathbf{r}^2 | \varphi_{nl} \rangle = \int d\mathbf{r} \mathbf{r}^2 |\varphi_{nl}(\lambda\mathbf{r})|^2 = \frac{2n + l + D/2}{\lambda^2}. \quad (\text{A.3})$$

Note that in $D = 1$, this result is not valid and the observable is instead given by $\langle \varphi_n | r^2 | \varphi_n \rangle = \frac{n+1/2}{\lambda^2}$.

A.1.1 Degeneracy of the harmonic oscillator

In D dimensions, some energy levels of the harmonic oscillator are degenerate. For simplicity, we will work with the band number $\mathcal{N} = \sum_i^D \nu_i = 2n + l$. For example, in $D = 2$, the states $(\nu_1, \nu_2) = (2, 0), (1, 1)$ and $(0, 2)$ are degenerate with $\mathcal{N} = 2$. We aim to derive a formula for the degeneracy $g(\mathcal{N}, D)$ of a given level \mathcal{N} in D dimensions.

First, ν_1 can take any value from 0 to \mathcal{N} . Then, ν_2 has $\mathcal{N} - \nu_1 + 1$ possibilities, ranging from 0 to $\mathcal{N} - \nu_1$. Next, ν_3 has $\mathcal{N} - \nu_1 - \nu_2 + 1$ possibilities, ranging from 0 to $\mathcal{N} - \nu_1 - \nu_2$, and so on. Ultimately, the last quantum number is automatically fixed as $\nu_D = \mathcal{N} - \nu_1 - \nu_2 - \dots - \nu_{D-1}$. The degeneracy of the level \mathcal{N} is given by the sum

$$\sum_{\nu_1=0}^{\mathcal{N}} \sum_{\nu_2=0}^{\mathcal{N}-\nu_1} \sum_{\nu_3=0}^{\mathcal{N}-\nu_1-\nu_2} \dots \sum_{\nu_{D-2}=0}^{\mathcal{N}-\nu_1-\dots-\nu_{D-3}} (\mathcal{N} - \nu_1 - \dots - \nu_{D-2} + 1). \quad (\text{A.4})$$

Rather than computing this sum directly, we can recast the problem as distributing \mathcal{N} indistinguishable balls into D distinct boxes, as illustrated in Fig. A.1.

Instead of viewing the system as D boxes, consider $D - 1$ walls separating \mathcal{N} balls. The number of ways to organise the system is $(\mathcal{N} + D - 1)!$. Since the permutation of identical balls or identical walls does not change the arrangement, the degeneracy of the level \mathcal{N} is

$$g(\mathcal{N}, D) = \frac{(\mathcal{N} + D - 1)!}{\mathcal{N}!(D - 1)!} = C_{\mathcal{N}+D-1}^{\mathcal{N}}. \quad (\text{A.5})$$

In particular, if $D = 1$, the degeneracy is $g(\mathcal{N}, 1) = 1$ as expected.

The degeneracy of the level \mathcal{N} can also be determined using spherical coordinates. The energy of the harmonic oscillator depends only on the radial quantum number n and the orbital quantum number l , but not on the magnetic quantum

numbers $\{\mu\}$. First, we calculate the degeneracy associated with a given orbital quantum number l [3], considering the constraint $l \geq \mu_1 \geq \mu_2 \geq \dots \geq |\mu_{D-2}|$,

$$W_l^D \equiv C_{l+D-3}^l \frac{2l + D - 2}{D - 2}. \quad (\text{A.6})$$

For instance, we verify that $W_l^3 = 2l + 1$ for $D = 3$, as expected. For a given level \mathcal{N} , the orbital quantum number l can take any value from 0 to \mathcal{N} , and the radial quantum number n is fixed to $\frac{1}{2}(\mathcal{N} - l)$ (if \mathcal{N} is even (odd), l must also be even (odd)). The degeneracy of the level \mathcal{N} is then given by the sum

$$\sum_{l \text{ even or odd}}^{\mathcal{N}} W_l^D, \quad (\text{A.7})$$

which yields the same result as (A.5).

A.2 N -body oscillator wavefunction

In Sec. 2.2, we demonstrated in equation (2.25) that the N -body harmonic oscillator for identical particles

$$H = \sum_{i=1}^N \frac{p_i^2}{2m} + \tilde{k} \sum_{i=1}^N (\mathbf{r}_i - \mathbf{R})^2 + k \sum_{i < j=2}^N (\mathbf{r}_i - \mathbf{r}_j)^2, \quad (\text{A.8})$$

can be expressed as a sum of $N - 1$ decoupled one-body harmonic oscillators in terms of the Jacobi coordinates $(\mathbf{x}_i, \mathbf{\Pi}_i)$ defined by (2.3). The wavefunction of the system is then

$$\psi = \prod_{i=1}^{N-1} \varphi_{n_i l_i \{\mu_i\}}(\lambda_i \mathbf{x}_i) \text{ with } \lambda_i^2 = \frac{i}{i+1} \sqrt{2m(Nk + \tilde{k})}. \quad (\text{A.9})$$

This wavefunction can be easily generalised to include K -body forces by substituting $k \rightarrow k C_{N-2}^{K-2}$. Note that to be complete, ψ must be multiplied by a wavefunction $\varphi(\mathbf{R})$ that depends on the CM position, which has been isolated. If no external forces act on the system, then $\varphi(\mathbf{R})$ can be taken as a plane wave. We also recall from Sec. 2.2 the definition of the global quantum number

$$Q(N) = \sum_{i=1}^{N-1} (2n_i + l_i + D/2), \quad (\text{A.10})$$

with (n_i, l_i) being the principal and orbital quantum numbers associated with the Jacobi coordinate \mathbf{x}_i .

A.2.1 Properties

The N -body wavefunction (A.9) is normalised since each individual wavefunction φ is normalised. It also possesses the following properties.

Parity

The parity operator \hat{P} switches the sign of the spatial coordinates $\mathbf{r} \rightarrow -\mathbf{r}$. It is known that the wavefunction φ_{nl} is an eigenstate of this operator with eigenvalue $P = (-1)^l$. Thus, the N -body wavefunction has the following parity eigenvalue

$$\begin{aligned} P &= \prod_{i=1}^{N-1} (-1)^{l_i} = (-1)^{\sum_i^{N-1} l_i} = (-1)^{\sum_i^{N-1} (2n_i + l_i)} \\ &= (-1)^{Q(N) - (N-1)\frac{D}{2}}, \end{aligned} \quad (\text{A.11})$$

Hence, all linear combinations of states $\{\psi\}$ with the same value of $Q(N)$ (and consequently the same value of the energy) have the same parity P .

Angular momentum

For $N > 2$, the wavefunction (A.9) does not have a well-defined angular momentum. However, by using the correct coupling coefficients, one can construct a wavefunction with total angular momentum L and projection M_L . We write this generically as

$$\psi_{M_L}^L = [[\dots [[l_1 l_2]^{l_{12}} l_3]^{l_{123}} \dots]^{l_{12\dots N-2}} l_{N-1}]_{M_L}^L, \quad (\text{A.12})$$

where $[\cdot]$ denotes the coupling of angular momenta. Note that $\sum_i^{N-1} l_i = L_{\max}$ is the maximum angular momentum L obtained by (A.12). Clearly, $L \neq L_{\max}$ in general, so L does not determine the parity of $\psi_{M_L}^L$.

Symmetry

The wavefunction ψ_α , where α denotes the set of quantum numbers $\{n_i, l_i, \{\mu_i\}\}$ with $i = \{1, \dots, N-1\}$, does not exhibit a particular symmetry under the permutations of particles in general. Nonetheless, by constructing suitable linear combinations of these functions, potentially including functions of other degrees of freedom if applicable, one can build a wavefunction with a given symmetry and angular momentum. Generically, we write this function as

$$\Psi = \sum_{\alpha} c_{\alpha} \psi_{\alpha} \phi_{\alpha}, \quad (\text{A.13})$$

where ϕ_{α} ¹ can be a spin, isospin, flavour or colour wavefunction, or may not exist if the only degree of freedom is spatial. The coefficients c_{α} are such that Ψ is normalised, has a well-defined angular momentum L and symmetry. Since Ψ is an eigenstate of H with eigenvalue (2.26) and parity (A.11), all $\{\psi_{\alpha}\}$ have the same value of $Q(N)$. For a given value of $Q(N)$ and a given symmetry, Ψ may not exist.

¹The functions ϕ_{α} are characterised by quantum numbers other than $\{n_i, l_i, \{\mu_i\}\}$. The index α here signifies that the function ϕ is associated with the function ψ_{α}

A.2.2 Bosonic ground state

We consider the ground state where $n_i = l_i = 0 \forall i$. According to (A.2),

$$\begin{aligned} \varphi_{0,0,\{0\}}(\lambda\mathbf{r}) &= \lambda^{D/2} \left[\frac{2}{\Gamma(D/2)} \right]^{1/2} e^{-\lambda^2 r^2/2} L_0^{D/2-1}(\lambda^2 r^2) Y_{\{0\}}^0(\hat{\mathbf{r}}) \\ &= \left(\frac{\lambda^2}{\pi} \right)^{D/4} e^{-\lambda^2 r^2/2}. \end{aligned} \quad (\text{A.14})$$

The N -body wavefunction (A.9) now reads

$$\psi = \prod_{i=1}^{N-1} \left(\frac{\lambda_i^2}{\pi} \right)^{D/4} e^{-\lambda_i^2 x_i^2/2} = \mathcal{R} \exp \left(-\frac{1}{2} \sum_{i=1}^{N-1} \lambda_i^2 x_i^2 \right), \quad (\text{A.15})$$

with $\mathcal{R} = \prod_i^{N-1} \left(\frac{\lambda_i^2}{\pi} \right)^{D/4}$. Then, we have

$$\begin{aligned} \sum_{i=1}^{N-1} \lambda_i^2 x_i^2 &= \sqrt{2m(Nk + \tilde{k})} \sum_{i=1}^{N-1} \frac{i}{i+1} x_i^2 \\ &= \sqrt{2m(Nk + \tilde{k})} \frac{1}{N} \sum_{i < j}^N (\mathbf{r}_i - \mathbf{r}_j)^2, \end{aligned} \quad (\text{A.16})$$

which is completely symmetric. The last equality is obtained through the transformation laws of Jacobi coordinates. The wavefunction (A.15) is thus the bosonic ground state and is characterised by positive parity and angular momentum $L = 0$. The associated global quantum number is

$$Q_{\text{BGS}} = (N-1) \frac{D}{2}. \quad (\text{A.17})$$

A.2.3 Fermionic ground state

The fermionic ground state (FGS) is more difficult to compute since two fermions cannot occupy the same level. Since we are only considering the spatial degree of freedom, we assume fermions have an intrinsic degeneracy d caused by other degrees of freedom, such as spin (e.g. electrons have $d = 2$). The main difficulty in computing the FGS is that the quantum numbers $(n_i, l_i, \{\mu_i\})$ are not associated with the individual coordinates but rather with the Jacobi coordinates. Here, we propose to compute only the global quantum number $Q(N)$ associated with the FGS.

Before proceeding, we will rearrange the harmonic oscillator Hamiltonian as follows [4]

$$\begin{aligned} H_{\text{ho}} &= \sum_{i=1}^N \frac{p_i^2}{2m} + \sum_{i < j=2}^N k(\mathbf{r}_i - \mathbf{r}_j)^2 - \frac{\mathbf{P}^2}{2Nm} \\ &= \sum_{i=1}^N \left(\frac{p_i^2}{2m} + Nk\mathbf{r}_i^2 \right) - \left(\frac{\mathbf{P}^2}{2Nm} + N^2k\mathbf{R}^2 \right) \\ &\equiv \sum_{i=1}^N H_i + H_{\text{CM}}. \end{aligned} \quad (\text{A.18})$$

The Hamiltonians H_i and H_{CM} are one-body oscillator Hamiltonians depending on the individual coordinates \mathbf{r}_i and the CM coordinate \mathbf{R} , respectively. Since these Hamiltonians commute, the energy of the many-body harmonic oscillator can be written as

$$E_{\text{ho}} = \sqrt{\frac{2}{m}} Nk \left(\sum_{i=1}^N (2\bar{n}_i + \bar{l}_i) + N\frac{D}{2} - (\mathfrak{N} + \frac{D}{2}) \right), \quad (\text{A.19})$$

where the quantum numbers (\bar{n}_i, \bar{l}_i) , with $i = \{1, \dots, N\}$, are now associated with the individual coordinates and \mathfrak{N} with the CM. With these quantum numbers, symmetry is easier to impose. Since we want the energy to be distributed on the internal variables only, we will set $\mathfrak{N} = 0$, leading to a new definition of the global quantum number

$$Q(N) = \sum_{i=1}^N (2\bar{n}_i + \bar{l}_i) + (N-1)\frac{D}{2}. \quad (\text{A.20})$$

Although this definition is similar to the previous one (A.10), the sum in the new definition runs from 1 to N , instead of $N-1$, reflecting the fact that the quantum numbers $\{\bar{n}_i, \bar{l}_i\}$ are related to the individual coordinates.

Using the result for the degeneracy of the harmonic oscillator (A.5), we can now fill the levels according to Fermi-Dirac statistics. Assuming the last occupied level is labelled by $\mathcal{N} = 2\bar{n}_i + \bar{l}_i = b$ and contains r particles, the total number of particles is given by

$$N = d \sum_{\mathcal{N}=0}^{b-1} C_{\mathcal{N}+D-1}^{\mathcal{N}} + r = d C_{b+D-1}^D + r. \quad (\text{A.21})$$

The global quantum number for the FGS is then given by

$$\begin{aligned} Q_{\text{FGS}}(N) &= \sum_{\mathcal{N}=0}^{b-1} \mathcal{N} d C_{\mathcal{N}+D-1}^{\mathcal{N}} + br + (N-1)\frac{D}{2} \\ &= d D C_{b+D-1}^{D+1} + br + (N-1)\frac{D}{2}, \end{aligned} \quad (\text{A.22})$$

with b the biggest integer such that $r = N - d C_{b+D-1}^D \geq 0$. In particular, in the one-dimensional case, if $d = 1$ and $r = 0$, we obtain $Q(N) = (N^2 - 1)/2$, which matches the result in [4]. An interesting limit of the above formula is when $N \rightarrow \infty$. Then [5],

$$Q_{\text{FGS}}(N \rightarrow \infty) \approx \frac{D}{D+1} \frac{(D!)^{1/D}}{d^{1/D}} N^{\frac{D+1}{D}}. \quad (\text{A.23})$$

A.3 Symmetrised three-body oscillator states

As previously stated, the N -body wavefunction (A.9) does not generally possess well-defined angular momentum and symmetry. In this section, we aim to explicitly construct these wavefunctions for $N = 3$ in three dimensions ($D = 3$). Starting from the N -body wavefunction (A.9), for $N = 3$, we have

$$\psi = \varphi_{n_1 l_1 \mu_1}(\lambda_1 \mathbf{x}_1) \varphi_{n_2 l_2 \mu_2}(\lambda_2 \mathbf{x}_2), \quad (\text{A.24})$$

where $\lambda_1 = \frac{1}{\sqrt{2}}[2m(\tilde{k}+3k)]^{1/4}$ and $\lambda_2 = \sqrt{\frac{2}{3}}[2m(\tilde{k}+3k)]^{1/4}$. For convenience, we define the variables $\mathbf{y}_i = \lambda_i \mathbf{x}_i$ and their conjugates $\boldsymbol{\rho}_i = \mathbf{\Pi}_i/\lambda_i$. The harmonic oscillator Hamiltonian (2.25) now reads

$$\begin{aligned} H &= \frac{1}{m} \mathbf{\Pi}_1^2 + \frac{1}{2}(\tilde{k} + 3k) \mathbf{x}_1^2 + \frac{3}{4m} \mathbf{\Pi}_2^2 + \frac{2}{3}(\tilde{k} + 3k) \mathbf{x}_2^2 \\ &= \sqrt{\frac{\tilde{k} + 3k}{2m}} [(\boldsymbol{\rho}_1^2 + \boldsymbol{\rho}_2^2) + (\mathbf{y}_1^2 + \mathbf{y}_2^2)]. \end{aligned} \quad (\text{A.25})$$

The three-body wavefunction (A.24) can now be endowed with angular momentum L and projection M_L

$$\begin{aligned} [\varphi_{n_1 l_1}(\boldsymbol{\rho}_1) \varphi_{n_2 l_2}(\boldsymbol{\rho}_2)]_{M_L}^L &= \sum_{\mu_1, \mu_2} (l_1 \mu_1 l_2 \mu_2 | L M_L) \\ &\quad \times \varphi_{n_1 l_1 \mu_1}(\boldsymbol{\rho}_1) \varphi_{n_2 l_2 \mu_2}(\boldsymbol{\rho}_2), \end{aligned} \quad (\text{A.26})$$

where $(l_1 \mu_1 l_2 \mu_2 | L M_L)$ is a Clebsch-Gordan coefficient². The Hamiltonian (A.25) is invariant under the rotation of coordinates

$$\begin{cases} \mathbf{r} &= C \mathbf{y}_1 - S \mathbf{y}_2 \\ \mathbf{s} &= S \mathbf{y}_1 + C \mathbf{y}_2 \end{cases} \quad \text{or} \quad \begin{cases} \mathbf{y}_1 &= C \mathbf{r} + S \mathbf{s} \\ \mathbf{y}_2 &= -S \mathbf{r} + C \mathbf{s} \end{cases}, \quad (\text{A.27})$$

with $C = \cos(\beta/2)$ and $S = \sin(\beta/2)$. Consequently, $[\varphi_{n l}(\mathbf{r}) \varphi_{\nu \lambda}(\mathbf{s})]_{M_L}^L$ is also an eigenstate of (A.25) with the same energy $2n+l+2\nu+\lambda = 2n_1+l_1+2n_2+l_2$. Therefore, one can write

$$\begin{aligned} [\varphi_{n_1 l_1}(\mathbf{y}_1) \varphi_{n_2 l_2}(\mathbf{y}_2)]_{M_L}^L &= \sum_{n, l, \nu, \lambda} \langle n l \nu \lambda; L | n_1 l_1 n_2 l_2; L \rangle_\beta \\ &\quad \times [\varphi_{n l}(\mathbf{r}) \varphi_{\nu \lambda}(\mathbf{s})]_{M_L}^L. \end{aligned} \quad (\text{A.28})$$

where $\langle n l \nu \lambda; L | n_1 l_1 n_2 l_2; L \rangle_\beta$ are the Brody-Moshinsky (BM) coefficients with angle β [6]. Note that the sum above is over all quantum numbers (n, l, ν, λ) consistent with the conservation of energy, the constraint of resultant angular momentum $|l - \lambda| \leq L \leq l + \lambda$, and parity $(-1)^{l_1+l_2} = (-1)^{l+\lambda}$. These coefficients will prove useful for computing the action of the symmetriser \mathcal{S}_σ on (A.26)

$$\mathcal{S}_\sigma = 1 + \sigma \hat{P}_{12} + \sigma \hat{P}_{13} + \sigma \hat{P}_{23} + \hat{P}_{13} \hat{P}_{12} + \hat{P}_{23} \hat{P}_{12}, \quad (\text{A.29})$$

where \hat{P}_{ij} is the permutation operator between particles i and j , and where $\sigma = 1$ corresponds to the symmetriser and $\sigma = -1$ to the antisymmetriser. First, the action of \hat{P}_{12} is simply given by

$$\hat{P}_{12} \mathbf{y}_1 = -\mathbf{y}_1 \quad \text{and} \quad \hat{P}_{12} \mathbf{y}_2 = \mathbf{y}_2, \quad (\text{A.30})$$

leading to

²This construction is only valid for massive particles. For massless particles, the helicity formalism must be used.

$$\hat{P}_{12}[\varphi_{n_1 l_1}(\mathbf{y}_1)\varphi_{n_2 l_2}(\mathbf{y}_2)]_{M_L}^L = (-1)^{l_1}[\varphi_{n_1 l_1}(\mathbf{y}_1)\varphi_{n_2 l_2}(\mathbf{y}_2)]_{M_L}^L. \quad (\text{A.31})$$

For symmetric states, l_1 must be even, and for antisymmetric states, l_1 must be odd. Next, the action of \hat{P}_{13} is given by

$$\hat{P}_{13}\mathbf{y}_1 = \frac{1}{2}\mathbf{y}_1 - \frac{\sqrt{3}}{2}\mathbf{y}_2 \text{ and } \hat{P}_{13}\mathbf{y}_2 = -\frac{\sqrt{3}}{2}\mathbf{y}_1 - \frac{1}{2}\mathbf{y}_2. \quad (\text{A.32})$$

These relations are similar to the rotations (A.27) with $\beta = 5\pi/3$. Thanks to the properties of the BM coefficients, one can show

$$\begin{aligned} & \hat{P}_{13}[\varphi_{n_1 l_1}(\mathbf{y}_1)\varphi_{n_2 l_2}(\mathbf{y}_2)]_{M_L}^L \\ &= (-1)^{l_1+l_2-L} \sum_{n,l,\nu,\lambda} \langle n l \nu \lambda; L | n_1 l_1 n_2 l_2; L \rangle_{\frac{5\pi}{3}} [\varphi_{\nu\lambda}(\mathbf{y}_1)\varphi_{nl}(\mathbf{y}_2)]_{M_L}^L. \end{aligned} \quad (\text{A.33})$$

A similar relation is found for the last permutation \hat{P}_{23} with $\beta = \pi/3$. The action of the symmetriser on our state is then given by

$$\begin{aligned} \Psi &= A (\sigma + (-1)^{l_1}) (\sigma [\varphi_{n_1 l_1}(\mathbf{y}_1)\varphi_{n_2 l_2}(\mathbf{y}_2)]_{M_L}^L + (-1)^{l_1+l_2-L} \\ &\quad \times \sum_{n,l,\nu,\lambda} (\langle n l \nu \lambda; L | n_1 l_1 n_2 l_2; L \rangle_{5\pi/3} + \langle n l \nu \lambda; L | n_1 l_1 n_2 l_2; L \rangle_{\pi/3}) \\ &\quad \times [\varphi_{\nu\lambda}(\mathbf{y}_1)\varphi_{nl}(\mathbf{y}_2)]_{M_L}^L). \end{aligned} \quad (\text{A.34})$$

The constant A is added for normalisation. For pedagogical purposes, the first symmetric wavefunctions $|\mathcal{N}, L^P\rangle$, with $\mathcal{N} = 2n_1 + 2n_2 + l_1 + l_2$ the band number, are explicitly written in terms of $|n_1, l_1, n_2, l_2; L\rangle$ [7]

$$|0, 0^+\rangle = |0, 0, 0, 0; 0\rangle, \quad (\text{A.35a})$$

$$|2, 0^+\rangle = \frac{1}{\sqrt{2}}(|1, 0, 0, 0; 0\rangle + |0, 0, 1, 0; 0\rangle), \quad (\text{A.35b})$$

$$|2, 2^+\rangle = \frac{1}{\sqrt{2}}(|0, 2, 0, 0; 2\rangle + |0, 0, 0, 2; 2\rangle), \quad (\text{A.35c})$$

$$|3, 1^-\rangle = -\frac{1}{2}|0, 0, 1, 1; 1\rangle + \frac{1}{\sqrt{3}}|0, 2, 0, 1; 1\rangle + \sqrt{\frac{5}{12}}|1, 0, 0, 1; 1\rangle, \quad (\text{A.35d})$$

$$|3, 3^-\rangle = \frac{1}{2}|0, 0, 0, 3; 3\rangle - \frac{\sqrt{3}}{2}|0, 2, 0, 1; 3\rangle. \quad (\text{A.35e})$$

Notably, symmetric states with $\mathcal{N} = 1$, $\mathcal{N} = 2$ and $L = 1$, $\mathcal{N} = 3$ and L even are forbidden.

A.4 Wavefunction in the envelope theory

In Sec. 2.3, an auxiliary Hamiltonian

$$\tilde{H} = \sum_{i=1}^N \frac{p_i^2}{2\mu_0} + \nu_0 \sum_{i=1}^N (\mathbf{r}_i - \mathbf{R})^2 + \rho_0 \sum_{i<j=2}^N (\mathbf{r}_i - \mathbf{r}_j)^2 + B(\mu_0, \nu_0, \rho_0), \quad (\text{A.36})$$

where B is a constant function of the auxiliary parameters (μ_0, ν_0, ρ_0) , was introduced to approximate the Hamiltonian H under study. The auxiliary Hamiltonian is a harmonic oscillator H_{ho} , and so are its eigensolutions. Specifically, the wavefunction is a product of $N - 1$ one-body harmonic oscillator wavefunctions (A.9) with $\lambda_i^2 = \frac{i}{i+1} \sqrt{2\mu_0(N\rho_0 + \nu_0)}$. However, it is more insightful to compute the wavefunction in terms of the more physical variables p_0 and r_0 defined by (2.53). In particular

$$\begin{aligned} r_0^2 &\equiv \langle (\mathbf{r}_i - \mathbf{r}_j)^2 \rangle = \frac{1}{C_N^2} \left\langle \sum_{i<j=2}^N (\mathbf{r}_i - \mathbf{r}_j)^2 \right\rangle \\ &= \frac{N}{C_N^2} \sum_{i=1}^N \frac{i}{i+1} \langle \mathbf{x}_i^2 \rangle \frac{N}{C_N^2} \sum_{i=1}^N \frac{i}{i+1} \frac{2n_i + l_i + D/2}{\lambda_i^2}, \end{aligned} \quad (\text{A.37})$$

where (n_i, l_i) are the quantum numbers associated with the Jacobi coordinate \mathbf{x}_i . The third equality is obtained from the transformation into Jacobi coordinates, and the fourth equality from the result (A.3). This yields

$$\sqrt{2\mu_0(N\rho_0 + \nu_0)} = \frac{N}{C_N^2} \frac{Q(N)}{r_0^2}. \quad (\text{A.38})$$

Ultimately, one obtains

$$\lambda_i = \sqrt{\frac{i}{i+1} \frac{2}{N-1} Q(N)} \frac{1}{r_0} = \sqrt{\frac{i}{i+1} \frac{N}{Q(N)}} p_0, \quad (\text{A.39})$$

where the last line is derived from (2.71c). Thus, by computing the value of r_0 or p_0 using the compact equations (2.71), one can determine the coefficients λ_i , which serves as an approximation of the original wavefunction. Thanks to (A.39), all the aforementioned results and properties of the harmonic oscillator can be applied within the framework of the envelope theory.

A.4.1 Modified global quantum number

In Sec. 2.4, a modified global quantum number

$$Q_\phi(N) = \sum_{i=1}^{N-1} \left(\phi n_i + l_i + \frac{D + \phi - 2}{2} \right), \quad (\text{A.40})$$

was introduced to enhance the accuracy of the envelope theory. How can we evaluate the value of Q_ϕ for the BGS and FGS? The idea is to consider that we are still dealing with harmonic oscillators and the levels have to be filled, but the energy of these levels has been artificially modified. By applying this procedure for bosons, we obtain

$$Q_{\phi\text{BGS}}(N) = (N-1) \frac{D+\phi-2}{2}. \quad (\text{A.41})$$

For the FGS, computations are more complex. For $\phi = 1$, one can use the same reasoning as the case $\phi = 2$, which corresponds to the usual harmonic oscillator, and obtain [3]

$$N = d C_{b+D-2}^{D-1} \frac{2b+D-2}{D} + r, \quad (\text{A.42a})$$

$$Q_{\text{FGS}}^{\phi=1} = d C_{b+D-2}^D \frac{2Db-2D+D^2+1}{D+1} + r b + (N-1) \frac{D-1}{2}. \quad (\text{A.42b})$$

For other values of ϕ , it does not seem possible to find a closed form solution as in (A.42). We propose the following procedure

1. Generate all possible quantum numbers $\{n, l\}$ and compute the occupation level $d W_l^D$ and associated energy $\phi n + l$.
2. Order the levels in increasing energy.
3. Fill each level $\{n, l\}$ with $d W_l^D$ particles, until N particles are exhausted.
4. Compute the value of Q_ϕ by summing, for each occupied pair $\{n, l\}$, the product of $\phi n + l$ with the number of particles occupying this level. At the end, we add $(N-1)(D+\phi-2)/2$.

An approximate value of Q_ϕ for large N can also be obtained [3]

$$Q_{\phi\text{FGS}}(N \rightarrow \infty) \approx \frac{D}{D+1} \left(\frac{\phi D!}{2d} \right)^{1/D} N^{\frac{D+1}{D}}. \quad (\text{A.43})$$

A final problem remains. To use the improvement procedure of the envelope theory, the angular part of $Q_\phi(N)$

$$\lambda = \sum_{i=1}^{N-1} l_i + (N-1) \frac{D-2}{2}, \quad (\text{A.44})$$

must be computed first. A priori, one could use the above procedure, but by summing only the quantum numbers l and adding $(N-1)(D-2)/2$ at the end. However, to start this process, one must know the value of ϕ beforehand, which is the exact goal of the improvement procedure. For bosons, this is not an issue since

$$\lambda_{\text{BGS}} = (N-1) \frac{D-2}{2}, \quad (\text{A.45})$$

which is independent of ϕ . However, this is not the case for fermions because levels with $n \neq 0$ have to be considered, and the arrangement of levels depends on ϕ . Therefore, the following solution is proposed. Since the wavefunctions are initially those of harmonic oscillators, the above procedure will be used but with $\phi = 2$, and $(N-1)(D+\phi-2)/2$ will be added at the end. In case some levels $\{n, l\}$ have the same energy, the filling step will begin with the levels with the lowest l .

Bibliography

- [1] Yáñez, R. J., Van Assche, W. & Dehesa, J. S. Position and momentum information entropies of the D -dimensional harmonic oscillator and hydrogen atom. *Phys. Rev. A* **50**, 3065 (1994).
- [2] Flügge, S. *Practical Quantum Mechanics* (Springer, Berlin, 1999).
- [3] Chevalier, C., Willemyns, C. T., Cimino, L. & Semay, C. Improvement of the envelope theory for systems with different particles. *Few-Body Syst.* **63**, 40 (2022).
- [4] Lévy-Leblond, J. M. Generalized uncertainty relations for many-fermion system. *Phys. Lett. A* **26**, 540 (1968).
- [5] Semay, C., Cimino, L. & Willemyns, C. Envelope theory for systems with different particles. *Few Body-Syst.* **61**, 19 (2020).
- [6] Silvestre-Brac, B. The cluster model and the generalized Brody-Moshinsky coefficients. *J. Phys. France* **46**, 1087 (1985).
- [7] Cimino, L., Tourbez, C., Chevalier, C., Lacroix, G. & Semay, C. Tests of the envelope theory for three-body forces. *Few-Body Syst.* **65**, 20 (2024).

Notions of the Poincaré group and $SO(3)$

B

The Poincaré group is the isometry group of Minkowski spacetime, comprising spacetime coordinate transformations $x \rightarrow x'$ that preserve the Minkowski metric $ds^2 = dt^2 - dx^2 - dy^2 - dz^2$, in natural units $\hbar = c = 1$. The elements of the Poincaré group can be categorised into four families

1. Spacetime translations $x^\mu \rightarrow x^\mu + a^\mu$, where a^μ is a constant 4-vector.
2. Spatial rotations $x^i \rightarrow R_j^i x^j$, where $R^t R = \mathbb{1}$.
3. Lorentz boost $x^\mu \rightarrow \Lambda_\nu^\mu x^\nu$, with $\Lambda^t g \Lambda = \mathbb{1}$ and $g = \text{diag}(1, -1, -1, -1)$.
4. Discrete transformations as parity $x^i \rightarrow -x^i$ and time reversal $x^0 = t \rightarrow -x^0$.

In this notation, Greek indices run from 0 to 3, while Latin indices run from 1 to 3. The Einstein summation convention is used, implying summation over repeated indices.

The Poincaré group contains several notable subgroups. Excluding the spacetime translations forms the homogeneous Poincaré group, also known as the Lorentz group $O(1, 3)$. The spatial rotations and Lorentz boosts form another subgroup, the proper-orthochronous Lorentz group. Lastly, spatial rotations alone form the rotation group $SO(3)$.

B.1 Poincaré algebra and generators

The Poincaré algebra, derived from the infinitesimal transformations of the Poincaré group (excluding parity and time reversal), consists of ten generators that satisfy specific commutation relations.

The spacetime translations can be expressed as $\exp(-iP_\mu a^\mu)$, where P_μ are the four translation generators. They commute with each other

$$[P_\mu, P_\nu] = 0 \quad \forall \mu, \nu. \quad (\text{B.1})$$

In quantum mechanics, these are interpreted as the four-momentum operators. Since they commute with each other, it is possible to construct vectors that are simultaneous eigenstates of the four operators.

Next, the spatial rotations are generated by three generators, denoted J_i , and follow the commutation relations of $SO(3)$

$$[J_i, J_j] = i\epsilon_{ijk}J_k, \quad (\text{B.2})$$

where ϵ_{ijk} is the completely antisymmetric Levi-Civita tensor. These generators do not necessarily commute with P_μ (the interested reader can refer to [1] for further information). In quantum mechanics, J_i are interpreted as the angular momentum operators.

Finally, the three last generators, denoted K_i , generate the Lorentz boosts along the three spatial directions. Their commutation relations are not essential for our discussion (see [1] for further information), but it is noteworthy that

$$[K_3, J_3] = 0, \quad (\text{B.3})$$

indicating that boosts along the z -direction commute with rotations around the z -axis. Lorentz boost and spatial rotation generators are often grouped under a single notation $M_{\mu\nu}$ defined by

$$J_i = \frac{1}{2}\epsilon_{ijk}M^{jk} \text{ and } K_i = M_{i0} = M_{0i}, \quad (\text{B.4})$$

corresponding to the six generators of the Lorentz group.

B.1.1 Casimir operators

A Casimir operator is a combination of the generators that commutes with all other generators. By their nature, Casimir operators can be used to classify¹ the irreducible representation of a group. For example, the Casimir of the group $SO(3)$ is $J^2 = J_i J^i$, and its eigenvalue is given by $j(j+1)$, where j is an integer or half-integer. Thus, the irreducible representations of $SO(3)$ are classified by the angular momentum j .

The Poincaré group possesses two Casimir operators, one quadratic and the other quartic [2]

$$P^2 = P_\mu P^\mu, \quad (\text{B.5})$$

$$W^2 = W_\mu W^\mu \text{ with } W_\mu = \frac{1}{2}\epsilon_{\mu\nu\rho\sigma}M^{\nu\rho}P^\sigma, \quad (\text{B.6})$$

where W^μ is the Pauli-Lubanski vector. By definition, the Casimir operator commutes with all the elements of the group, implying in our case that they are Lorentz invariant. The first Casimir, (B.5), is the squared momentum, and its eigenvalue is logically interpreted as the squared mass m^2 . This reaffirms the well-known fact that mass is a Lorentz invariant.

¹Consider a group G and a representation U with its vector space V . Let $|v\rangle \in V$ be a vector, and denote the eigenvalue of the Casimir operator by c . Acting on $|v\rangle$ with the group's elements results in a new vector $|w\rangle$. If the representation is irreducible, then $|w\rangle \in V$. Since the Casimir operator commutes with any element of the group, the eigenvalue of the Casimir operator on $|w\rangle$ remains c . Hence, the irreducible representation U can be labelled by c .

The second Casimir, (B.6), the Pauli-Lubanski operator, is more complicated to interpret, and we need to distinguish between the massive and massless cases.

Massive particles

For massive particles, $m \neq 0$, the Pauli-Lubanski operator can be evaluated for a particle at rest, implying $P^i = 0 \forall i$ and $P^0 = m$. It is always possible to find a Lorentz boost such that a massive particle comes to rest. Since boosts commute with P^2 , the eigenvalue of the state remains m^2 . In this scenario, the Pauli-Lubanski vector W_i reduces to $-m J_i$ and $W_0 = 0$. The Casimir (B.6) reads

$$W^2 = -m^2 J^2, \quad (\text{B.7})$$

where J^2 is the squared angular momentum operator, which is the Casimir operator of $SO(3)$. Since the particle is at rest, the angular momentum is associated with the spin. Thus, the spin is a Lorentz invariant for massive particles.

Massless particles

For massless particles, $m = 0$, the Pauli-Lubanski operator does not yield additional information, as $W^2 = 0$. However, another combination of the generators proves to be Lorentz invariant in the massless case [2]

$$\Lambda = \frac{J_1 P_1 + J_2 P_2 + J_3 P_3}{\sqrt{P_1^2 + P_2^2 + P_3^2}} = \frac{\mathbf{J} \cdot \mathbf{P}}{\sqrt{\mathbf{P}^2}}. \quad (\text{B.8})$$

This operator, called the helicity operator, is interpreted as the angular momentum projection along the momentum direction. Even though helicity is a Lorentz invariant only for massless particles, eigenstates of this operator can be constructed for massive particles (see Sec. 3.1).

B.1.2 Classification of particles

Following the discussion in Sec. 3.1, we aim to describe a particle by a Lorentz invariant. Thus, we decide to characterise them by the eigenvalues of the Poincaré Casimir operators. Formally, we associate a particle with an irreducible representation of the Poincaré group. To construct a one-particle state, we choose it to be an eigenstate of a set of commutative operators. Firstly, it is an eigenstate of P^2 , whose eigenvalue is related to the mass m , and of W^2 , whose eigenvalue is related to the spin s for massive particles. Moreover, we choose the state to be an eigenstate of all four-momentum operators P_μ , since they commute with each other, ensuring that the one-body state has a well-defined four-momentum. Finally, for massive particles, the one-body state is also an eigenstate of W_3 , since $[P_\mu, W_3] = 0 \forall \mu$, with the eigenvalue related to the z -projection of the spin. Therefore, massive particles are characterised by $2s + 1$ degrees of freedom.

For massless particles, the one-body state is chosen as an eigenstate of Λ , the helicity operator. A priori, massless particles have only one degree of freedom. However, it is evident from (B.8) that the action of the parity operator will switch the sign of the helicity eigenvalue. Hence, massless particles have two degrees of freedom. This is why it is often said that photons are spin-1 particles:

they are described by a vector state but have only two projections, ± 1 , of the spin. The explicit expressions of the one-body states are given in Chapter 3.

B.2 Little group and $SO(3)$

The rotation group $SO(3)$ plays an important role in the Poincaré group. Indeed, it corresponds to the so-called *little group* for massive particles. Consider a particle in the irreducible representation $P^2 = m^2$ of the Poincaré group. By applying Lorentz boosts, all four-momenta \bar{p} satisfying $\bar{p}^2 = m^2$ can be reached, forming the orbit of the particle. Since all these states remain in the same irreducible representation, a reference four-momentum can be chosen to describe all states in the orbit. For massive particles, it is convenient to choose the rest state $\bar{p} = (m, \mathbf{0})$. The set of transformations that leave the reference four-momentum invariant is called the little group, which, for massive particles, corresponds to $SO(3)$ [1]. This is another way to understand why a massive particle is characterised by spin.

A similar reasoning can be applied to massless particles, for which the reference four-momentum is chosen as $\bar{p} = (1, 0, 0, 1)$. The corresponding little group is $ISO(2)$, the isometry group of two-dimensional Euclidean space [1]. Starting from $ISO(2)$, one can derive the notion of the helicity operator.

Returning to $SO(3)$, since rotations frequently appear in the helicity formalism presented in Chapter 3, a review of $SO(3)$ is helpful.

B.2.1 Wigner- D matrices

As explained above, the generators of $SO(3)$ are the three angular momentum operators J_i . In the formalism of the Euler angles (α, β, γ) , an arbitrary rotation R can be expressed as [3]

$$R(\alpha, \beta, \gamma) = \exp(-i\alpha J_3) \exp(-i\beta J_2) \exp(-i\gamma J_3). \quad (\text{B.9})$$

Other rotation formalisms exist, such as the axis-angle representation, but the Euler angles prove to be more practical for our purposes. The matrix elements of a rotation operator $R(\alpha, \beta, \gamma)$ between eigenstates of angular momentum j are defined as

$$\langle j m' | U(R(\alpha, \beta, \gamma)) | j m \rangle \equiv D_{m' m}^j(\alpha, \beta, \gamma), \quad (\text{B.10})$$

where $D_{m' m}^j$ are the Wigner D -matrices [3]. In (B.10), the notation $U(\cdot)$ specifies the representation j . For instance, if $j = 1/2$, the generators J_i are expressed in terms of the Pauli matrices. Thus, the action of a rotation operator on a state $|j m\rangle$ can be expressed as

$$U(R(\alpha, \beta, \gamma)) | j m \rangle = \sum_{m'=-j}^j D_{m' m}^j(\alpha, \beta, \gamma) | j m' \rangle. \quad (\text{B.11})$$

Properties

The Wigner D -matrices exhibit many interesting properties (for further details, see [3]). Here are some that will be useful in the derivations in Chapter 3

1. Orthogonality and completeness relations

$$\int_0^{2\pi} d\alpha \int_0^\pi d\beta \sin \beta \int_0^{2\pi} d\gamma D_{m\mu}^{j*}(\alpha, \beta, \gamma) D_{m'\mu'}^{j'}(\alpha, \beta, \gamma) = \frac{8\pi^2}{2j+1} \delta_{jj'} \delta_{mm'} \delta_{\mu\mu'}, \quad (\text{B.12a})$$

$$\sum_{j=0, \frac{1}{2}, 1, \dots}^{\infty} \sum_{m=-j}^j \sum_{m'=-j}^j \frac{2j+1}{16\pi^2} D_{mm'}^{j*}(\alpha_1, \beta_1, \gamma_1) D_{mm'}^j(\alpha_2, \beta_2, \gamma_2) = \delta(\alpha_1 - \alpha_2) \delta(\cos \beta_1 - \cos \beta_2) \delta(\gamma_1 - \gamma_2). \quad (\text{B.12b})$$

2. Addition of two D -matrices

$$\sum_{m''=-j}^j D_{mm''}^j(\alpha_2, \beta_2, \gamma_2) D_{m''m'}^j(\alpha_1, \beta_1, \gamma_1) = D_{mm'}^j(\alpha, \beta, \gamma), \quad (\text{B.13})$$

where (α, β, γ) are the Euler angles obtained after successive rotations of angles $(\alpha_1, \beta_1, \gamma_1)$ and $(\alpha_2, \beta_2, \gamma_2)$.

3. Unitarity

$$(D_{mm'}^j(\alpha, \beta, \gamma))^{-1} = D_{m'm}^{j*}(\alpha, \beta, \gamma). \quad (\text{B.14})$$

4. Symmetry

$$D_{mm'}^{j*}(\alpha, \beta, \gamma) = (-1)^{m-m'} D_{-m-m'}^j(\alpha, \beta, \gamma). \quad (\text{B.15})$$

5. Expansion in Clebsch-Gordan coefficients

$$D_{m\mu}^j D_{m'\mu'}^{j'} = \sum_J (j m j' m' | J M) (j \mu j' \mu' | J N) D_{MN}^J, \quad (\text{B.16})$$

where $|j - j'| \leq J \leq j + j'$, $M = m + m'$ and $N = \mu + \mu'$

6. Relation to spherical harmonics

$$D_{m0}^l(\alpha, \beta, \gamma) = \sqrt{\frac{4\pi}{2l+1}} Y_m^{l*}(\beta, \alpha). \quad (\text{B.17})$$

Wigner d -matrices

Substituting (B.9) into (B.10), and noting that $J_3 |j m\rangle = m |j m\rangle$, one finds

$$D_{mm'}^j(\alpha, \beta, \gamma) = \exp(-im\alpha) d_{mm'}^j(\beta) \exp(-im'\gamma), \quad (\text{B.18})$$

where $d_{mm'}^j(\beta) = D_{mm'}^j(0, \beta, 0) = \langle j m' | \exp(-i\beta J_2) | j m \rangle$ are the Wigner d -matrices. They are real and have the following orthogonality and completeness relations

$$\int_0^\pi d\beta \sin \beta d_{m\mu}^j(\beta) d_{m'\mu'}^{j'}(\beta) = \frac{2}{2j+1} \delta_{jj'} \delta_{mm'} \delta_{\mu\mu'}, \quad (\text{B.19a})$$

$$\sum_{j=0, \frac{1}{2}, 1, \dots}^{\infty} \frac{2j+1}{2} D_{mm'}^j(\beta_1) D_{mm'}^j(\beta_2) = \delta(\cos \beta_1 - \cos \beta_2). \quad (\text{B.19b})$$

A specific value of the d -matrices that will be frequently used is

$$d_{mm'}^j(\pi) = (-1)^{j+m} \delta_{m-m'} = (-1)^{j-m'} \delta_{-mm'}. \quad (\text{B.20})$$

Bibliography

- [1] Weinberg, S. *The Quantum Theory of Fields. Volume I: Foundations* (Cambridge University Press, Cambridge, 2005).
- [2] Bogolubov, N. N., Logunov, A. A., Oksak, A. I. & Todorov, I. T. *General Principles of Quantum Field Theory* (Springer, Dordrecht, 1990).
- [3] Varshalovich, D. A., Moskalev, A. N. & Khersonskii, V. K. *Quantum Theory Of Angular Momentum* (World Scientific, Singapore, 1988).

The Lagrange-mesh (LM) method, which is both highly accurate and user-friendly, is employed to solve the two-body system of the quark core-gluon interaction in Chapter 4. For systems involving particles with spin, the method has been described in detail in [1, 2]. In the context of the quark core-gluon system, the general wave function is approximated by the expansion

$$|\psi_{\text{LM}}\rangle = \sum_{\alpha=1}^{N_h} \sum_{i=1}^{N_{LM}} C_{i\alpha} |f_i; J^P; J_C; \alpha\rangle, \quad (\text{C.1})$$

where the basis $\{|f_i; J^P; J_C; \alpha\rangle\} = \{|f_i\rangle \otimes |J^P; J_C; \alpha\rangle\}$ is used, and

$$\langle J^P; J_C; \beta | J^P; J_C; \alpha \rangle = \delta_{\beta\alpha}. \quad (\text{C.2})$$

The summation runs over N_h helicity channels $\{|J^P; J_C; \alpha\rangle\}$ defining the state, and N_{LM} Lagrange radial functions $\{f_i\}$ such that

$$\langle \mathbf{r} | f_i; J^P; J_C; \alpha \rangle = \frac{1}{\sqrt{hr}} f_i\left(\frac{r}{h}\right) |J^P; J_C; \alpha\rangle. \quad (\text{C.3})$$

These functions are associated with N_{LM} dimensionless mesh points $\{x_i\}$, are orthonormal (at the Gauss approximation), and vanish at all mesh points but one. The coefficients $C_{i\alpha}$ are computed by diagonalising the Hamiltonian matrix with elements $\langle f_j; J^P; J_C; \beta | H | f_i; J^P; J_C; \alpha \rangle$, and h is the sole non-linear parameter that sets the system's scale (the method is not highly sensitive to the value of this parameter).

When only one channel is present, the computation of the matrix elements is described in [1]. The primary difference is replacing the mean values $l(l+1) = \langle \mathbf{L}^2 \rangle$ with their helicity counterparts $\langle J^P; J_C; \alpha | \mathbf{L}^2 | J^P; J_C; \alpha \rangle = w_{\alpha\alpha}$ (see Sec. 3.3.3). Let us note that the computation of $\langle \sqrt{\mathbf{p}^2 + m^2} \rangle$ first involves calculating the eigenvalues of the operator $\mathbf{p}^2 + m^2$ in the basis, which is easy to perform [1].

For some J^P quantum numbers, multiple channels must be considered. In equation (C.1), the same number of mesh points and the same value of the scale parameter are chosen for all helicity channels. This uniform choice simplifies the computation of non-diagonal matrix elements due to the orthogonality condition

on the functions $\{f_i\}$. Since the interaction is purely central, the coupling of helicity channels arises only from the operator \mathbf{L}^2 in \mathbf{p}^2 . For $\beta \neq \alpha$, it can be shown that [3]

$$\langle f_j; J^P; J_C; \beta | \mathbf{p}^2 + m^2 | f_i; J^P; J_C; \alpha \rangle = \frac{w_{\beta\alpha}}{h^2 x_i^2} \delta_{ji}, \quad (\text{C.4})$$

$$\langle f_j; J^P; J_C; \beta | V(r) | f_i; J^P; J_C; \alpha \rangle = 0. \quad (\text{C.5})$$

Bibliography

- [1] Semay, C., Baye, D., Hesse, M. & Silvestre-Brac, B. Semirelativistic Lagrange mesh calculations. *Phys. Rev. E* **64**, 016703 (2001).
- [2] Baye, D. The Lagrange-mesh method. *Phys. Rep.* **565**, 1 (2015).
- [3] Cimino, L., Willemyns, C. T. & Semay, C. Quark core-gluon model for heavy hybrid baryons. *Phys. Rev. D* **110**, 034032 (2024).

